

Department of Chemical Engineering

**Synthesis of Polymeric Nanocomposite Membranes for Aqueous and
Non-aqueous Media**

Babak Rajaeian

This thesis is presented for the degree of

Master of Philosophy

of

Curtin University

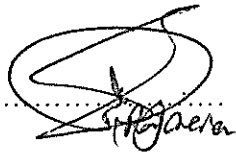
December 2012

Declaration

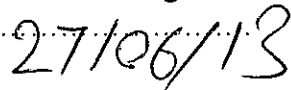
To the best of my knowledge and belief this thesis contains no material previously published by any person except where due acknowledgment has been made.

This thesis contains no material which has been accepted for the award of any other degree or diploma in any university.

Signature:

A handwritten signature in black ink, appearing to read 'S. H. Gaera', written over a dotted line.

Date:

A handwritten date '27/06/13' in black ink, written over a dotted line.

Abstract

Thin film composite (TFC) membranes have long been used by many large-scale applications (i.e., water and wastewater treatment). Recently, conventional polymeric TFC membranes are facing with short longevity due to high fouling tendency and susceptibility at extreme operational conditions. On the other hand, ceramic membranes are also suffering from disadvantages like low selectivity, unreliable control over porosity and pore size which makes it difficult to achieve a reproducible final product. The aim of this project was to develop a high selective TFC membranes incorporated by functionalized TiO₂ nanoparticles for aqueous and non-aqueous media applications.

In order to obtain high permeable aromatic polyamide thin film nanocomposite (TFN) nanofiltration membrane, the conventional interfacial polymerization (*IP*) reaction was applied as the embedding media for functionalized nanoparticles. For this purpose, TFN nanofiltration membrane with appropriate structural and separation properties was developed by dispersing the aminosilanized TiO₂ nanoparticles inside the diamine monomer and polymerizing the monomer in the presence of these particles. Surface-modified ceramic substrate was used to obtain high mechanical resistant composite membrane. Results from spectrometry analyses represent that the silane coupling agent called AAPTS has been successfully grafted onto the external surface of TiO₂ after the chemical modification. Upon incorporation of TiO₂ nanoparticles, thermal stability of nanocomposite is significantly improved in comparison with TFC membrane. Morphological investigations prove that the functionalized TiO₂ nanoparticles could effectively change the surface properties and roughness of NF membranes. Performance results show that ultra-low concentration (0.005 wt%) of amine functionalized TiO₂ nanoparticles improves the salt rejection as well as water flux. Flux can be further improved by the incorporation of higher percentage of the modified TiO₂ into polymer membrane.

In order to obtain nanofiltration membrane with high permeability and antifouling properties, TFN membrane was synthesised by dip-coating of a hydrophilized porous

poly(vinylidene fluoride) (PVDF) support in different poly(vinyl alcohol) (PVA) aqueous solution. In order to improve the interfacial adhesion of nanoparticles in PVA blend, an endothermic carboxylation reaction under acidic condition was carried out on the TiO_2 surface using chloroacetic acid (ClCH_2COOH). Glutaraldehyde (GA) was used as a cross-linker to bond resultant PVA chains and enhances the stability of the coated PVA layer, accordingly. TiO_2 nanoparticles were dispersed in PVA solution in pure and functionalized forms. Scanning electron microscopy (SEM) identified various topographies by the incorporation of TiO_2 nanoparticles. Performance results showed a 40% rejection improvement of divalent salt (MgSO_4) by the incorporation of 1.0 wt% surface-carboxylated TiO_2 nanoparticles into PVA solution. A simultaneous 57% retention improvement was achieved for uncharged solute (PEG 2000). After PVA coating with TiO_2 incorporation, the flux recovery ratio of PVDF membrane was significantly improved from 45 to 94%.

In order to apply TFN membranes in non-aqueous media, a range of thin film nanocomposite solvent resistant nanofiltration membranes (SRNF) were fabricated by interfacial polymerization technique. TiO_2 nanoparticles were used as inorganic fillers into polyamide chain network. TiO_2 nanoparticles' surfaces were functionalized in order to improve their compatibilization inside the polyamide matrix. For this purpose, Monoethanolamine (MEOA) and triethylenetetramine (TETA) agents were applied to aminate TiO_2 nanoparticles, while thionyl chloride (TCl) was used to chlorinateation. Morphological investigations identified various topographies formed by the incorporation of TiO_2 nanoparticles with different chemistry. Transport properties of membranes were evaluated by two different dyes: positively-charged Crystal Violet (CV) (408 Da) and neutral Bromothymol Blue (BTB) (624 Da). Performance results reveal that high rejection was achieved by the TFN membrane fabricated by TCl-modified TiO_2 with BTB and CV rejection of 90 and 93%, respectively. These satisfactory rejection data for both charged and uncharged dyes can be attributed to formation of a dense structure after exposing the chlorinated TiO_2 nanoparticles into interfacial polymerization reaction on membrane surfaces.

List of Publications during the postgraduate study in Curtin

1. **Babak Rajaeian**, A. Rahimpour, Moses Tade, Shaomin Liu, Fabrication and Characterization of Polyamide Thin Film Nanocomposite (TFN) Nanofiltration Membrane Impregnated with TiO₂ nanoparticles, *Desalination, Desalination*, 313, (2013) 176-188.
2. **Babak Rajaeian**, Moses Tade, Shaomin Liu, Synthesis, Characterization, and Antifouling Properties of TiO₂-PVA Thin Film Nanocomposite (TFN) Membranes, *Separation and Purification Technology*, under review.
3. **Babak Rajaeian**, Moses Tade, Shaomin Liu, The effects of functionalized TiO₂ nanoparticles on properties and performance of polyimide-based thin film composite membranes in non-aqueous media, in preparation.
4. A. Rahimpour, M. Jahanshahi, S. Khalili, A. Mollasosseini, A. Zirepour, **Babak Rajaeian**, Novel functionalized carbon nanotubes for improving the surface properties and performance of Polyethersulfone (PES) membrane, *Desalination* 286 (2012) 99–107

Acknowledgement

Although I like referring to this work as “my thesis”, it actually belongs to many people, thanks to whom I developed myself professionally and personally.

First and foremost, I would like to express my sincere gratitude to my supervisors, *Professor Shaomin Liu* and *Professor Moses O Tade* for their patience, supports and trust on my abilities which was steering me through this gruelling journey.

I gratefully acknowledge the Centre for Material Research (CMR) at Curtin University and especially PhD candidate *Mr. Kun Zhang* for assistance with SEM and EDX imaging characterizations and also special thanks to *Dr. Thomas Becker* for his help in AFM and water contact angle analyses. I would like to acknowledge *Ms. Karen Haynes*, *Mrs. Roshanak Doroushi* and *Mr. Jason Wright* for their assistance in laboratory equipment and instruction.

Of course this period would not have been the same without all the nice Post Graduate colleagues. Thanks guys, for building up a happy and harmonious environment for my study here, especially for the good “tea-time” shared moments. I would like to extend my heartfelt appreciation to my Persian fellows *Mansoor Hasani*, *Amirpiran Amiri* and *Amir Memar*, for unconditional helping me many times. I was proud being part of you.

Last but not the least, I would like to give plenty of loves to my parents and my sister for their endless support and motivation they used to provide despite being far away and never let me realize that they are living on the other side of the world.

Table of Contents

Abstract.....	ii
List of Publications during the postgraduate study in Curtin	iv
Acknowledgements	v
Table of contents	vi
List of Figures	ix
List of Tables	xii
Nomenclature	xiii
Chapter 1	1
Introduction	
Chapter 2	4
Literature Review	
2.1 Membrane basics	4
2.2 Membranes structure	4
2.2.1. Membranes structure based on porosity	4
2.2.2. Membrane structure based on symmetry	6
2.3 Phase inversion method for formation of support layer	9
2.4 Mechanism of formation of the thin selective barrier layer	11
2.4.1. Interfacial polymerization using monomers	11
2.4.2. Interfacial crosslinking using polymers	15
2.5 Thin film Nanocomposite (TFN) membranes	17
2.6 Scope of the Research	20
Chapter 3.....	21
Fabrication and Characterization of Polyamide Thin Film Nanocomposite (TFN)	
Nanofiltration Membrane Impregnated with TiO ₂ Nanoparticles	
3 Abstract.....	21
3.1 Introduction.....	22
3.2 Experimental Section	23

3.2.1 Materials and Chemicals.....	23
3.2.2 Carboxylation of TiO ₂ nanoparticles	24
3.2.3 Surface modification of TiO ₂ nanoparticles	26
3.2.4 Fabrication of Polyamide and Titania-Polyamide thin films	26
3.2.5 Membrane Characterization	27
3.2.6 Membrane performance test and the determination of pore size and effective thickness/porosity	28
3.3 Results and discussion	31
3.3.1 Characterization of modified TiO ₂ nanoparticles	31
3.3.2 TFC and TFN membranes characterizations by FTIR, SEM, AFM and hydrophilicity evaluation	35
3.3.3 Separation performance and membrane pore size determination	46
3.4 Conclusions.....	50
Chapter 4.....	51
Synthesis, Characterization, and Antifouling Properties of TiO ₂ -PVA Thin Film Nanocomposite (TFN) Membranes	
4 Abstract	51
4.1 Introduction.....	52
4.2 Experimental Section	54
4.2.1 Materials and Chemicals.....	54
4.2.2 Surface modification of TiO ₂ nanoparticles	54
4.2.3 Preparation of PVDF support membrane	55
4.2.4 Preparation of composite and nanocomposite membranes	56
4.2.5 Membrane characterization	56
4.2.6 Filtration performance and fouling analysis	57
4.3 Results and discussion	58
4.3.1 Characterization of Carboxylated of TiO ₂ nanoparticles	58
4.3.2 Composite and Nanocomposite membranes characterized by FTIR, SEM.	62

4.3.3 Membrane hydrophilicity, fouling resistance and performance evaluation	67
4.4 Conclusion	74
Chapter 5.....	75
The effects of functionalized TiO ₂ nanoparticles on properties and performance of polyimide-based thin film composite membranes in non-aqueous media	
5 Abstract	75
5.1 Introduction.....	76
5.2 Experimental Section	77
5.2.1 Materials and Chemicals.....	77
5.2.2 TiO ₂ functionalization procedure	78
5.2.3 Ultrafiltration Polyimide (PI) membranes preparation	78
5.2.4 Fabrication of TFC and TFN SRNF membranes	79
5.2.5 Characterization of SRNF membranes	80
5.3 Results and discussion	82
5.3.1 FTIR analysis.....	82
5.3.2 Membrane surface morphology.....	83
5.3.3 Membrane hydrophilicity and performance evaluation.....	89
5.4 Conclusion	93
Chapter 6.....	94
Conclusions and Recommendations	
6.1 Conclusions	94
6.2 Recommendations	95
References.....	97

List of Figures

- 2.1** Schematic illustration of three main structures [9]
- 2.2** Classification of membranes based on structural symmetry[1]
- 2.3** Microstructures of (a) macro-porous ceramic membrane[2] and (b) polyester fibres[3]
- 2.4** Layer by layer schematic of a composite structured membrane
- 2.5** Changes of the casting solution through the three-component phase diagram from the initial polymer casting solution (A) to the final membrane (D) [4]
- 2.6** The schematic illustration of the chemistry of the interfacial polymerization of phenylene diamine with trimesoyl chloride on a microporous polysulfone support[5]
- 2.7** Schematic *IP* reaction profile at time t [6]
- 2.8** Illustration of crosslinking reaction between polyvinyl alcohol and glutaraldehyde[7, 8]
- 2.9** Conceptual cross-section of a (A) thin film composite; (B) thin film nanocomposite containing zeolite molecular-sieve[9]
- 2.10** Schematic and SEM illustration of CNT-embedded have also formed a similar IP-based polyamide membrane[10]
- 2.11** Schematic diagram of the (A) TFC and (B) TFN membranes and the (C) mechanism for nanofiltration of water and ions[11]
- 3.1** Preparation of polyethersulfone (PES) composite support (The dotted red lines exhibit hydrogen bonding interactions between the sulfonic groups of PES and hydroxyl groups of alumina support
- 3.2** Schematic diagram of nanofiltration system. (I) Feed tank; (II) Thermal coil; (III) Pump; (IV) Thermometer; (V) Needle valve; (VI) Pressure gauges; (VII) Permeate; (VIII) Hollow fibre membrane house; (IX) Composite hollow fibre nanofiltration membrane; (X) By-pass; (XI) Concentrate
- 3.3** (a) Un-modified hydrophilic nanoparticles dispersed in organic solution, (b) AAPTS-modified low-hydrophilic TiO_2 nanoparticles in aqueous solution
- 3.4** (a) XRD patterns, (b) UV-vis diffuse reflectance absorption spectra and (c) ATR-FTIR spectra of pure and AAPTS-functionalized TiO_2 nanoparticles

3.5 Photographs of dispersion qualities of AAPTS-functionalized and pure TiO_2 nanoparticles scattered in the m-PDA aqueous and TMC organic solutions respectively after hours

3.6 Cross-sectional SEM images of ceramic-supported PES membrane (a) Polymer selective layer, (b) Ceramic-polymer whole view

3.7 ATR-FTIR spectra of TFC and TFN membranes

3.8 Thermal Gravimetric Analysis for TFC and TFN nanofiltration membranes

3.9 SEM top-view images of (a) PES composite support, TFC (b), P-TFN (c), A-TFN₁ (d), TFN₂ (e) and TFN₃ (f) membranes

3.10 SEM surface images and EDX analysis and low-magnification of 0.1 wt% pure TiO_2 thin-film nanocomposite nanofiltration (TFN) membrane

3.11 Schematics for dispersion quality of unmodified and AATPS-modified TiO_2 nanoparticles in TMC and m-PDA solutions respectively result in polyamide mixed matrix thin film nanocomposite. (The dotted red arrows indicate flow paths for water transport)

3.12 Three dimensional AFM images for PES composite support, TFC and TFN membranes

3.13 Proposed nucleophilic substitution reaction mechanism between AAPTS-functionalized TiO_2 nanoparticles and produced HCl during the polycondensation process

3.14 (a) Flux and (b) salty organic solution rejection behaviours of TFC and TFN nanofiltration membranes. (Average of three replicates was reported)

4.1 A depiction of the interactions between hydroxyl groups of PVA chains TiO_2 nanoparticles in raw and carboxylated forms

4.2 ATR-FTIR spectra of pure and carboxylated TiO_2 nanoparticles

4.3 TEM observations of (a) raw and (b) carboxylated TiO_2 nanoparticles dispersed in deionized water followed by 10 min ultrasonication

4.4 ATR-FTIR spectra of all prepared membranes.

4.5 Cross-sectional SEM images of the cross-section of the M-1 (a, b and d) and M-2 (c) membranes, in different magnifications were 500 \times (a); 1000 \times (b); 3000 \times (c) and 5000 \times (d)

4.6 SEM surface images of composites and nanocomposites membranes: (A) M-1, (B) M-2, (C) M-2 (Supported by unmodified PVDF), (D) M-3, (E) M-4 and (F) M-5.

- 4.7** EDX-mapping analyses of composites and nanocomposites membranes: (a) M-3, (b) M-4 and (c) M-5
- 4.8** Effect of applied pressure on pure water flux values of developed membranes
- 4.9** Rejection data for the composite and nanocomposite membranes
- 4.10** Three steps Flux versus Time for the developed membranes at 400 KPa: pure water flux for 90 min, BSA solution flux for 90 min, and pure water flux of cleaned membranes for 90 min
- 4.11** Pure water flux recovery after filtration of BSA solutions
- 4.12** Fouling resistance ratios of all prepared membranes
- 5.1** ATR-FTIR spectra of aminated TiO₂ nanoparticles
- 5.2** SEM images of the cross-section of the TFC SRNF membrane, in different magnifications were 1000× (top); 5000× (middle) and 20000× (bottom).
- 5.3** Surface SEM images of the TFC and TFN SRNF membranes
- 5.4** EDX-mapping analyses of nanocomposite SRNF membranes and schematic settlements of (A) physical, (B) chemical functionalization of TiO₂ nanoparticles by TETA
- 5.5** Three dimensional AFM images for the TFC and TFN SRNF membranes
- 5.6** Fluxes of pure solvent (methanol) and two employed dye-solutes for composite and nanocomposite SRNF membranes
- 5.7** Dye-solute rejection behaviours of the TFC and TFN SRNF membranes

List of Tables

- 2.1 phenomenological equations[12]
- 3.1 Surface roughness parameters and water contact angles of PES composite support and TFC and TFN nanofiltration membranes
- 3.2 Structural and transport properties of TFC and TFN nanofiltration membranes
- 4.1 Summary of the membranes' recipe
- 4.2 The free energy of interaction between the surface and water droplet ($-\Delta G_{SL}$) calculated from water contact angle (θ)
- 4.3 Review of water flux recovery ratio (FRR) in nanocomposite membranes
- 5.1 Fabrication recipes of the TFC and TFN SRNF membranes
- 5.2 Molecular structures and physical properties of Dye-Solutes in this study
- 5.3 Surface roughness parameters of the TFC and TFN SRNF membranes
- 5.4 Water contact angle measurements for the TFC and TFN SRNF membranes

Nomenclatures

A_0	constant defined in Eq. (2.7) ($\text{m}^5/\text{kmol s}$)
B_0	constant defined in Eq. (2.8) ($\text{m}^6/\text{kmol s}$)
C_0	constant defined in Eq. (2.9) ($\text{m}^7/\text{kmol s}$)
$C(r, t)$	concentration of monomer A in the thin film at position r and time t , as shown in Figure 7.2 (kmol/m^3)
C_b	concentration of monomer B in the organic phase, as shown in Figure 7.2 (kmol/m^3)
$C_I(r, t)$	concentration of monomer A in the support-membrane phase at time t , as shown in Fig. 1 (kmol/m^3)
D	diffusion coefficient of monomer A in the thin film (m^2/s)
D_0	constant defined in Eq. (2.10) ($\text{m}^8/\text{kmol s}$)
D_M	constant defined as $D_M = D_M U \rho P$ ($\text{m}^5/\text{kmol s}$)
E_0	constant defined in Eq. (2.11) ($\text{m}^9/\text{kmol s}^2$)
k	apparent reaction rate constant defined as $k = k_r \delta$ ($\text{m}^4/\text{kmol s}$)
k_I	constant defined as $k_I = k_r \delta / \rho P$ ($\text{m}^7/\text{kmol}^2 \text{s}$)
k_r	second-order reaction rate constant ($\text{m}^3/\text{kmol s}$)
K	partition coefficient of monomer A between the support-membrane phase and the thin-film phase (dimensionless)
L	length of the support membrane, as shown in Figure 7.2 (m)
M_i	molecular weight of component i (kg/kmol)
P	average degree of polymerization (dimensionless)
r	radial coordinate normal to the surface of a cylindrical membrane, as shown in Figure 7.2 (m)
S	membrane area (m^2)
t	polymerization time (s)
X	thickness of the thin film (m)
δ	thickness of the reaction zone, as shown in Figure 7.2 (m)
A_k	effective porosity of the membranes
$D_{i,\infty}$	bulk diffusivity (m^2/s)
J_v	volume flux (based on membrane area) (m/s)

j_w	pure water flux (based on membrane area) (m/s)
$K_{i,c}$	hindrance factor for convection
$K_{i,d}$	hindrance factor for diffusion
Pe_m	Peclet number
ΔP	applied pressure
r_p	effective pore radius (m)
r_s	stokes radius of ions and solutes (m)
R_{real}	real rejection
Δx	effective membrane to thickness (m)
Φ	steric partition term
λ	ratio of ionic or solute radius/pore radius
η	dynamic viscosity of solution (Pa s)

Chapter 1 Introduction

Nowadays water demand has been increased dramatically with the development of urban life and industrialization. Global water scarcity has become one of the most challenging problems facing human beings with the advancement of civilization. Approximately half of the available water sources are used for industrial and agricultural activities and the other part is used for domestic purposes [13-15]. Moreover, water shortage is becoming worse day by day as the existing usable water resources are continuously suffering from contaminants of industrial wastes or discharges. Serious water shortage speeds up the necessity of using seawater or brackish groundwater, river water for a public potable water supply.

As a chemical engineering-related solution, desalination is a process which is employed to provide purified water to a drinking quality by removing salt and particulates from these naturally undrinkable-water resources. Currently, three desalination technologies are employed to separate extra salt from water. The first one is to use thermal method to change the water phase (to vapour or solid), followed by physically separating the new phase from the remaining salt solution, and recovering the thermal energy[16]. The second desalination method is based on chemical approaches which include ion exchange, liquid-liquid extraction, and gas hydrate or other precipitation methodologies[17, 18]. Finally, the third approach for desalination is the physical separation of components using a membrane in which the externally applied driving force for mass transfer is pressure gradient.

Recent works, targeting at efficient desalination processes [19-23], have demonstrated a remarkable low specific energy of seawater desalination in new membrane system which potentially proves membrane process effectiveness in water desalinating. Polymeric thin film composite (TFC) reverse osmosis (RO) is the most commercially successful membrane desalination technology which has overtaken conventional thermal and chemical approaches. Nowadays, nanofiltration (or "loose RO") membranes provide a valuable alternative to reverse osmosis, requiring a low operating pressure and energy cost. In addition to the ongoing research into conventional polymeric TFC nanofiltration (NF) membrane materials,

nanotechnology has offered synergistic approach by incorporating nanomaterials into their top-separating layer. This new generation called thin film nanocomposite (TFN) membranes have been targeted in this research to develop novel materials to attain optimized fabrication conditions.

This dissertation focuses on the fabrication and performance evaluation of thin film nanocomposite membranes including six chapters.

Chapter 1 summarizes the necessity of developing the present polymeric TFC membranes to TFN ones which was the starting point of this project.

Chapter 2 presents a background and literature review of the technological evolution of conventional thin film composite membranes followed by recent developments of advanced thin film nanocomposite membranes. As the composite membranes generally comprise of two layers supported by macro-porous substrate, the theoretical and modelling studies of each membrane layer was reviewed.

Chapter 3 proposes a novel method to incorporate surface-modified TiO₂ nanoparticles into polyamide layer of nanofiltration membranes supported by the polyethersulfone-coated porous aluminium oxide ceramic hollow fibres with high area/volume. This type of membrane provides nearly defect-free tailored semipermeable TFN barrier layer with improvement in water permeability and salt rejection efficiency.

Chapter 4 presents the investigation on fouling-resistant poly(vinyl alcohol) (PVA) nanocomposite selective layer on porous poly (vinylidene fluoride) (PVDF) support embedded by TiO₂ nanoparticles. To improve the interfacial adhesion of nanoparticles in PVA blend, an endothermic carboxylation reaction was employed to modify the TiO₂ surface.

Chapter 5 explores polyamide thin film nanocomposite solvent resistant nanofiltration membrane (SRNF) developed by conventional interfacial polymerization method on a porous polyimide support. Surface functionalization of TiO₂ nanoparticles again was employed to improve compatibilization of nanoparticles inside the polymer matrix. In this chapter, EDX-mapping analysis was

carried out to investigate the dispersion quality of modified TiO₂ nanoparticles throughout the hybrid polyamide thin films. Transport properties of membranes were evaluated by methanol solutions of two different positively-charged and uncharged dyes.

Chapter 6 gives the general conclusions refereeing to all the previous chapters. Concise recommendations for future works arising out of the studied materials and methods are also presented.

Chapter 2 Literature Review

2.1 Membrane basics

During the recent years, membranes have received increasing attention in separation industries and different fields of liquid and gas mixture purification such as: food[24], chemical[25], petrochemical [26, 27] pharmaceutical [28] industries, desalination plants[29], gas refining[30] and so on. A membrane is a permeable or semi-permeable phase which acts as a permselective barrier against passing or permeation of other components. Performance of a membrane is determined by two factors: permeability/selectivity and stability. Productivity or permeability of a membrane is defined as the amount of permeate divided by the membrane area, time, pressure difference and membrane thickness. Selectivity or separation factor which is normally used for gases mixtures and miscible liquids is the ratio of the concentration in permeate divided by that in the feed for two components[31]. For example, oxygen purification in the field of air separation, O_2/N_2 selectivity is the capability of membrane to separate oxygen from nitrogen. Rejection is also defined as a percentage of the component which does not pass through the membrane.

2.2. Membranes structure

Based on materials and the methods for membranes fabrication, various structures appear. In literatures, different models and names are used to categorize membranes structure such as porous or non-porous membranes, symmetrical or asymmetrical membranes and so on. More detailed structure classification has been described as follows.

2.2.1. Membranes structure based on porosity

Various materials can be used for membranes fabrication. Different techniques can also be used to transform the material into the membrane. Depending on the type of material and required structure, fabrication method is selected. Based on separation principles, three basic classifications are considered:

1. Porous membrane
2. Non-porous membrane
3. Carrier membrane

It should be noted that the above classification does not contain all membrane structures. For example, Reverse Osmosis (RO) and Nanofiltration (NF) membranes have purgatorial state between porous and non-porous categories. Figure 2.1 depicts these three structures.

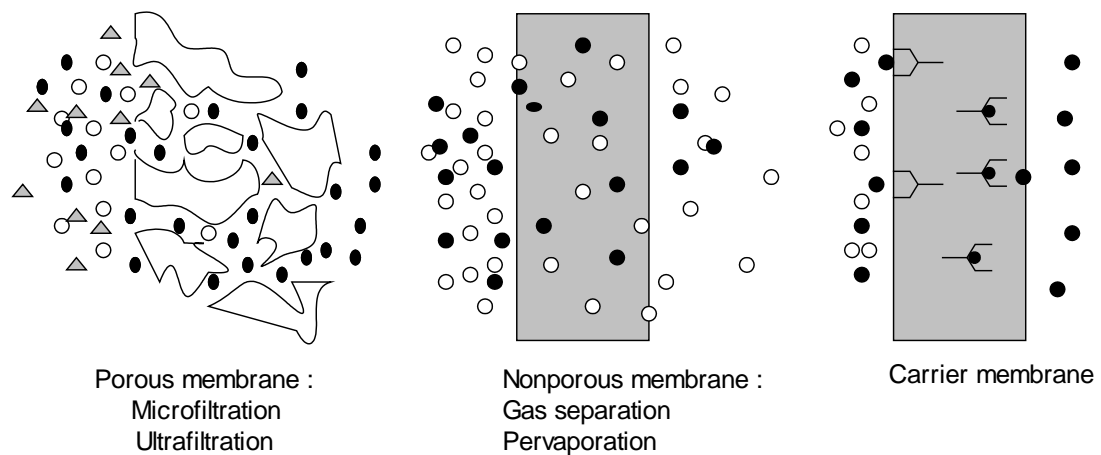


Figure 2.3 Schematic illustration of three main structures [9]

Basically, porous or non-porous structures are mostly related to polymeric membranes[32]. The size of the holes in the porous membranes is one of the most important factors to determine their separation efficiency. Ultrafiltration (UF) and microfiltration (MF) membranes are mostly fallen into this category. Obviously, when the size of the particles in solution is significantly different with the membrane pores, high selectivity will be expected as only smaller particles allowed to pass through. Therefore, it is clear that this type of membrane separation is a function of particle size, pore size and pore size distribution of the membrane[33]. Non-porous membranes have the ability to separate the gases or vapours. In fact, difference in solubility or diffusion of components in the bulk polymer is the main factor to separate components of a mixture in non-porous membranes. Non-porous or dense membranes are composed of a dense layer and the separation is driven by the pressure, concentration, and temperature or voltage difference. Proportionality between flux and driving force can be written as[12]

$$J = A \frac{dX}{dx} \quad (2.1)$$

where A is phenomenological coefficient and dX/dx is the driving force expressed as the gradient of the X (pressure, concentration, temperature and voltage difference) along a coordinate x perpendicular to the transport barrier. A list of phenomenological coefficients is shown in Table 2.1.

Table 2.1 phenomenological equations[12]

Mass flux	$J_m = -D \frac{dc}{dx}$	✓ (Fick law)
Volume flux	$J_v = -L_p \frac{dp}{dx}$	✓ (Darcy law)
Heat flux	$J_h = -\lambda \frac{dT}{dx}$	(Fourier law)
Momentum flux	$J_n = -\nu \frac{dv}{dx}$	(Newton law)
Electrical flux	$J_i = -\frac{I}{R} \frac{dE}{dx}$	(Ohm law)

The Pore-flow model based on Darcy's Law is used to explain the pressure-driven convection of flow through these micro and nano porous membranes, while the solution-diffusion model based on Fick's Law is applied to explain non-porous and dense membranes. The last category is carrier membranes. The membrane performance is somewhat similar to cell membranes[12]. As an example, liquid membranes are mostly fall into this category. In this group of membranes, the separation is performed via a specific carrier agent. The carrier agent reacts with one permeating component on the feed side of the membrane and then diffuses across the membrane to release the permeate on the product side of the membrane[34]. The type of the carrier molecule determines the selectivity of the membrane based on the components into the feed solution. Obviously, the high level of selectivity can be achieved by choosing an appropriate carrier agent.

2.2.2. Membrane structure based on symmetry

The above classification was based on the presence or absence of pores, and the membranes were divided into three general categories. However, membranes can also be classified based on symmetry or lack of symmetry in their structure. Therefore, two following categories have mostly been considered:

1. Symmetrical membrane
2. Asymmetric or anisotropic membrane

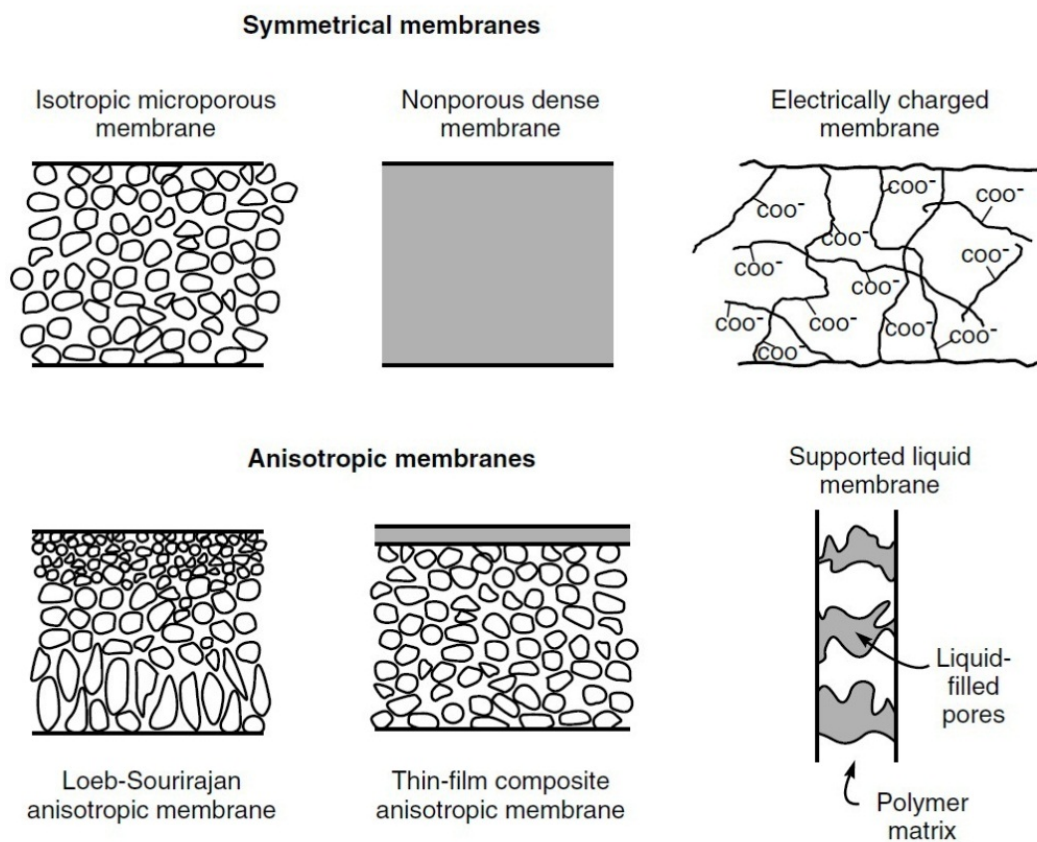


Figure 4.2 Classification of membranes based on structural symmetry[1]

Although this classification is mostly used for polymeric membranes, the ceramic and metal membranes can also be fallen into symmetric or asymmetric structure categorization. This thesis deals with thin-film composite anisotropic membranes. Composite membranes generally consist of two different layers. One of them acts as a substrate or support and the other one function as a high selective skin layer which is mostly coated on the substrate. Sometimes an additional layer in the lowest part of

the polymeric membrane is used to amplify the mechanical resistance against a variety of stresses exerted on the membrane. This layer is normally made of polyester fibres with high porosity. Hence, ceramic microfiltration membranes can also be used as the lowest part of composite membranes when high operational resistance is needed[35]. SEM pictures of both mentioned substrates are shown in Figure 2.3.

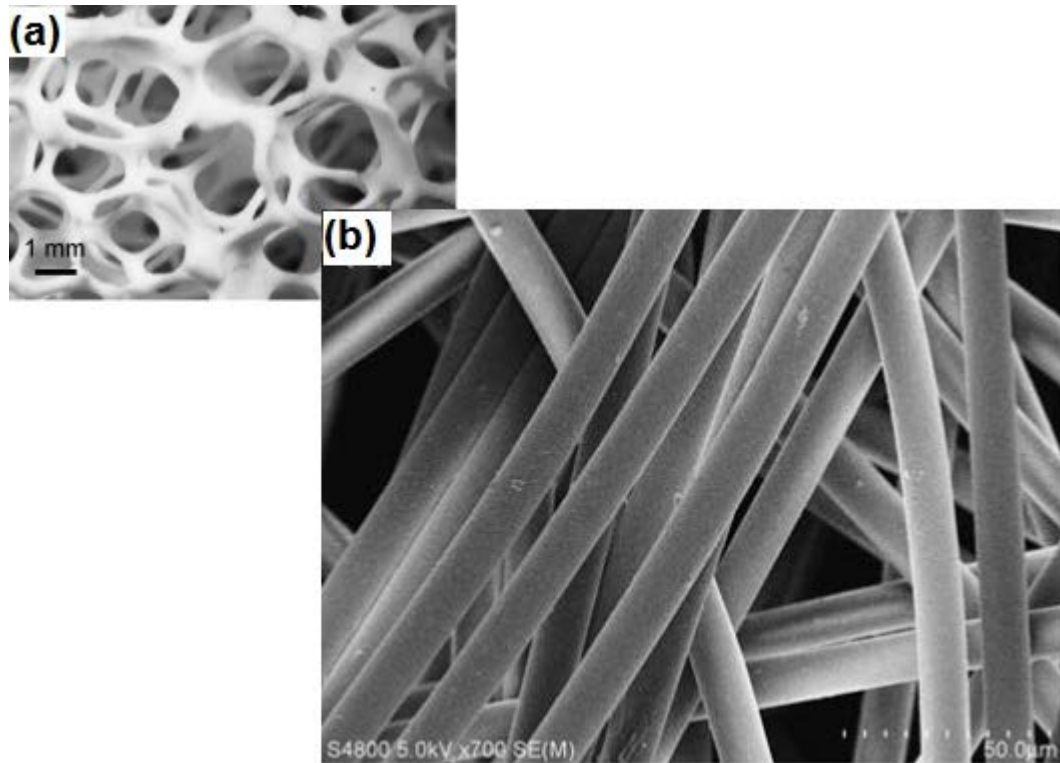


Figure 2.3 Microstructures of (a) macro-porous ceramic membrane[2] and (b) polyester fibres[3]

Figure 2.4 depicts a schematic of a composite structured membrane that consists of dense top layer, a porous support layer and a layer of polyester as substrate. A layer that is used as a porous support has general asymmetric structure which is mostly prepared by phase inversion method. This method is very versatile to achieve both porous and dense structured membranes which is described in the following section[12].

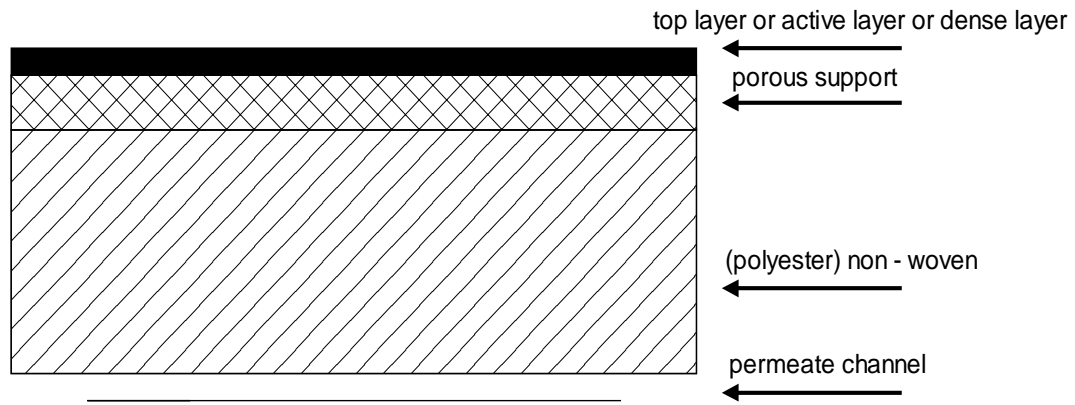


Figure 2.4 Layer by layer schematic of a composite structured membrane

2.3. Phase inversion method for formation of support layer

Phase inversion is a physical transformation of a polymer solution to form a solid polymer through a controlled process. Phase inversion process is also called ‘solidification’ where the initial polymer solution is coagulated as a solid phase due to the removal of the solvent from the casting solution. Similarly, during all phase inversion processes, a one-phase polymeric solution which is thermodynamically stable is transformed into two distinct phases under a certain condition. This transformation is called ‘demixing’. Over the demixing process, the system is separated into two phases; a polymer-rich solid phase and polymer-poor liquid phase. The membrane structure can be varied by controlling the factors influencing the phase inversion process[12]. Due to multiplicity of controllable parameters in phase inversion in comparison with the other fabrication methods of polymeric membranes, the optimum properties can be attained based on experiments as well as mathematical models [36]. This method, known as polymer precipitation or phase separation, can be applied by different techniques such as precipitation by solvent evaporation, precipitation by controlled evaporation, precipitation from the vapour phase, thermal precipitation and immersion precipitation[12]. However, most of the membranes attained by phase inversion method are fabricated by immersion precipitation technique. The more accurate thermodynamic studies of the phase inversion method are also concisely investigated. All of the transformations of polymeric solution from initial formation to end of solidification are demonstrated by a curve in the phase diagram (Figure 2.5)

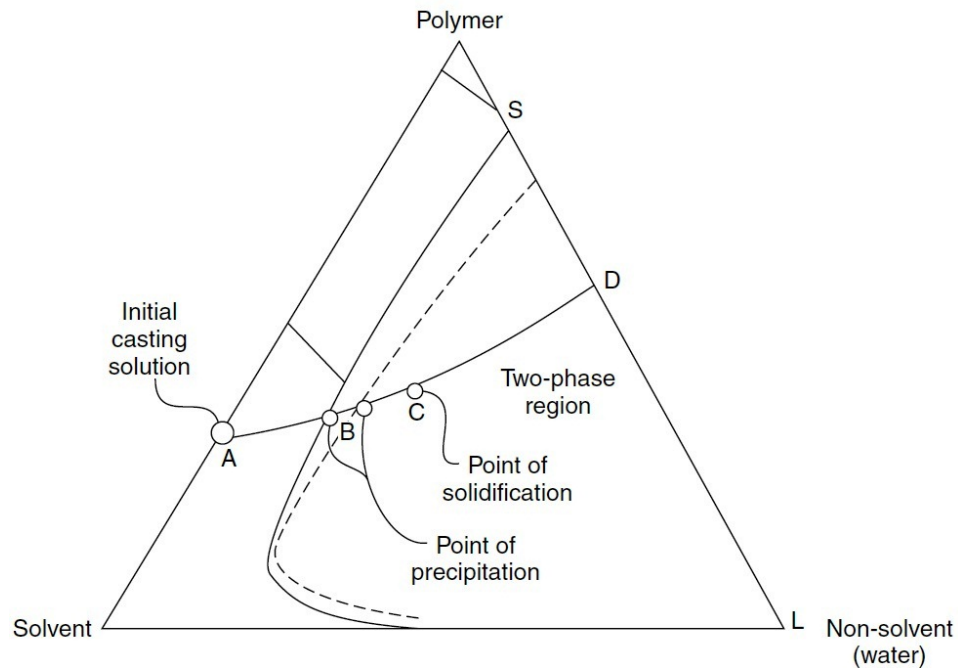


Figure 2.5 Changes of the casting solution through the three-component phase diagram from the initial polymer casting solution (A) to the final membrane (D) [4]

As it is clearly shown, the composition of polymeric solution is changing from stage A to D. In fact, point A corresponds to initial polymer casting solution while D stands for final membrane. Similarly, point S illustrates a rich solid polymer membrane comprises the membrane effigy and point L shows polymer-poor liquid phase appeared in membrane pores and void structure. Hence, the composition of each point in each phase, three lines can be drawn parallel to the three sides of triangle. Three sides of triangle are divided into ten equal parts. Then, the composition of each point is computed by counting the plotted interval against each vertex of triangle. The position of D on the S-L line determines the porosity of membrane. The total precipitation process passes through A-D pathway where the displacement of solvent and non-solvent took place. Point B indicates the direction in which the polymer precipitation begins. Along with beginning the precipitation of polymer solution in coagulation bath, the more solvent is removed from polymer solution and non-solvent or water replaces instead. As precipitation proceeds, more solvent is removed and precipitant is impregnated by the polymer-rich phase, so the viscosity rises[4]. Finally, the polymer reaches the highest possible viscosity (point C) which can be assumed as a solid. The top active layer acts as a thin selective

barrier skin which allows some particles and solutes pass through but not others. Several methods are applicable for coating the active layer on the porous intermediate layer including interfacial polymerisation[37] in-situ polymerisation[38] dip coating[39] and plasma polymerisation[40]. Except for dip coating, the other techniques involve polymerization, which generates new polymers in a very thin layer. During the fabrication of a composite membrane, the major challenge is how to form a thin, defect free and homogeneous high selective and high flux polymer layer onto the porous substrate. For instance, interfacial polycondensation is known as an interesting method for direct synthesis of polymer film which allows the simultaneous polymerization and formation of the high selective membrane with controllable morphology and properties by the reaction mechanism[41]. Moreover, dip coating has also gained high popularity mostly because of its easy operation for both hollow fibre and flat sheet substrates. Therefore, in this project, interfacial polymerization and dip coating methods are employed for formation of thin selective layer.

2.4. Mechanism of formation of the thin selective barrier layer

2.4.1. Interfacial polymerization using monomers

Linking up of the single monomers to build up a long chain is called polymerization. Interfacial polymerization is an alternative for high temperature bulk polymerization of condensation polymers. In this method, two immiscible solvents are used. Reaction occurs between monomers of two phases. The chemical equation and conceptual stoichiometry of this reaction in formation of interfacial polyamide Thin Film Composite membrane is shown in Figure 2.6.

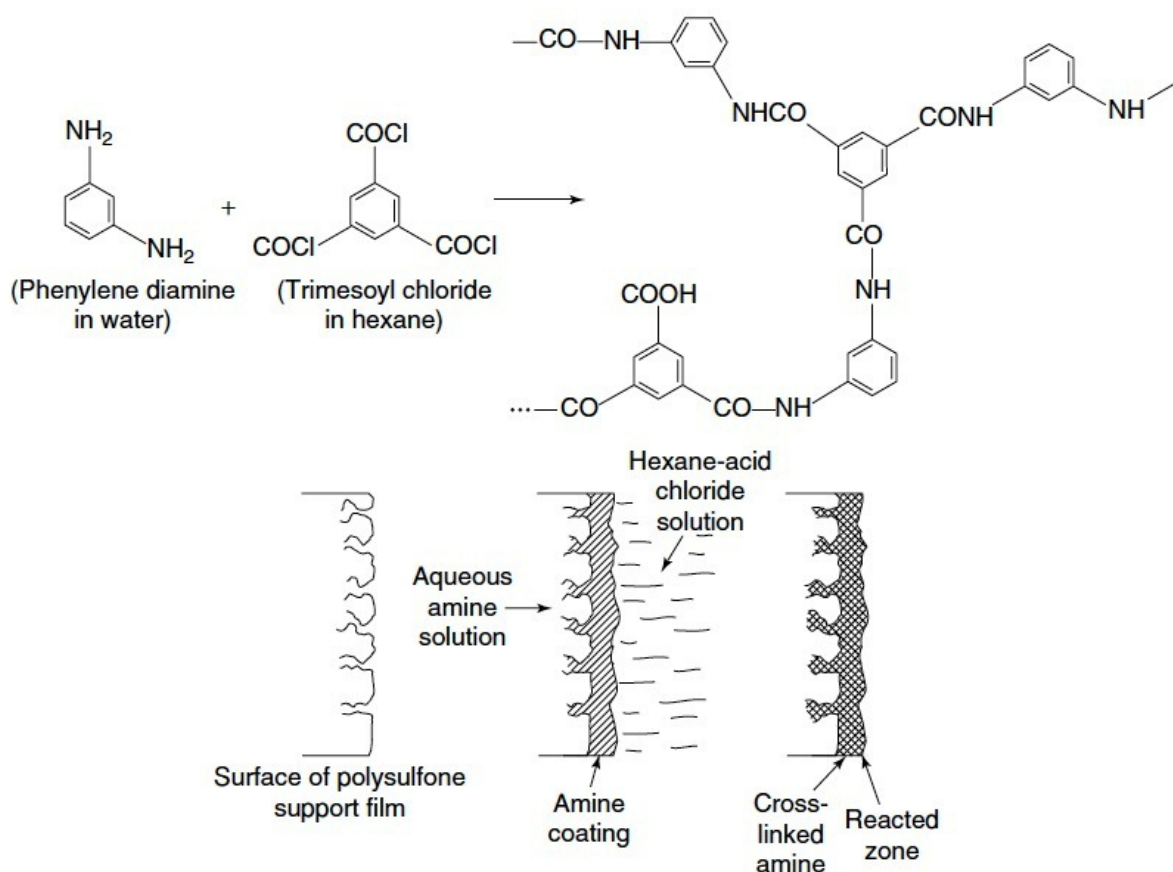


Figure 2.6 The schematic illustration of the interfacial polymerization of phenylene diamine with trimesoyl chloride on a microporous polysulfone support[5]

In this type of reactions, 1,3-phenylenediamine, as bifunctional amine monomer, reacts with trimesoyl chloride as trifunctional acyl halide monomer at the interface of the organic and aqueous phases. However, polymerization occurs predominantly in the organic phase due to the relatively low solubility of most acid chloride in water. Therefore, it is common to use a large excess of amine over acid chloride, which drives partitioning and diffusion of the amine into the organic phase. The general mathematical model based on reaction as well as diffusion under non-steady state boundary conditions was firstly developed by Ji et al. [6]. They assumed the formation of distinct uniform reaction zone while concentration profile of amine solution was linear across the newly formed film. The degree of polymerization reaction was constant with second-order kinetics. This profile is schematically shown in Figure 2.7.

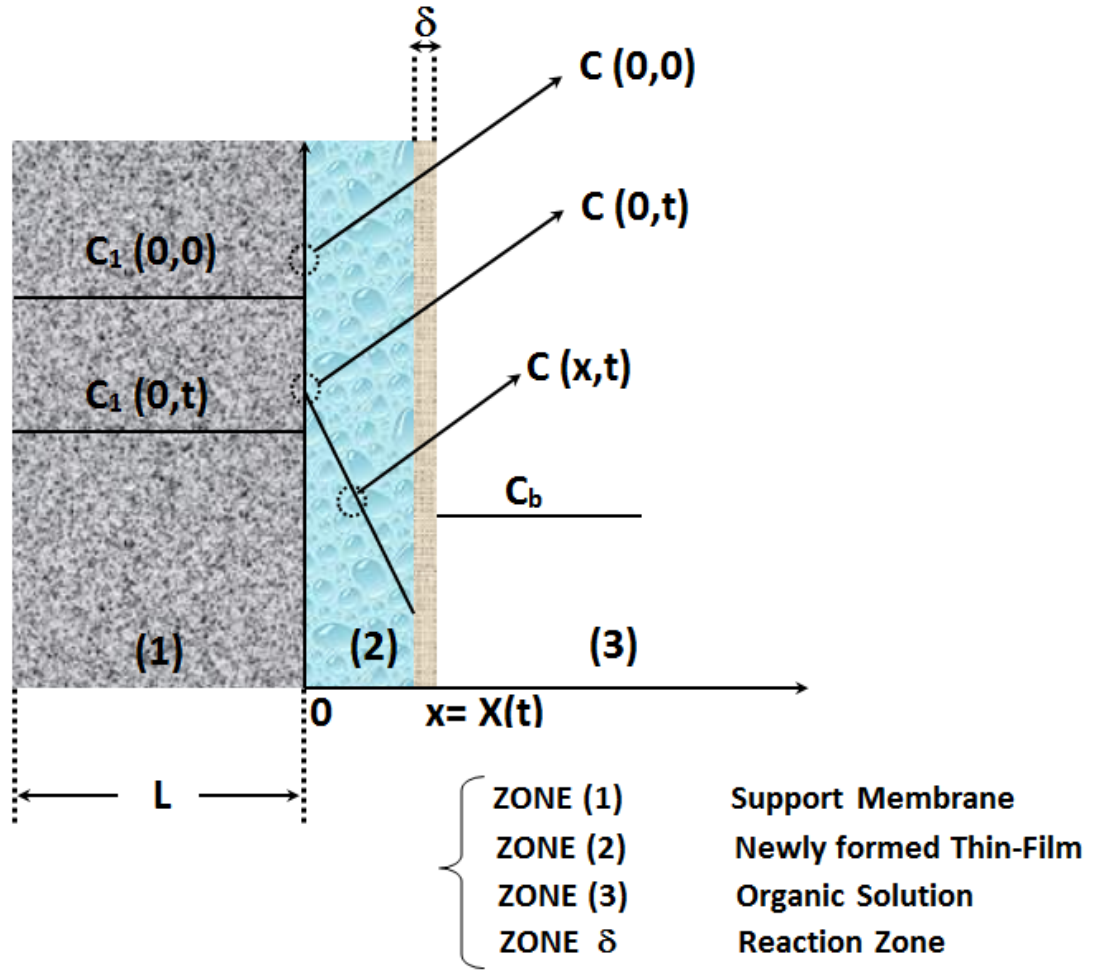


Figure 2.7 Schematic of *IP* reaction profile at time t (Adopted from [6])

The reaction rate is proportional to the concentrations of both monomers. Thin film growth versus time can be predicted based on mass balance at interface with consideration of reaction and diffusion rates. With respect to time, according to second-order interfacial polymerization reaction and the amine monomer diffusion to the reaction zone can be as follows

$$\frac{dX}{dt} = \frac{1}{\phi_p} k_I C(X,t) C_b \quad (2.1)$$

$$\frac{dX}{dt} = \frac{D_M [C(0,t) - C(X,t)]}{X \phi_p^2} \quad (2.2)$$

$$\phi_p = \frac{M_U \rho_w}{M_U \rho_w + M_w \rho_p \beta} \quad (2.3)$$

where dX/dt is the growth rate of the thin-film thickness, $C(X,t)$ is the concentration of amine monomer in the reaction zone at time t , C_b is the concentration of acid halide monomer in the organic phase, δ is the reaction zone thickness, β is the molar ratio of water to amine monomer transported (J_{water}/J_{amine}) and D_M is defined as $D_P M_U / \rho_P$. Assuming that diamine aqueous monomer diffuses constantly from the saturated support-membrane to the reaction zone, a material balance on the fraction of the amine monomer on the membrane surface can be used to obtain its un-steady-state concentration, $C(0,t)$

$$\underbrace{\frac{C(0,t)fLS}{K}}_{\text{Zone (1)}} + \underbrace{\int_0^x C(x,t)Sdx}_{\text{Zone (2)}} + \underbrace{\frac{2\phi_P XS\rho_P P}{M_P}}_{\text{Zone } \delta} = \underbrace{\frac{C(0,0)fLS}{K}}_{\text{Initial}} \quad (2.4)$$

where S is membrane area. In fact, amine monomers along with reaction with acyl halide monomers in organic phases, they can also act as an acid acceptor by neutralizing hydrogen chloride produced during amide formation. Therefore, Ji and co-workers assumed two molecules of amine are consumed for each molecule of acyl halide. Thus, Eq 4 can be integrated as follows

$$\int_0^x C(x,t)Sdx = \frac{XS[C(0,t) + C(X,t)]}{2} \quad (2.5)$$

Substitution of Eqs 2.1, 2.4 and 2.5 into Eq 2.2 followed by mathematical rearrangement based on film growth (dX/dt) gives

$$C(X,t) = \frac{\phi_P}{k_I C_b} \frac{A_0 - B_0 X}{C_0 X^2 + D_0 X + E_0} \quad (2.6)$$

where A_0 , B_0 , C_0 , D_0 and E_0 are constant parameters as defined in (2.7) - (2.11) equations.

$$A_0 = \frac{2D_M k_I C_b C(0,0)fL}{\phi_P^3} \quad (2.7)$$

$$B_0 = \frac{4KD_M k_I C_b \rho_P}{M_U \phi_P^2} \quad (2.8)$$

$$C_0 = \frac{Kk_I C_b}{\phi_P} \quad (2.9)$$

$$D_0 = \frac{2k_I C_b fL}{\phi_P} + \frac{2KD_M}{\phi_P^2} \quad (2.10)$$

$$E_0 = \frac{2D_M fL}{\phi_P^2} \quad (2.11)$$

Substitution of Eq 2.5 and 2.6 into mass balance Eq 2.4 results in

$$C(0,t) = \frac{1}{\frac{fL}{K} + \frac{X}{2}} \left[\frac{C(0,0)fL}{K} - \frac{2\phi_P X_{\rho_P}}{M_U} - \frac{C(X,t)}{2} X \right] \quad (2.12)$$

Finally, based on kinetic and diffusion equations (1 and 2), subject to boundary conditions of eqs 6 and 12, the correlation between time (t) and the film thickness (X) achieve as

$$t = - \left(\frac{E_0}{B_0} + \frac{A_0 D_0}{B_0^2} + \frac{C_0 A_0^2}{B_0^3} \right) \ln \left(1 - \frac{B_0 X}{A_0} \right) - \frac{C_0}{2B_0} X^2 - \left(\frac{D_0}{B_0} + \frac{C_0 A_0}{B_0^2} \right) X \quad (2.13)$$

The separation mechanism of thin-film nanofiltration membrane is influenced by both electrical (Donnan) and/or steric (sieving) size effects[42] which is described based on extended Nernst-Planck equation[43, 44] and extensively applied as Donnan/steric pore model by many researchers[45-50]. Therefore, this generation of membranes remarkably grown because of their unique ability to separate and fractionate polyvalent ions[51, 52], and relatively low-molecular weight organic species [53].

2.4.2. Interfacial crosslinking using polymers

Another mechanism for the formation of thin selective layer on the UF support is crosslinking reaction between a dense hydrophilic polymer and an aldehyde like poly vinyl alcohol (PVA) and glutaraldehyde (GA). Hence, this reaction is performed in presence of sulfuric acid as a catalyst. In fact, PVA is soluble to water after coating on the UF support. Therefore, it is not stable for separations of aqueous mixtures.

Chemical crosslinking of PVA using glutaraldehyde is a straightforward method to improve the mechanical and chemical integrity of PVA as well as its permeability [54, 55]. The schematic surface modification with examples of crosslinking reaction of PVA with GA are illustrated below

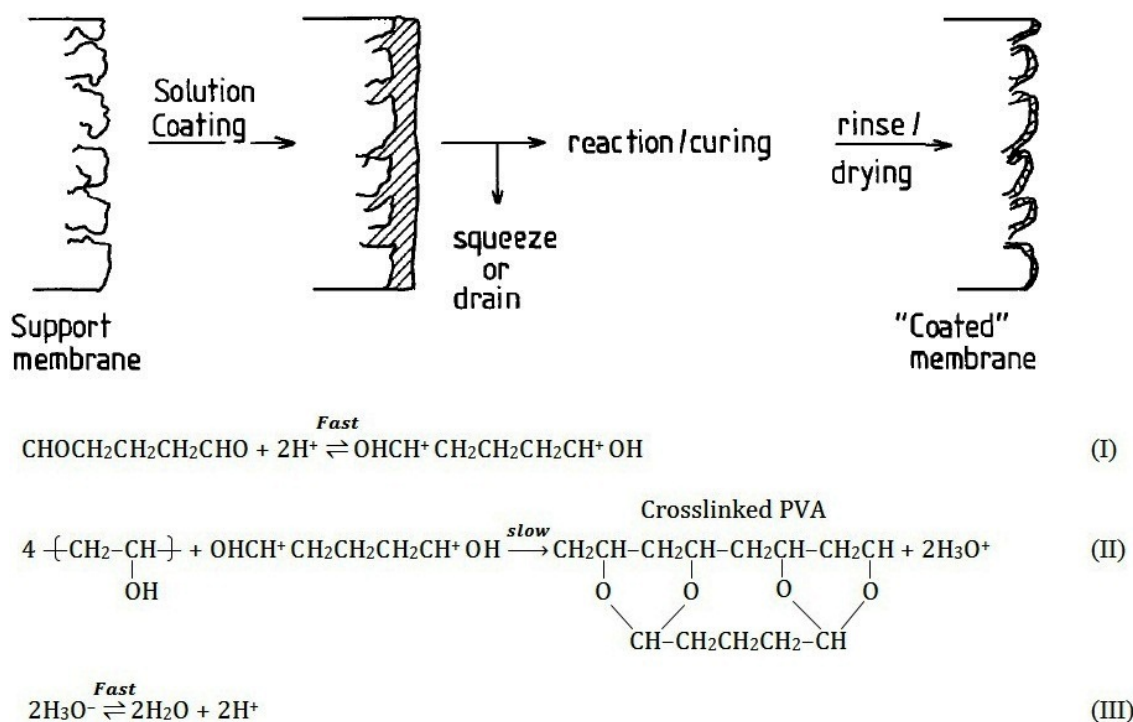


Figure 2.8 Illustration of crosslinking reaction between polyvinyl alcohol and glutaraldehyde[7, 8]

According to Kim et al.[7], the general reaction rate equation can be written based on Eq (II) as follows

$$-\frac{dG}{dt} = k H^\alpha G^\beta S^\gamma \quad (2.14)$$

where k is the overall rate constant, H is the hydroxyl group concentration of PVA polymer film, G and S are the concentrations of GA and Sulfuric acid, respectively. α , β and γ are the reaction orders with respect to the each reactant concentration. Kim and co-workers comprehensively investigated the effects of variation of these measurable variables based on results from correlation. The overall rate equation of crosslinking reaction was obtained as follows

$$-\frac{dG}{dt} = 7.78 \times 10^2 \exp\left(-\frac{2.90 \times 10^3}{T}\right) H^{0.95} G^{1.07} S^{1.15} \quad (2.15)$$

where T is the absolute temperature. Based on these fundamental results, many studies have been done in desalination application. Lang et al. explored the appropriate fabrication conditions for PVA-polysulfone based TFC membrane by aldehyde and dicarboxylic acid crosslinking agents [39]. Jegal and co-authors [56-58] studied another polysulfone-based TFC nanofiltration membrane by coating dilute poly (vinyl alcohol) (PVA) and sodium alginate (SA) blend solutions. They have succeeded to increase chemical stability of the TFC membranes in the wide range of pH from 1 to 13 without sacrificing the flux and rejection.

2.5. Thin Film Nanocomposite (TFN) membranes

Currently, polymers are still the main materials in membrane technology with the advantages of good film forming ability, flexibility and low cost. However, the limited chemical, mechanical and thermal resistance restricts the application of polymer materials. On the other hand, inorganic materials have higher thermal and chemical resistance as well as a longer lifetime, but they are suffering the high cost and brittleness. Therefore, membranologists have decided to combine the good properties of organic and inorganic materials. They offered specific advantages for the preparation of nanofiltration membranes by introducing a new concept called “Thin Film Nanocomposite (TFN)”. Nanoparticles have been added inside the thin films of TFC membranes in order to take advantage of the good properties of the nanomaterials [59]. TFN technology demonstrates a breakthrough in the membrane design with improved separation performances, good thermal and chemical resistance and adaptability to harsh environments [60]. This new generation of thin-film nanocomposites was initiated by Jeong et al. [9] to improve the high water permeability and salt rejection. As shown in Figure 2.9, they incorporated the zeolite molecular-sieve into polyamide thin films by presenting nanoparticles in the isopar-TMC monomer solution during the preparation.

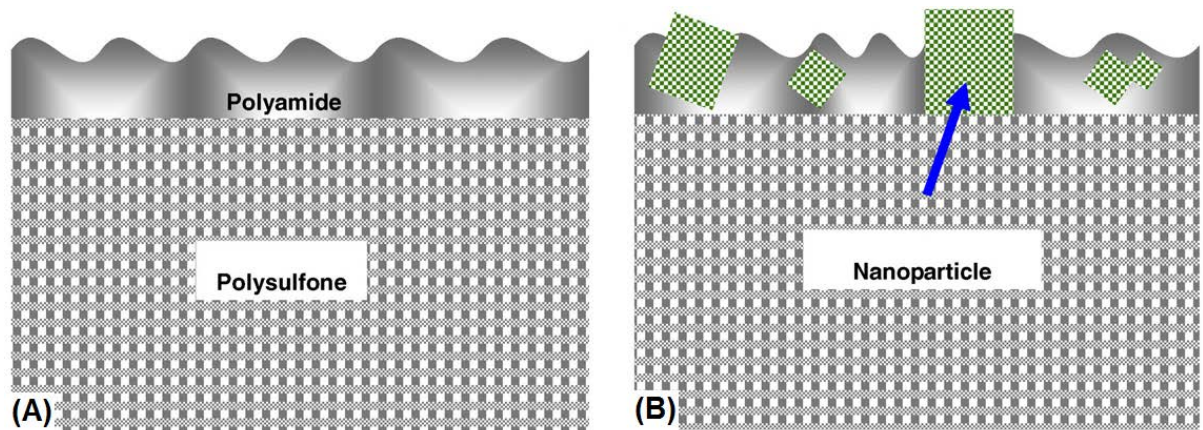


Figure 2.9 Conceptual cross-section of a (A) thin film composite; (B) thin film nanocomposite containing zeolite molecular-sieve[9]

Thereafter, thin-film nanocomposites have also been developed by other researchers. Lind et al. [60] employed silver-exchange zeolites to yield membranes with enhanced antimicrobial activities. However, encapsulation of synthesised nanocrystals within polyamide thin film imparted significant reduction in bactericidal properties. They investigated the combined influences of zeolite crystal size and polymerization chemistry on zeolite-polyamide thin film nanocomposite membranes and found that the better membrane permeability and higher solute rejection were achieved simultaneously by the addition of smaller zeolites [62]. Subsequently, Lind and co-workers tailored the zeolite-polyamide TFN RO membranes followed by different physical-chemical post-treatments[61]. In order to reduce the nanoparticle aggregation in organic monomer solution, zeolite hydration was carried out during the interfacial polymerization reaction. Furthermore, Fathizadeh et al. [62] proposed a polyamide thin film nanocomposite RO membrane by using self-made nanozeolite NaX to improve thermal stability, product flux and salt rejection efficiency. With respect to TFN membranes, some other researches have already been carried using different nanoparticles into polyamide layer. Lee et al. [63] structured a stable high-loaded TiO_2 polyamide TFN via in-situ interfacial polymerization. Immobilization of silver nanoparticles onto thin film composite membrane was also investigated to prepare nanofiltration membranes resistant to fouling and biofouling [64, 65]. The interest of TFN membranes was also brought by Roy et al. [10] to fabricate highly productive solvent-resistant nanofiltration membranes using both hydrophilized and hydrophobized Multi-Walled Carbon Nanotubes (MWCNTs).

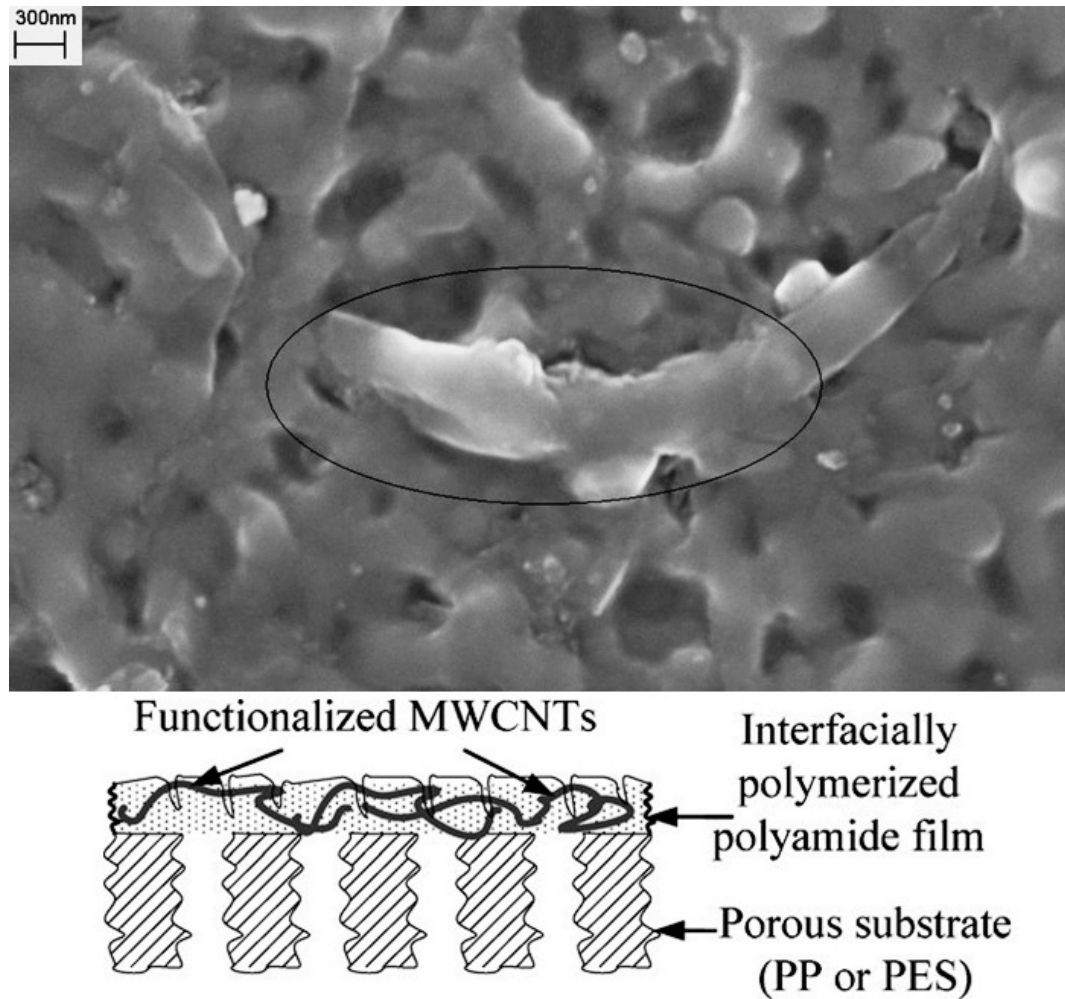


Figure 2.10 Schematic and SEM illustration of CNT-embedded polyamide membrane [10]

They concluded that the methodology of functionalization can effectively amend the poor matrix-particle compatibilization by decreasing the nanogap dimensions. Therefore, they could optimize the transport corridor between an individual MWCNT (nanogaps) and the surrounding polymer chains, resulting in low-resistance pathway for solvent and water transport. Interestingly, the efforts toward the nanocomposite coating have recently been continued for the formation of crosslinked PVA RO and NF membranes. Baroña et al. [11] successfully developed polysulfone-based PVA nanocomposite membrane for NF application. To reach their purpose, they firstly dispersed aluminosilicated single-walled nanotubes (SWNTs), into the PVA solution; subsequently, they employed aldehyde crosslinker solution to increase the stability of PVA-coated layer. Figure 2.11 illustrates an

imogolite acting as a negatively charged nanochannel which causes both steric hindrance and electrostatic repulsion to achieve high water flux ion rejection.

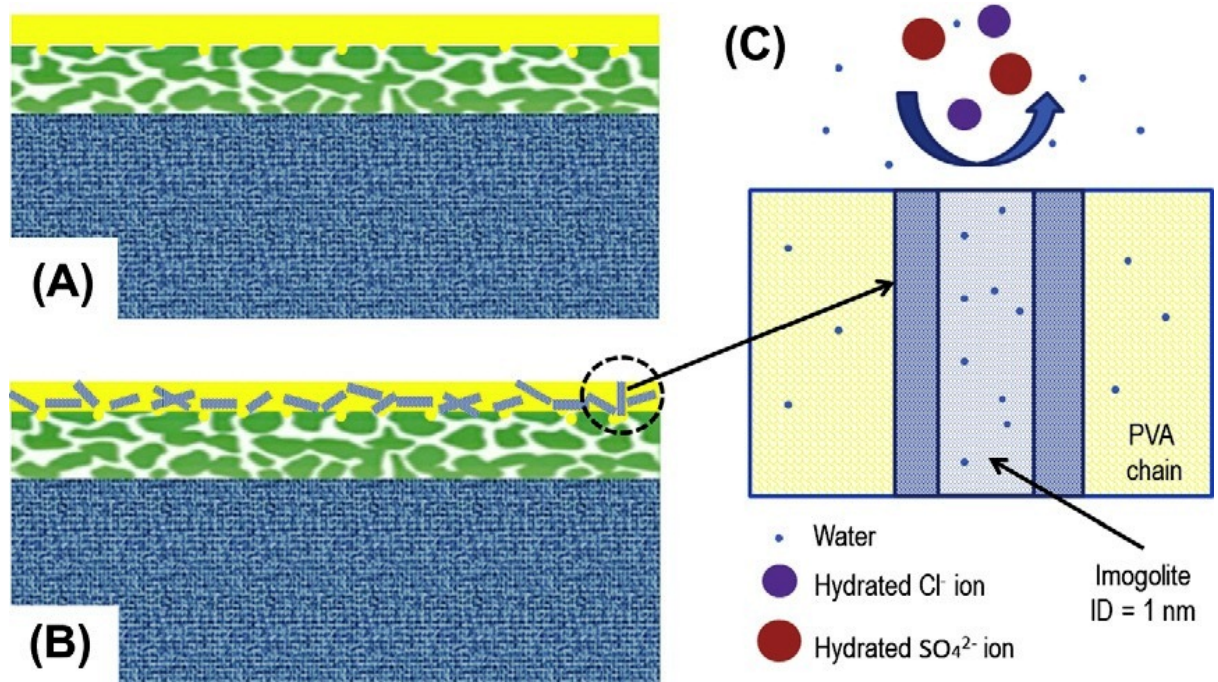


Figure 2.11 Schematic diagram of the (A) TFC and (B) TFN membranes and the (C) mechanism for nanofiltration of water and ions[11]

2.6 Scope of the Research

This brief literature survey provides a certain knowledge base and background to understand and achieve high-performance membranes applicable for aqueous and non-aqueous applications via TFN technique. The potential application of nanoparticles proposes a new basement for innovative methods either in concept and sustainability or operation. In this thesis, TiO₂ nanoparticles have been employed as an inorganic nanophase due to their high potentiality and widespread applications. We modify nanoparticles by covalently-bonded chemical groups on their surface prior to incorporate into polymer phase. We hypothesize that chemical functionalization not only stabilize TiO₂ nanoparticles into polymeric matrix, but also have the potential to improve selectivity and permeability.

Chapter 3 Fabrication and Characterization of Polyamide Thin Film Nanocomposite (TFN) Nanofiltration Membrane Impregnated with TiO₂ Nanoparticles

Abstract

A novel thin-film nanocomposite nanofiltration membrane has been developed via interfacial incorporation of aminosilanized TiO₂ nanoparticles. Polyethersulfone (PES) barrier coating on a porous α -Al₂O₃ ceramic hollow fibre membrane was employed as the substrate layer. TiO₂ nanoparticles were incorporated in pure and functionalized forms into trimesoyl chloride (TMC) organic phase and *m*-phenylenediamine (*m*-PDA) aqueous phase, respectively. The surface functionalization of TiO₂ nanoparticle was confirmed by XRD, FTIR and UV-vis reflectance spectral analysis. Surface properties of the fabricated composite membranes were investigated using SEM, EDX, AFM and contact angle goniometry. Heat resistibility of polyamide layers were examined using thermo-gravimetric analysis (TGA). Membranes intrinsic properties such as: the permeability, selectivity and pore size determination were also elucidated. The silane coupling agent containing amino-functional groups reinforced TiO₂ nano fillers for the good dispersion inside the polyamide skin layer by reducing their surface energy. At Ultra-low concentration (0.005 wt%) of functionalized TiO₂ nanoparticles improved the salt rejection to 54% as well as water flux to 12.3 l/m² h. By incorporating 10 times higher concentration of TiO₂ nanoparticles, water flux was increased approximately 2-fold compared with the pure polyamide membrane with negligible rejection loss. These results demonstrated competency of using functionalized inorganic nanoparticles to achieve the increment of product flux and the separation efficiency.

3.1 Introduction

Nanofiltration (NF) or "loose reverse osmosis (RO)" membranes have been recently developed with performance characteristics between reverse osmosis and ultrafiltration membranes. Lower operation cost, higher water flux and good rejection of salt or organic compounds with low molecular weights (200 to 500 g.mol⁻¹) are the most significant advantages of these new membranes compared to the traditional RO membranes[66-73]. NF membranes mostly fall into two categories namely: 1. asymmetric bulk structure containing a very thin, permselective dense skin layer supported on a more porous sublayer of the same polymer, commonly formed by a phase inversion process induced by immersion precipitation technique [74-78]; 2. thin-film composite structure with a thin polymer layer supported by one or more porous layers in different polymers. Interfacial polymerization (*IP*) is the most widely-used method to prepare thin-film composite NF membranes.

In this regard, interfacially cross-linked aromatic polyamide on a polyarylsulfone support layer has increasingly been recognized as one of the best processes for production of these membranes [79-82]. Efforts toward the improvement of conventional polyamide thin-film composite membranes are still going on and have dramatically been directed to a new concept called "thin film nanocomposite (TFN)" which demonstrates a breakthrough on how to synthesize and incorporate super-hydrophilic nanoparticles into the polyamide thin film[83]. This new generation of thin-films thereafter has been applied by many researchers to incorporate of zeolite nanoparticles into polyamide thin films through dispersing the nanoparticles in the isopar-TMC monomer solution [9, 60-62, 84]. High-loaded TiO₂ polyamide thin film nanocomposite membrane structured by Lee et al. using interfacial polymerization technique[63]. In case of antibacterial nanocomposite membranes some researchers immobilized silver nanoparticles into polyamide thin film [64, 65]. Since dispersion of hydrophilic nanoparticles in non-polar organic solvents is unstable, very small-sized silica nanoparticles have been dispersed into *m*-phenylenediamine (MPD) aqueous solution just before interfacial reaction by Jadav et al. [85]. In fact, large hydrophilic nanoparticles in water are difficult to be phase-transferred to nonpolar organic solvent[86], therefore properties of nanoparticles cannot be conferred to polyamide layer.

In all of these studies, nanoparticle agglomerations could not be avoided which severely impedes the TFN membrane to realize their potentials. Recently, the chemically surface modification of nanoparticles prior to use has attained special interest to overcome nanoparticle agglomerations drawback. For this purpose, utilizing a strategy based on the interaction or lack of interaction between the external surface of the nanoparticles and the resultant polymer matrix has been targeted in this study. In this approach, TiO₂ nanoparticles have initially been treated with an aminosilane coupling agent called “N-[3-(Trimethoxysilyl) propyl] ethylenediamine” (AAPTS). Then, different concentrations of modified nanoparticles were dispersed into the diamine aqueous solution prior to IP reaction. It is hypothesized that the Silanization treatment by AAPTS has dual effect on TiO₂ settlements into resultant polyamide matrix; firstly, minimizing the particle/particle interaction and consequent agglomeration accounts for reducing their surface energy; secondly, enabling inhomogeneous dispersion of nanoparticles throughout the polyamide matrix due to the presence of organic monolayer onto the TiO₂ surface. It is anticipated that the anchored-TiO₂ nanoparticles will provide tailored semipermeable TFN barrier layer with improvement in terms of permeability and selectivity.

3.2 Experimental Section

3.2.1 Materials and Chemicals

Commercially available aluminium oxide powder with particle diameter of 0.3 μm (gamma/alpha, surface area $15\text{m}^2\text{ g}^{-1}$) was used as hollow fibre support material. Polyethersulfone (PES) [Radel A-300, Solvay Advanced Polymers, USA], and 1-methyl-2-pyrrolidinone (NMP) (HPLC grade, Sigma-Aldrich) were used for preparing the polymer solution. Polyvinylpyrrolidone (PVP, K90) [GAF® ISP Technologies Inc., $M_w = 630,000$] was used as an additive. Isopropanol and methanol were supplied by Ajax Finechem Pty Ltd. All other chemicals including m-Phenylenediamine flakes, $\geq 99\%$, 1,3,5-Benzenetricarbonyl trichloride (TMC), Triethylamine (TEA), n-Hexan, Titanium (IV) oxide nanopowder (TiO₂ $\sim 21\text{ nm}$), N-[3-(Trimethoxysilyl)propyl]ethylenediamine (AAPTS) and Glucose were purchased from Sigma-Aldrich. Sodium Chloride (NaCl $\geq 98\%$) was purchased from

RHEOCHEM LTD, WA, Australia. Deionized water has been used throughout this study unless otherwise indicated.

3.2.2 Preparation of ceramic hollow fibre-supported PES ultrafiltration Membranes

The detailed procedure of the preparation of alumina hollow fibre supports was described previously [87-89]. The Al_2O_3 powder was added to a mixture of solvent (N-methyl-2-pyrrolidinone (NMP)) and binder of polyetherimide (PEI) in the ratio of 5:1:4 (w/w) to create the spinning dope. The mixture was constantly stirred for a period of 24 h to ensure a uniform mixture. The viscosity of the mixture was adjusted with <1%, w/w polyvinyl pyrrolidone. Distilled water and tap water were used normally as the internal and external coagulants, respectively. The dope mixture was extruded via a tube-in-orifice spinneret with Outside Diameter (OD) = 2.5 mm and Inside Diameter (ID) = 0.8 mm into thin hollow fibres which were gelled by immersion in tap water. Subsequently, the extruded Al_2O_3 hollow fibres were dried, cut in short lengths of 15 cm, and sintered at 1500 °C for 4 h with a ramping and cooling rate of 2 °C min⁻¹ in non-flowing air atmosphere to obtain the robust hollow fibre supports.

As schematically is shown in Figure 3.1, the prepared hollow fibre substrates were firstly cleaned in deionized water bath by ultrasonic cleaner several times to remove the loose particles on the surfaces. After this, the hollow fibre support was treated by boiling in hydrogen peroxide (30% (v/v)) for 15 min to further clean the surface as well as to introduce OH groups on the surface. Finally, the hollow fibre was thoroughly washed in deionized water for subsequent polymer coating.

Polyethersulfone (PES) solution was prepared by dissolving 20 wt% PES powder in 1-methyl-2-pyrrolidinone (NMP) and evacuated overnight to remove the gas-bubbles. Prior to the coating, the Al_2O_3 hollow fibre with both ends sealed by Teflon was soaked in NMP for 3 hours to displace air bubbles present in the fibre pores and restrict the penetration of polymer solution inside the porous structure during dip coating process [90]. Hollow fibre was immersed vertically inside the PES solution for 5 minutes and then transferred to non-solvent bath (the mixture of water (80% v)

and 2-propanol (20%)) for fast precipitation and finally soaked in deionized water 24 h to guarantee the complete phase separation. The immersion process was carried out at room temperature. Finally, membranes were placed between two sheets of filter papers for 24 hours at room temperature to facilitate the drying.

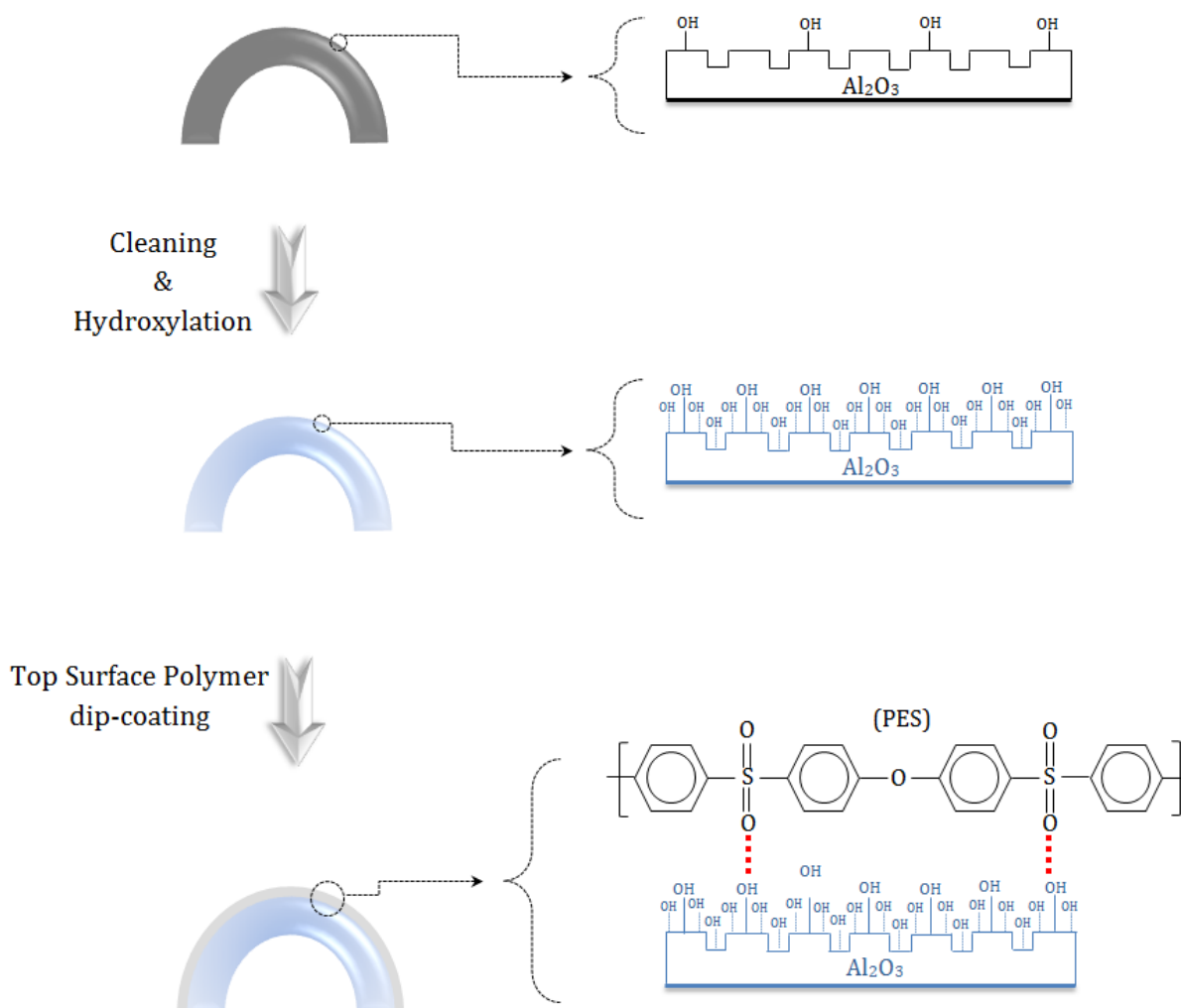


Figure 3.1 Preparation of polyethersulfone (PES) composite support (The dotted red lines exhibit hydrogen bonding interactions between the sulfonic groups of polyethersulfone and hydroxyl groups of alumina support.

3.2.3 Surface modification of TiO₂ nanoparticles

Chemical surface modification of TiO₂ nanoparticles was carried out by the reflux method. Briefly, two gram of dry TiO₂ was placed in 150 ml methanol and homogeneously dispersed at ambient temperature for 30 min in an ultrasonic mixer (UNISONICS PTY LTD, SYDNEY, AUSTRALIA). Thereafter, 40 ml APTS was added slowly to the resulting mixture stirring on a magnetic stirrer. After stirring for 3 h at 70 °C (above the boiling point of the methanol), the mixture was cooled and washed with pure methanol several times to separate TiO₂ nanoparticles and the unreacted coupling agent molecules. The final separation of TiO₂ particles from the solution was carried out in a centrifuge at 4000 rpm for 30 min. The resulting particles were then dried in an oven at 150 °C for 24 h to affect tethering of the physisorbed silane and to remove residual solvent and silane from the crude product. It should be noted that, it is extremely difficult to avoid accruing the self-condensation between aminosilane to form Si–O–Si silane-treated nanoparticles. The product was then grounded with a mortar and pestle. The presence of organic groups on the surface of modified nanoparticles was confirmed by FT-IR and UV-vis spectrums.

3.2.4 Fabrication of Polyamide and Titania-Polyamide thin films

Various thin film composite (TFC) and thin film nanocomposite (TFN) NF membranes were prepared with different compositions summarised in Table 3.1.

Table 3.1 Surface roughness parameters and water contact angles of PES composite support and TFC and TFN nanofiltration membranes

Membrane	Pure-TiO ₂ (wt%)	APTS-TiO ₂ (wt%)	Roughness (nm)			Contact angle (°)
			<i>RMS</i>	<i>R_a</i>	<i>R_{max}</i>	
Composite PES support	—	—	14.6	11.2	214	87.3
TFC	—	—	95	75	598	79
P-TFN	0.1	—	82.3	65.4	554	69.8
A-TFN ₁	—	0.005	98.8	79.2	650	75.8
A-TFN ₂	—	0.05	73.7	57.6	534	62.7
A-TFN ₃	—	0.1	72	56	518	59

For the preparation of pure polyamide composite membrane, the PES-coated hollow fibre membrane was vertically immersed in aqueous solution containing 1 wt% *m*-PDA for 2 min. A spherical hollow rubber was employed to drain off excess amine solution from the support surface. The saturated membrane was then immersed vertically inside 0.1 wt% TMC in *n*-hexane solution. After 30 s of interfacial reaction, the obtained membrane was cured at 70 °C for 5 min, washed thoroughly with deionized water to remove unreacted amine.

TiO₂ polyamide nanocomposites were synthesised using the same procedure as mentioned above, except that various amount of APTS-modified and just 0.1 wt% of unmodified TiO₂ nanoparticles were dispersed in *m*-PDA and TMC solution, respectively. In order to reach good dispersion of nanoparticles, ultrasonication bath was employed for 1 hour at ambient temperature immediately prior to the interfacial polymerization.

3.2.5 Membrane Characterization

In order to examine the surface wetting characteristics of different TFC and TFN NF membranes, water contact angle was measured using the contact angle detecting instrument [KSV Cam Optical Contact Angle and Pendant Drop Surface Tension Software Version 3.81, Finland]. De-ionized water was used as the probe liquid in all measurements. Functional identification of the prepared thin films and modified TiO₂ nanoparticles were demonstrated by using FTIR spectral analysis. All FTIR spectra were recorded by the attenuated total reflection (ATR) technique using Spectrum 100-FT-IR Spectrometer (Perkin-Elmer). Owing to the brittleness of ceramic hollow fibres under ATR crystal plate configuration, the thin polyamide film needed to peel off from composite support. For this purpose, all membranes were placed in NMP for 30 min to completely dissolve PES intermediate layer. Ceramic supports were then taken out and thin skin layers were collected and dried in the oven at 70 °C for 24 h to evaporate the residual NMP. Optical properties of pure and APTS modified TiO₂ nanoparticles were performed utilizing UV-vis reflectance spectra.

The UV–visible diffuse reflectance spectra (DRS) were recorded on a V-570 UV–visible spectrometer (Jasco, Japan) equipped with an integrating sphere. In this approach the same concentration of samples was prepared in which BaSO₄ was used as a reference material. The crystalline structure of raw and functionalized TiO₂ nano-powders was measured with using powder X-ray diffraction (XRD). The spectra were obtained on a D8-Advance X-ray diffractometer (Bruker, Germany) with Cu K α radiation ($\lambda = 1.5418 \text{ \AA}$), at 40 kV, 40 mA, in the interval $20^\circ \leq 2\theta \leq 80^\circ$. The thermal stability of polyamide films was investigated using Thermo-gravimetric analysis (TGA) in air on a Mettler-Toledo, STAR^e system. In each run, about 5 mg of each extracted polyamide samples was loaded into a pan and heated to 110 °C for 30 min and then heated up to 700 °C at a rate of 5 °C/min. The gas flow rate was maintained at 10 ml/min.

Morphologies of thin film composite and nanocomposite membranes were observed using scanning electron microscopy (SEM) (Zeiss EVO 40XVP). Pt sputtered coating was performed on the samples under vacuum before the morphological observation. The elemental composition of membrane surfaces were conducted using an EDS X-ray detector equipped by the scanning electron microscopy. Atomic force microscopy (Digital Instruments NanoScope IIIA) was used to measure the topography of the prepared membranes. The membrane surfaces were imaged in a scan size of 5 $\mu\text{m} \times 5 \mu\text{m}$ by contact mode operation in air. The surface roughness parameters of the membranes which are expressed in terms of the mean roughness (Ra), the root mean square of the Z data (RMS) and the maximum vertical distance between the highest and lowest data points within the cursor box (Rmax) were calculated from AFM images by NanoScope software 6.13 at scan areas of 5 $\mu\text{m} \times 5 \mu\text{m}$.

3.2.6 Membrane performance test and the determination of pore size and effective thickness/porosity

The nanofiltration experiments were conducted using self-assembled Water manifold system purchased from Swagelok, USA, is schematically depicted in Figure 3.2. The hydraulic diameter of the tubes and connector fittings were similarly 3/8 in to avoid pressure drop in flow channels. Based on [91] the concentration polarization can be

minimized under turbulent cross flow. In this approach, feed velocity was roughly fixed at 4m/s which give Reynolds Number equal to 38000 accounts for turbulent flow regime. Immediately after membrane preparation, one fibre with an effective area 8.5 cm^2 was sealed inside membrane module utilizing Epoxy resin. The membrane permeation or rejection properties were examined using pure water, aqueous solution containing small organic molecules (500 ppm Glucose) and salt (2000 ppm NaCl), respectively. All experiments were carried out at 110 Psi and 25°C. The concentrations of NaCl and Glucose in permeates were analysed by TPS WP-81 (Thermo Fisher Scientific Inc., Australia) or Shimadzu TOC-5000 CE analyser.

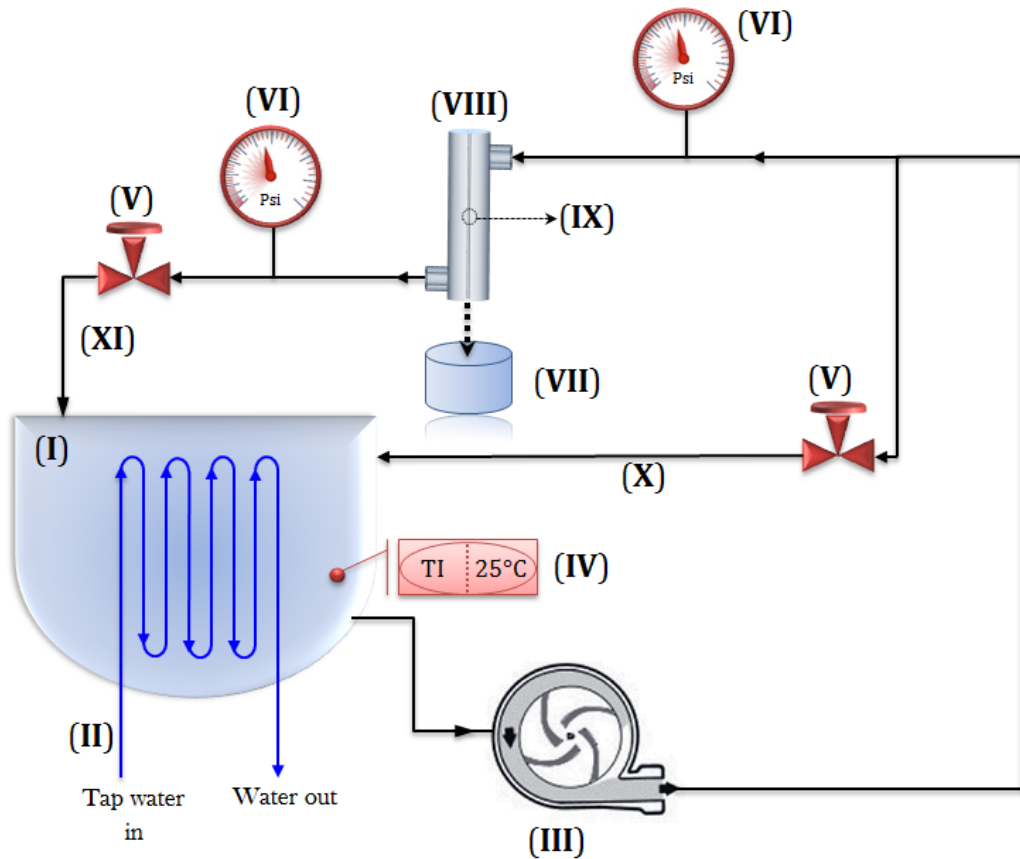


Figure 3.2 Schematic diagram of nanofiltration system. (I) Feed tank; (II) Thermal coil; (III) Pump; (IV) Thermometer; (V) Needle valve; (VI) Pressure gauges; (VII) Permeate; (VIII) Hollow fibre membrane house; (IX) Composite hollow fibre nanofiltration membrane; (X) By-pass; (XI) Concentrate.

Structural properties of NF membranes were investigated using the Donnan steric pore model (DSPM).[92].We applied this model as summarized below:

Firstly, the glucose molecular radius (r_s) obtained from the formula given by Aimar et al.[93]:

$$r_s = 0.33M_w^{0.46} \quad (3.1)$$

Then, the correlation between the pore size and the real solute rejection were applied as follow:

$$R_{real} = 1 - \frac{K_{i,c} \Phi}{1 - \exp(-Pe_m)[1 - \Phi K_{i,c}]} \quad (3.2)$$

where Φ , λ , $K_{i,c}$ and Pe_m are defined as

$$\Phi = (1 - \lambda)^2 \quad (3.3)$$

$$\lambda = \frac{r_s}{r_p} \quad (3.4)$$

$$K_{i,c} = (2 - \Phi)(1.0 + 0.054\lambda - 0.988\lambda^2 + 0.441\lambda^3) \quad (3.5)$$

$$K_{i,d} = 1.0 - 2.3\lambda + 1.154\lambda^2 + 0.224\lambda^3 \quad (3.6)$$

$$Pe_m = \frac{K_{i,c}}{K_{i,d}} \frac{J_v}{D_{i,\infty}} \frac{\Delta x}{A_K} \quad (3.7)$$

where r_p is the pore radius, $D_{i,\infty}$ the diffusion coefficient of glucose equal to $6.9 \times 10^{-10} \text{ m}^2 \text{ s}^{-1}$ [94], J_v the volume flux (based on membrane area) (m s^{-1}), Δx the effective thickness and A_K is the porosity of membrane. Considering the Hagen-Poiseuille equation for flow across the active layer of the membrane with assuming a negligible pressure drop through its support layer gives following equation:

$$J_w = \frac{r_p^2 \Delta P}{8\eta \left(\frac{\Delta x}{A_K} \right)} \quad (3.8)$$

where J_w is the pure water flux ($\text{m}^3 \text{m}^{-2} \text{s}^{-1}$), ΔP the applied transmembrane pressure (kPa) and η is dynamic viscosity of the solution (kPa s). In order to estimate $\Delta x/A_K$ and r_p , a set of algebraic equations (Eq. 2-7) was solved using MATLAB[®] (2010b) numerical facility.

3.3 Results and discussion

3.3.1 Characterization of modified TiO₂ nanoparticles

Nanoparticle arrangements in thin polymer are schematically depicted in Figure 3.3. Figure 3.3(a) illustrates the conventional arrangement of unmodified nanoparticles into polyamide structure after dispersion in TMC organic phase. As anticipated, due to hydroxyl groups on the nanoparticle surfaces the hydrogen bonds between particles lead to consequent agglomeration. A major requirement for the creation of organic monolayer on the surface of nanoparticles is improving the poor interaction between the raw nanoparticles. In fact, introducing the interfacial organic region around the nanoparticles can effectively reduce their percolation threshold, resulting in better disturbance to the matrix chain packing around it[95]. As shown in Figure 3.3 (b), in this work, we propose that prior to the incorporation inside the polymer; particle surface should be modified with proper functional group like aminosilane. This can effectively minimize the probability of the formation of Oxygen Bridge bonds between TiO₂ nanoparticles and consequent particle agglomeration phenomenon. To fabricate TiO₂-polyamide nanocomposite membranes, aminosilanized TiO₂ nanoparticles were homogeneously dispersed into *m*-phenylenediamine aqueous solution and then interfacially polymerized in presence of Trimesoyl chloride in organic phase.

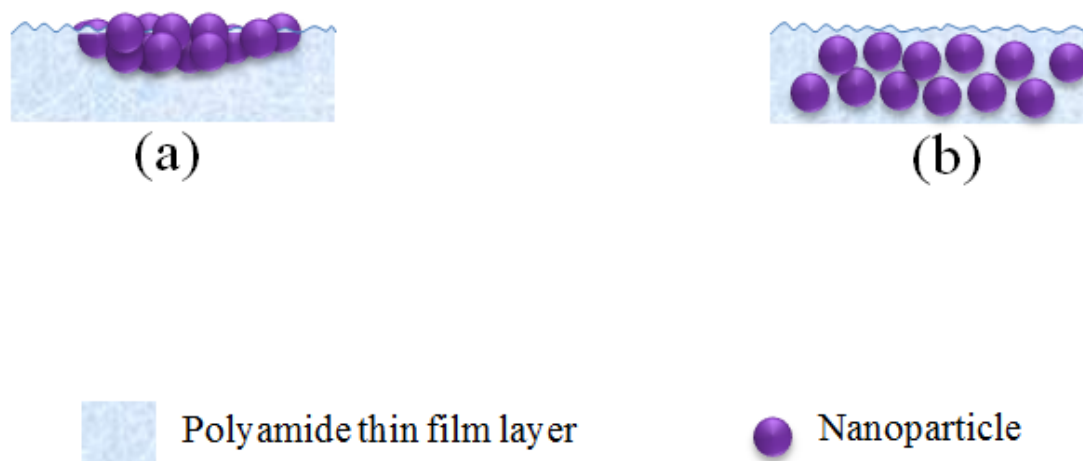


Figure 3.3 (a) Un-modified hydrophilic nanoparticles dispersed in organic solution, (b) APTS-modified low-hydrophilic TiO_2 nanoparticles in aqueous solution

Figure 3.4(a) shows the XRD patterns of the TiO_2 nanoparticles before and after modification with the amino-silane functionalization. As can be seen, both samples exhibit similar XRD patterns and the surface functionalization does not significantly change the crystalline structure of the TiO_2 powder. Figure 3.4(b) displays different optical properties of TiO_2 samples. Pure TiO_2 shows negligible absorption intensity in the visible light region, whereas the absorption edge of the modified TiO_2 nanoparticles is shifted into visible region. which can be attributed by the excitation of electrons from the valence band to the conduction band of TiO_2 [96]. In fact, the presence of NH_2 groups in the vicinity of TiO_2 nanoparticles narrows the energy band gap between the HOMO and LUMO orbitals[97]. FTIR spectral analysis was also carried out to verify the particle functionalization with results showing in Figure 3.4(c). The spectrum of unmodified TiO_2 reveals a broad peak from 3000 to 3600 cm^{-1} which can be associated with the O–H stretching vibration of the absorbed water on TiO_2 surface [98]. Interestingly, the peak intensity of O–H groups in the functionalized TiO_2 spectrum becomes weaker since part of the hydroxyl groups on the TiO_2 surface reacted with APTS which confirms the introduction of low hydrophilic amino-functional silanes on TiO_2 surface. In addition, the appearance of new bands at 1600 corresponds to the primary amine groups [N–H]. Although the other amine bands vibration arose around 3434 cm^{-1} which was covered by strong

water band in the region from 3300 to 3500 cm^{-1} . In the spectra of AAPTS-modified TiO_2 , the peak at 2927 cm^{-1} is due to alkyl groups [C–H] with stretching vibration. Furthermore, the absorption peaks at around 1075 and 1103 can be attributable to Si–O–C group vibration of surface modified TiO_2 nanoparticles [99]. In addition to FTIR, the dispersion of TiO_2 nanoparticles with certain concentrations inside aqueous amine and organic TMC solutions were visually compared.

Figure 3.5(a-c) displays transparent colloidal suspension of AATPS-modified TiO_2 nanoparticles in *m*-PDA aqueous solution due to particle functionalization by an organic layer. In Fig.5 (d) a fast TiO_2 precipitation of pure TiO_2 was observed in nonpolar TMC organic solution. We believe that fast precipitation and instability of high energy TiO_2 nanoparticles in organic phase can be evidence for their incapability to interact with polymeric phase during interfacial polymerization reaction.

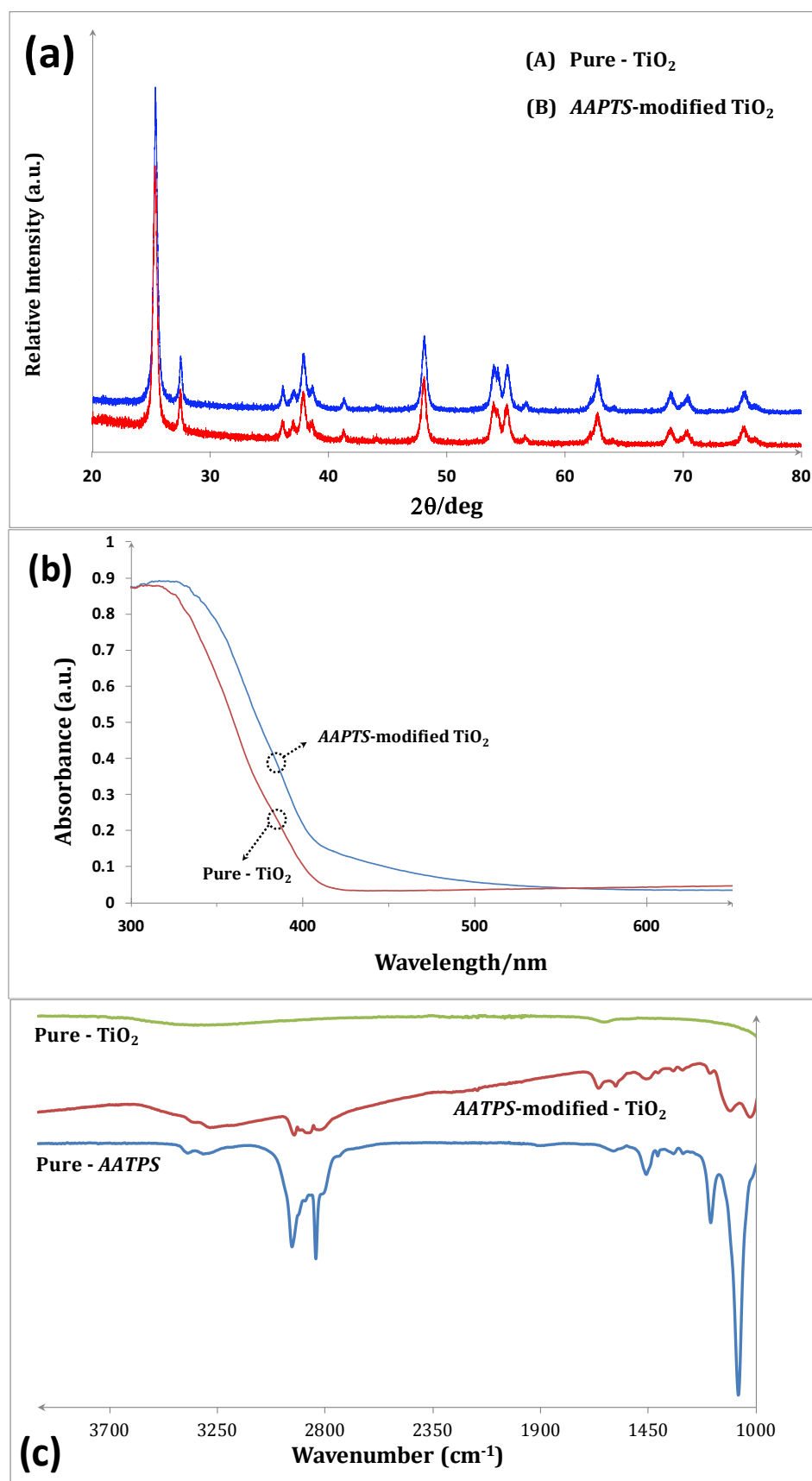


Figure 3.4 (a) XRD patterns, (b) UV-vis diffuse reflectance absorption spectra and (c) ATR-FTIR spectra of pure and AAPTSS-functionalized TiO_2 nanoparticles

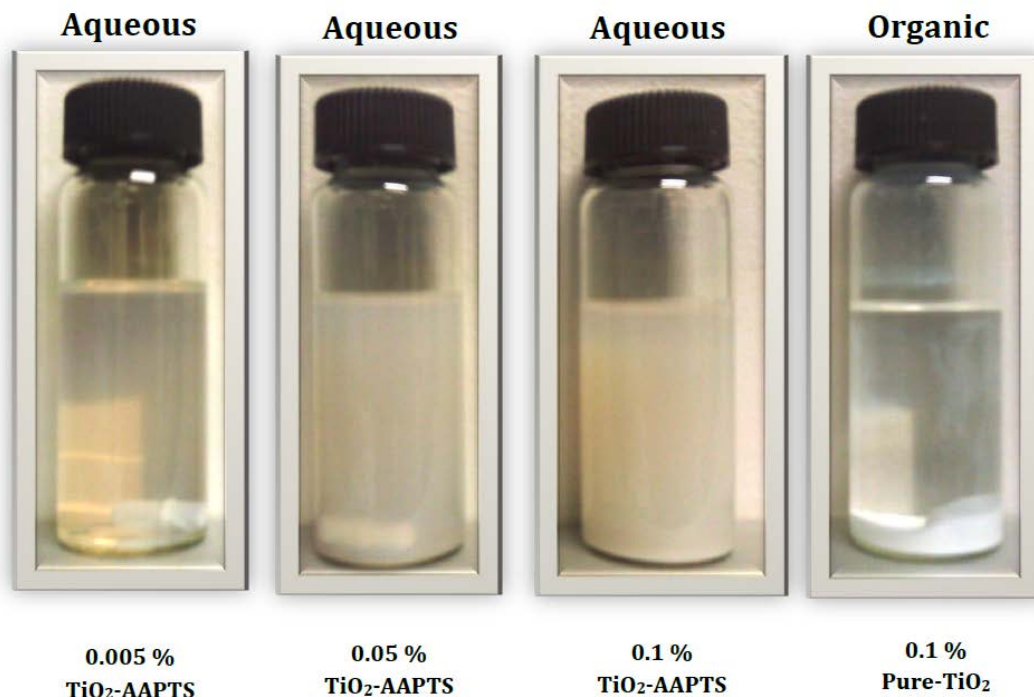


Figure 3.5 Photographs of dispersion qualities of AAPTTS-functionalized and pure TiO₂ nanoparticles homogenised in the *m*-PDA aqueous and TMC organic solutions respectively after hours

3.3.2 TFC and TFN membranes characterizations by FTIR, SEM, AFM and hydrophilicity evaluation

Figure 3.6 exhibits cross sectional morphology of the ceramic-supported PES composite membrane with thin skin layer on the top and finger-like porous structure underneath. Although the sample was fractured quickly after taking out from liquid nitrogen, but polymer deformation still can be observed in membrane cross sectional area. The PES coverage with a thickness around 70 microns over the alumina substrate is clearly demonstrated (marked with arrow shapes in Figure 3.6 (b)). The adhesion between alumina and PES phase can be attributed to van der Waals force or hydrogen bonds between hydrophilized ceramic and polymer.

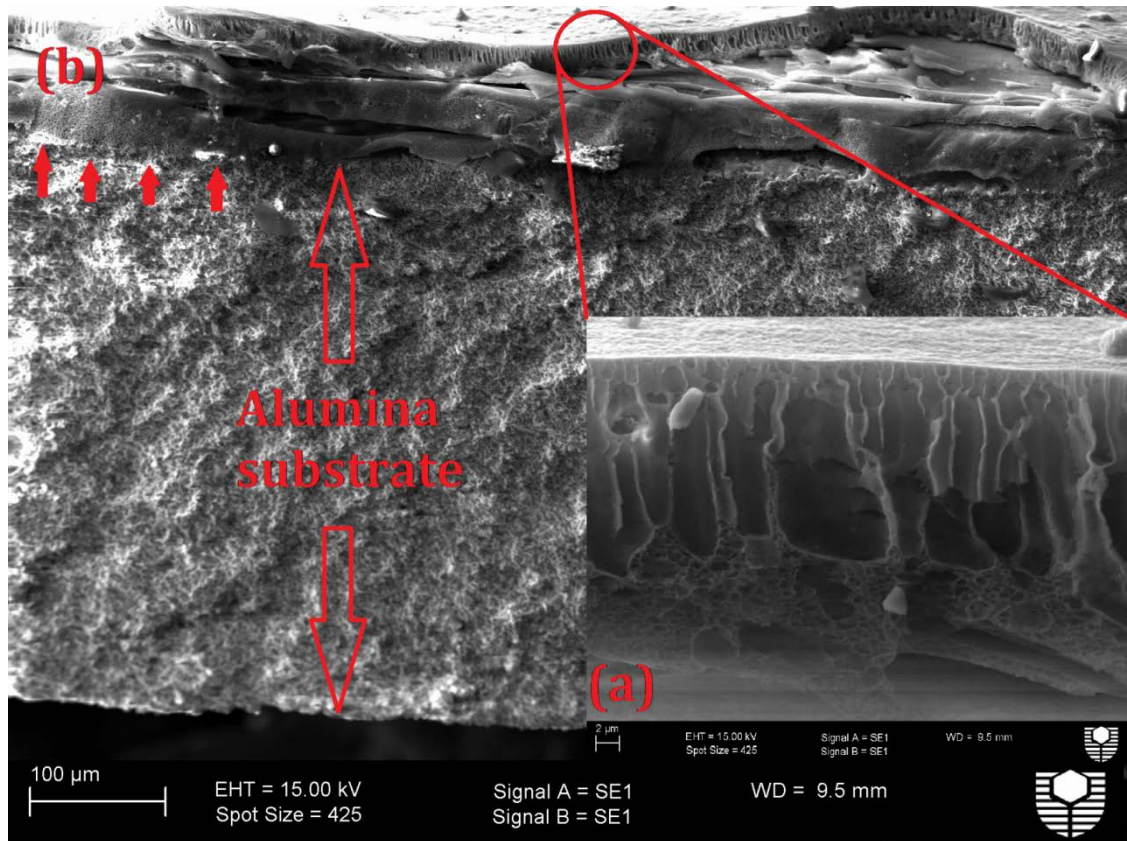


Figure 3.6 Cross-sectional SEM images of ceramic-supported PES membrane (a) Polymer selective layer, (b) Ceramic-polymer whole view

ATR-FTIR spectra of polyamide layer of TFC and TFN membranes over wave numbers of $1800 - 700 \text{ cm}^{-1}$ are given in Figure 3.7. The peak at 1663 cm^{-1} can be ascribable to the amide I band, C=O and C–N stretching vibrations. The peak around 1609 cm^{-1} is assigned to aromatic amide [C=C ring] breathing as well as N–H deformation vibration. Another peak at 1541 cm^{-1} can be assigned to N–H bending and N–C stretching of –CO–NH– group.

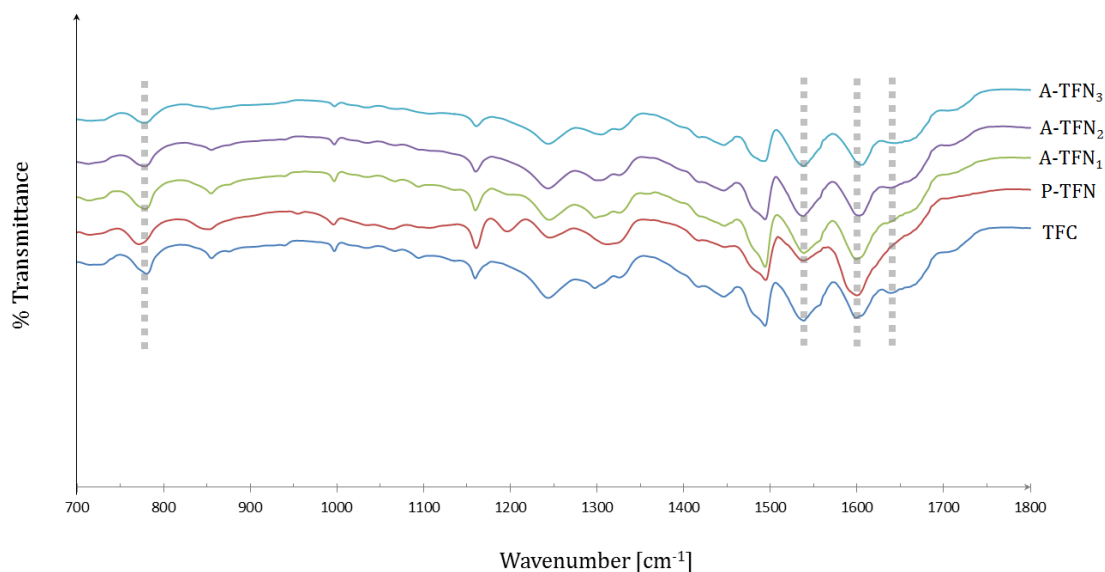


Figure 3.7 ATR-FTIR spectra of TFC and TFN membranes

Figure 3.8 shows TGA profiles of the TFC and TFN thin-films in Air. Different regions could be identified for the curves of weight loss against temperature. The initial region appeared at about 50 °C up to 200 °C with about 3% weight loss for all samples, which be assigned to evaporation of residual organic precursors and physically adsorbed water in composites after extraction and drying process. Thermochemically decomposition of the samples was occurred at second stage between 200 and 600 °C. The maximum weight loss observes in neat TFC profile, whereas A-TFN_{1,2} exhibit the best stability. The strength of the interaction between the filler and the polymer mainly depends on the property of the interface [100]. Therefore, the amount and distribution of TiO₂ into the polyamide network are likely to be the most important factors to determine the properties of the composite products. In general, the high quantity of TiO₂ defects interfacial adhesion between functionalized TiO₂ nanoparticles and polyamide matrix on the film's stability since it can disorder the polymeric chains.

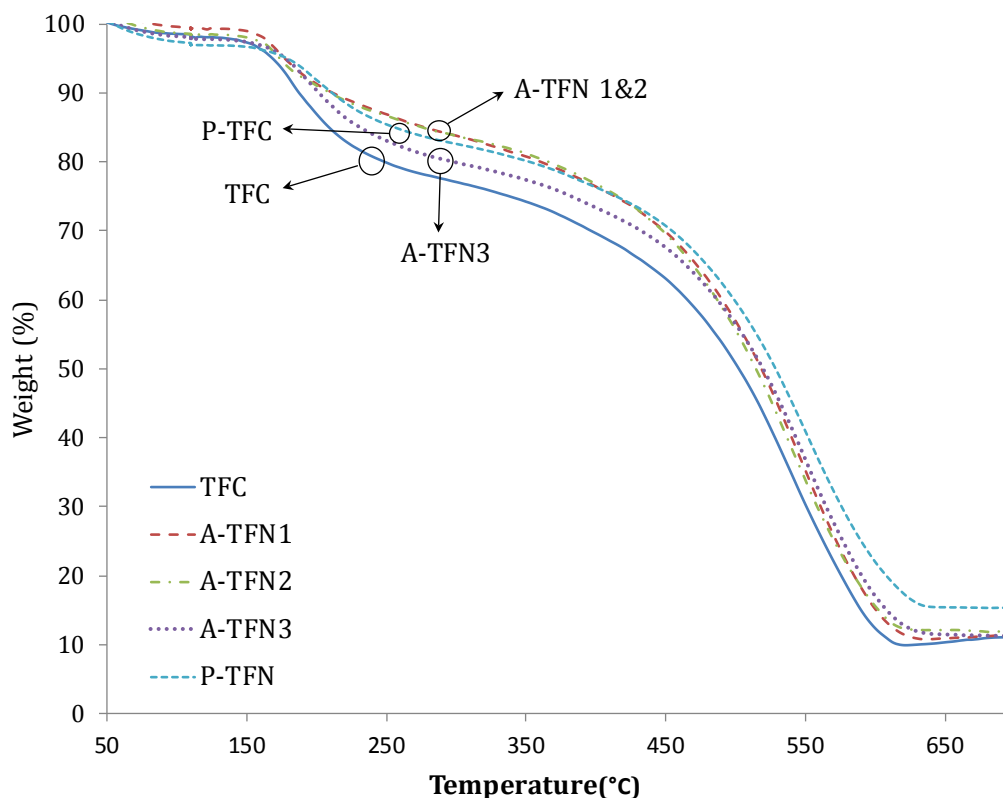


Figure 3.8 Thermal Gravimetric Analysis for TFC and TFN nanofiltration membranes

SEM and AFM analyses were carried out to verify the formation of ultra-thin skin layer over the composite ultrafiltration support as well as the influence of TiO_2 concentrations on the final membrane surface structure. SEM image in Figure 3.9 (a) of the composite support indicates that a uniform porous polymeric PES film was formed on the ceramic support. After the interfacial polymerization reaction, the polyamide membrane surface displays a typical morphology of peaks-and-valley structure (Figure 3.9(b-f)). In compare with the original TFC membrane(Figure 3.9 (b)), a denser structure is visible on pure TiO_2 incorporated thin-film nanocomposite (P-TFN) membrane surface (Figure 3.9 (c)), which provides a morphological evidence of potentiality to decline the permeability [101]. In case of the P-TFN membranes, severe TiO_2 particle agglomeration was evidenced by the SEM image in Figure 3.10 and subsequent EDX mapping analysis verified the presence of TiO_2 phase. These observations are in good agreement with results from other researchers

[63]. Previous report indicated the loading with 5 wt% TiO_2 nanoparticles was an optimum concentration for interfacial polymerization with higher water flux [26].

Different with TFC and the P-TFN membranes, A-TFN₁ and A-TFN₂ membranes display the more “leaf-like” morphologies. Meanwhile, with the increase of modified- TiO_2 nanoparticle loadings, the membrane surface becomes smoother. Interestingly, ultra-low concentration of modified- TiO_2 nanoparticles (0.005 wt%) remarkably changed the surface morphology of mixed matrix polyamide thin film. These observations demonstrate better settlements of nanoparticles throughout the polyamide matrix due to the presence of the silane functional layer onto the TiO_2 surface which can provide final polyamide network with appropriate nano-gaps so-called defects.

Figure 3.11 illustrates the different arrangements of the unmodified and modified TiO_2 nanoparticles along with the polyamide matrix formation with and without the presence of polymerizable groups. It is hypothesized that the presence of silane functional groups onto the TiO_2 surface allows monomer molecules to diffuse to the surface of the particles resulting in polydispersity of the polymer chains and the more dispersible TiO_2 nanoparticles into polymer matrix [102, 103].

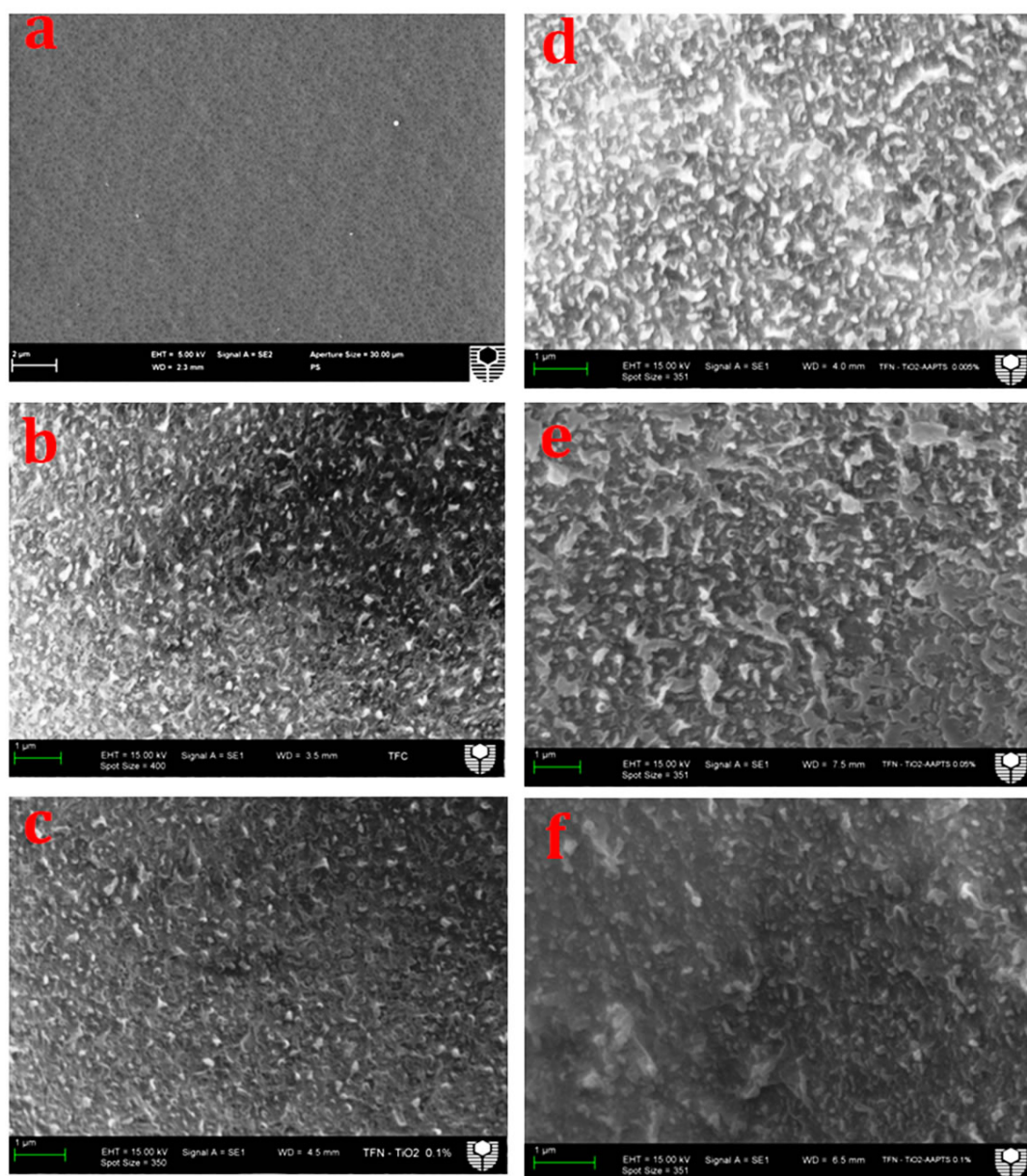


Figure 3.9 SEM top-view images of (a) PES composite support, TFC (b), P-TFN (c), A-TFN₁ (d), A-TFN₂ (e) and A-TFN₃ (f) membranes

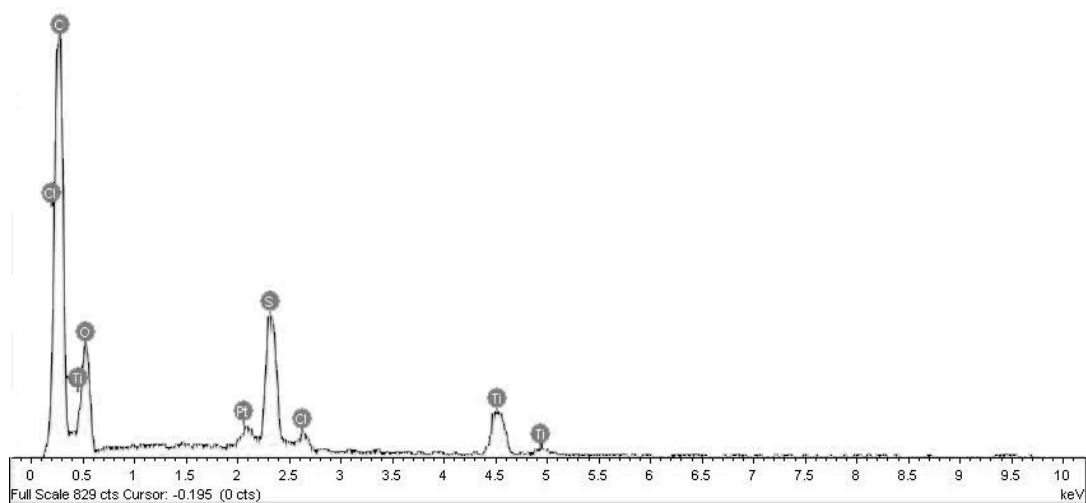
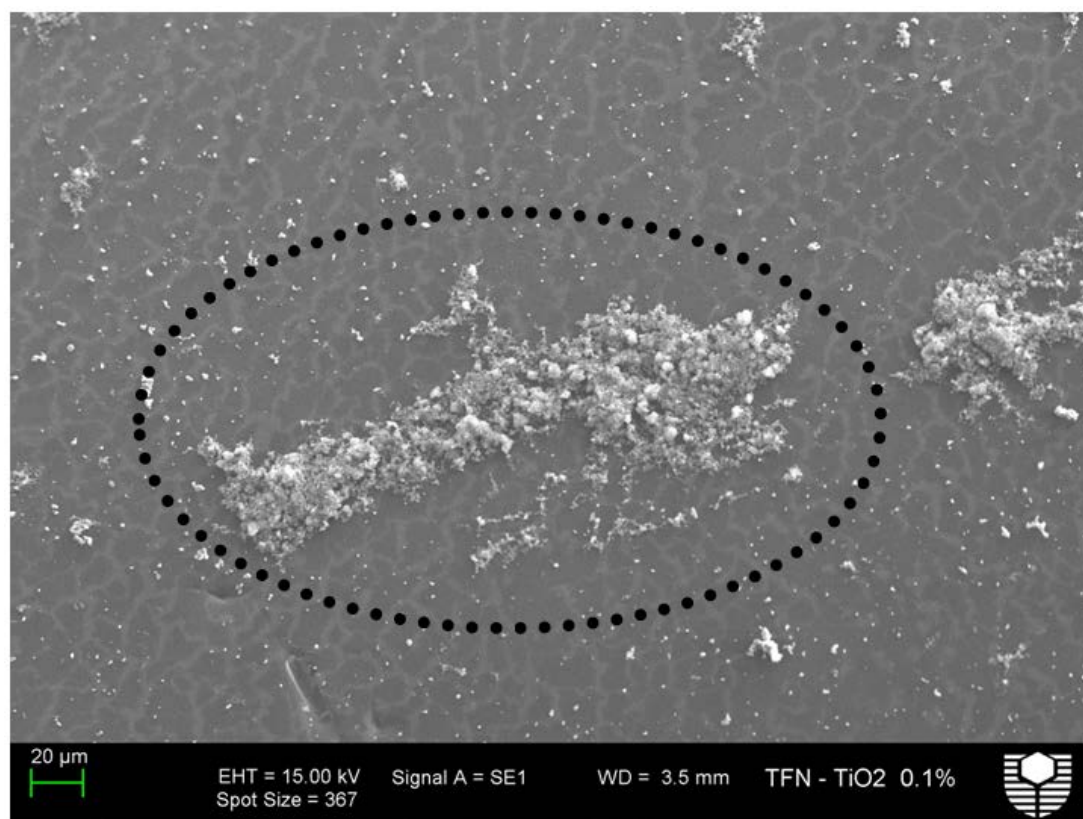


Figure 3.10 SEM surface images and EDX analysis and low-magnification of P-TFN membrane

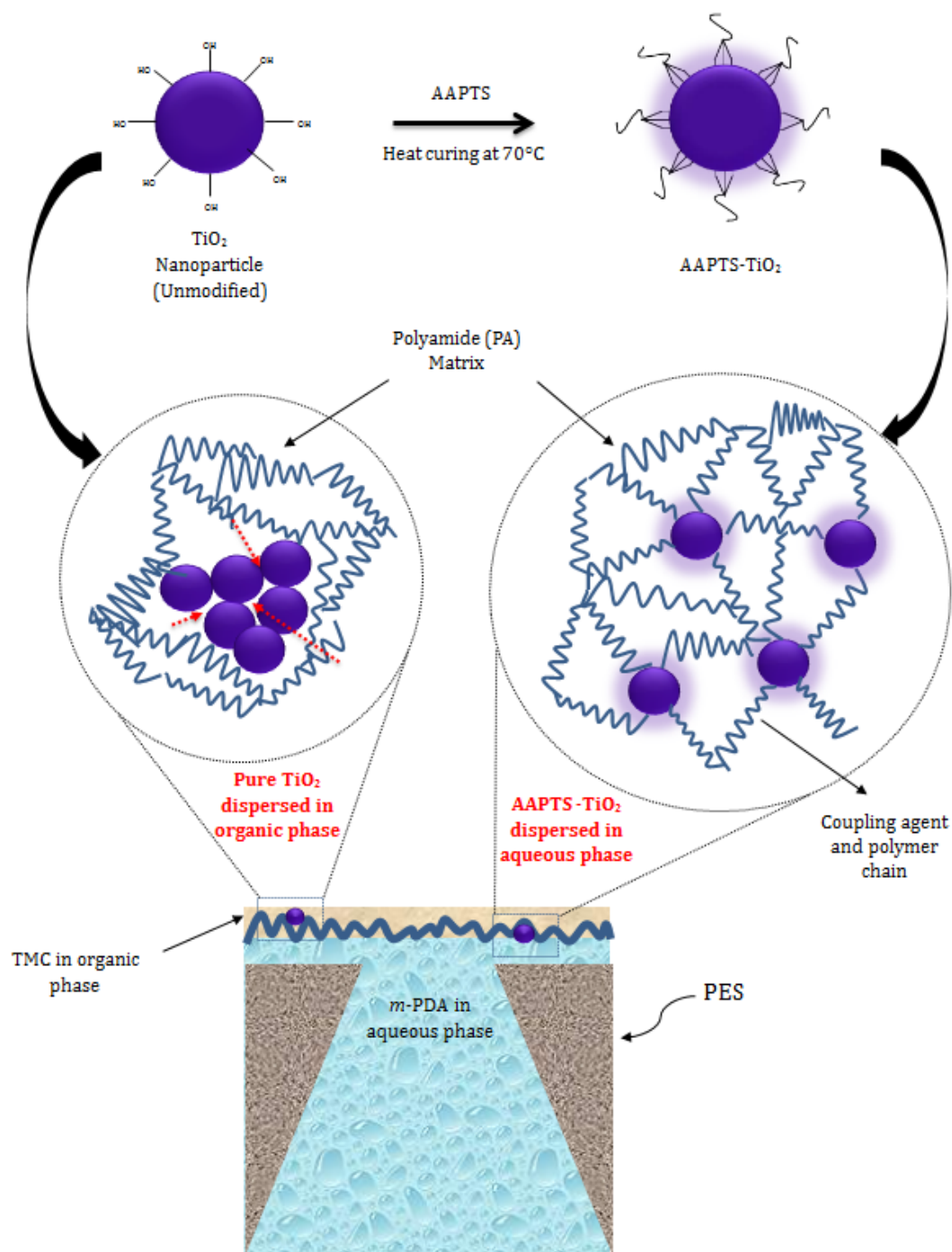


Figure 3.11 Schematics for dispersion quality of unmodified and AATPS-modified TiO_2 nanoparticles in TMC and m-PDA solutions respectively result in polyamide mixed matrix thin film nanocomposite. (The dotted red arrows indicate flow paths for water transport)

AFM images were also taken to compare the surface morphologies of all the fabricated membranes. Table 1 reveals the statistical roughness information in terms of average roughness (R_a), root mean square roughness (RMS) and maximum difference in height between the highest and lowest point (R_{max}). A glance at Figure 3.12 will easily identify the rougher morphologies of all the interfacial polymerized nanofiltration membranes than the PES composite support membrane. Uniform distribution of peak-to-valley morphology can also be observed for fresh TFC, P-TFN and A-TFN membranes.

The roughness quantitative data indicates A-TFN₁ membrane has the roughest surface in good agreement with SEM observation. In general, any factors that alter the solubility and diffusivity of the amine monomer in the organic phase affect the reaction rate, and thus, the morphology and structure of the resulting polyamide film [104]. By blending Ultra-low concentration (0.005 wt%) of aminosilanized TiO₂ nanoparticles with m-PDA solution, increasing the surface roughness is observed. This can be attributed as follows. Existence of strong nucleophiles on the aminosilanized TiO₂ nanoparticles including primary and secondary amine groups can be acted as hydrogen chloride scavengers during polycondensation process. In other words, presence of amine groups on TiO₂ surfaces accelerates the m-PDA–TMC reaction by naturalizing the hydrogen chloride produced during amide formation. This phenomenon is further illustrated in Figure 3.13. By incorporating higher concentrations aminosilanized TiO₂ nanoparticles, another possible reaction pathway is hypothesized. In fact, because of competing the AAPTS's amine groups with m-PDA for reaction with TMC in addition to the reaction with HCl. As a result, the less polymerization and consequently looser and smoother polyamide film will be formed. However, in P-TFN membrane a dense and smooth morphology is observed by depositing TiO₂ nanoparticles. This clearly indicates that TiO₂ nanoparticles are distributed on the membrane surface so that the peak-to-valley structures of the membrane surface are filled with nanoparticles.

To evaluate the hydrophilicity, the contact angle analysis was carried out on all prepared NF membranes with data showing in Table 3.1. The PES composite support has the highest water contact angle expressing the lowest hydrophilic surface comparing to other thin film polymerized nanofiltration membranes, which can be

attributed to the existence of the strong hydrophilic polar amide functional groups introduced onto the PES surface[33, 52]. All TiO_2 incorporated thin film nanocomposites show higher hydrophilicity than the TFC membrane due to the hydrophilic nature of TiO_2 nanoparticles. However, differences are also observed among the TFN membranes accounting for the diversity in chemistry as well as contents of TiO_2 nanoparticles. As observed, the higher TiO_2 concentration reveals higher hydrophilic surface. The more hydrophilic properties in A-TFN₂ than the P-TFN membrane is explained by the correlation between the surface roughness hydrophilicity based on Wenzel's equation[105]; surface roughness will decrease the contact angle for a droplet on a hydrophilic surface and increase the contact angle for a droplet on a hydrophobic surface.

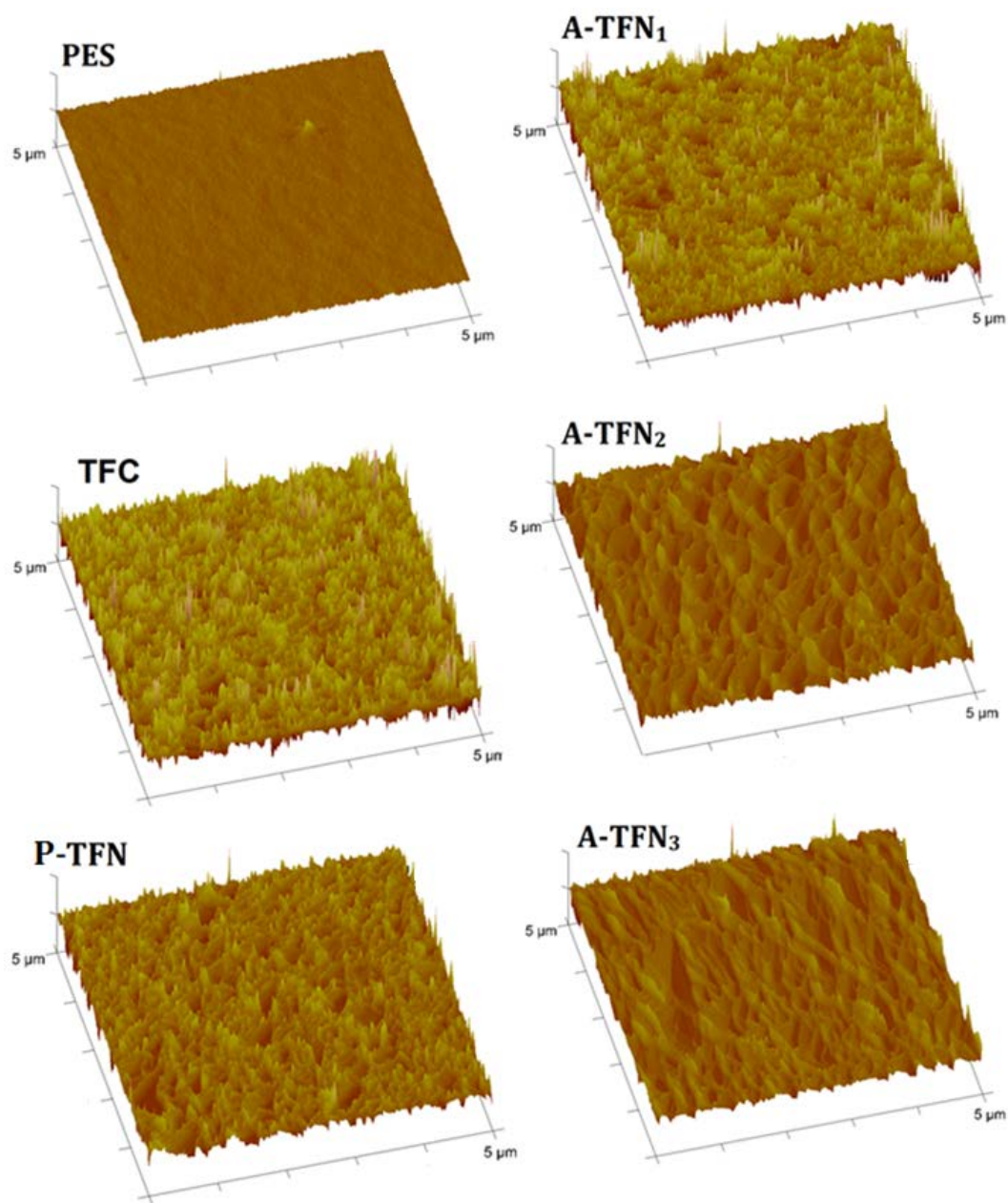


Figure 3.12 Three dimensional AFM images for PES composite support, TFC and TFN nanofiltration membranes

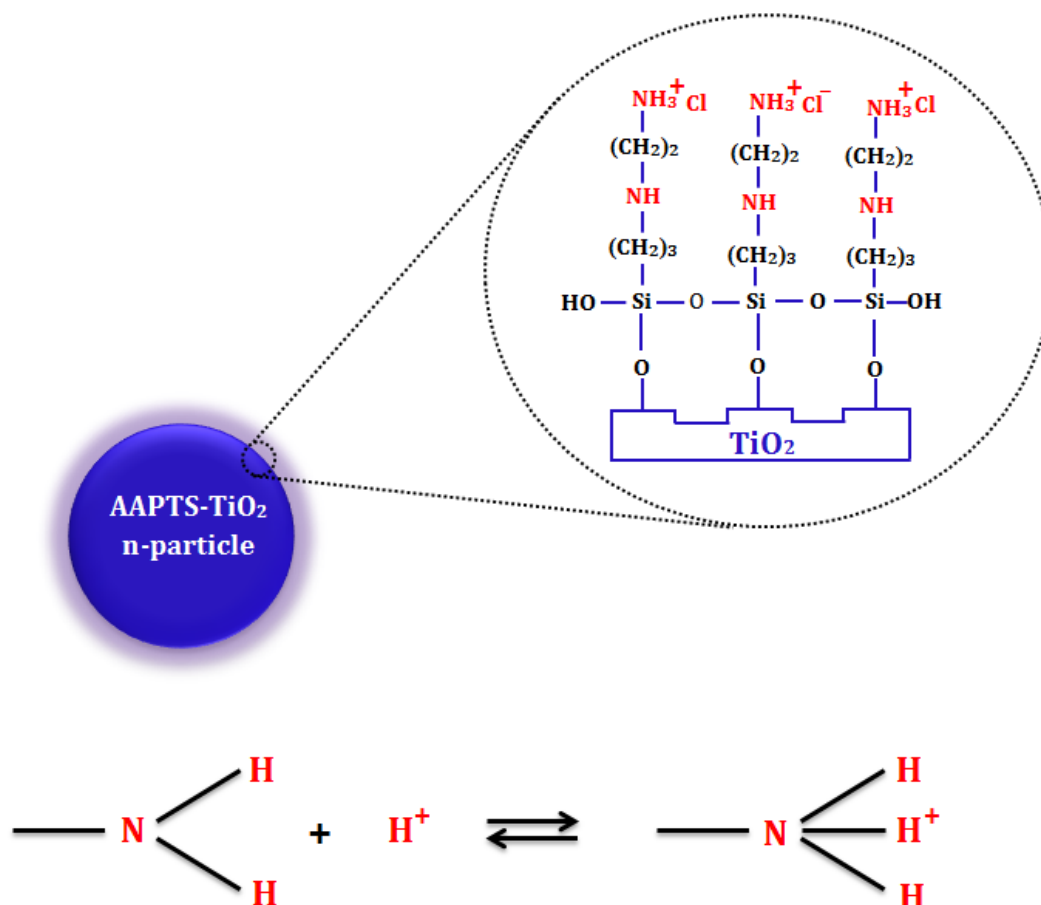


Figure 3.13 Proposed nucleophilic substitution reaction mechanism between AAPTS-functionalized TiO₂ nanoparticles and produced HCl during the polycondensation process

3.3.3 Separation performance and membrane pore size determination

Fig. 14 depicts flux and salt rejection behaviours for TFC, TFN membranes using ultra-pure water and organic NaCl solution. Pure water flux is varied between 11.2 and 27 l/m² h for TFN and A-TFN₃ membranes, respectively. A similar flux profile is also observed in case of solute permeation where the flux increased from 10 to 23 l/m² h for P-TFN and A-TFN₃ membranes. In case of P-TFN, the inefficiency of raw TiO₂ nanoparticles as a flux enhancer is illustrated, where the addition of hydrophilic nanoparticles, has led to lower pure water as well as productivity flux in compare with TFC membrane. The lower flux of P-TFN can be attributed by clogging into surface valleys resulting dense aggregation on polyamide skin layer just after

polycondensation taking place at the interface. In fact, appearance of carboxyl and amide groups after polycondensation corresponds to the main parameter for settling of TiO₂ nanoparticles or self-assembly on the membrane surface. In the meantime, the salt rejection increased to 55% for this membrane as a result of pores blockage by raw TiO₂ nanoparticles.

For A-TFN₁₋₃ nanofiltration membranes modified by functionalized TiO₂ nanoparticles, two major effects on the flux and rejection behaviour are observed: (i) the increase of hydrophilicity consequently enhancing the productivity flux and (ii) nucleophilic substitution reaction due to amino groups on the AAPTS-modified TiO₂ surfaces thus acting as a HCL acceptor to avoid less polymerization which results in recovered salt rejection. As a result, the enhancement of NaCl rejection of TFC membrane has been observed to 54% when ultra-low concentration of AAPTS-TiO₂ was incorporated into polyamide network (A-TFN₁). In fact, presence of chemical functional groups on the modified TiO₂ surfaces can obviously increase the binding affinity of TiO₂ nanoparticles to polyamide chain network during interfacial reaction. Specifically, aminosilanized TiO₂ nanoparticles may interact with the by-product of interfacial polymerization (HCl). By incorporating high loading of AAPTS-modified TiO₂ nanoparticles (0.05 and 0.1 wt%) into *m*-PDA aqueous solution, interfacial polycondensation reaction would be impaired by amine functional groups grafted on nanoparticles. This leads to a lower degree of polymerization resulting in the shrinkage of the cross-linked film and equivalent variation of pore size in the diffusion determining layer of polyamide matrix. It should be also noticed that, the reason for turning down the salt rejection for all NF membranes can be assigned to back diffusion of NaCl ions in the concentration polarization layer due to the presence of organic components (glucose) in feed solution. This hindrance results in the rejection reduction while no obvious change of glucose rejection with presence of NaCl ions was observed. [106, 107].

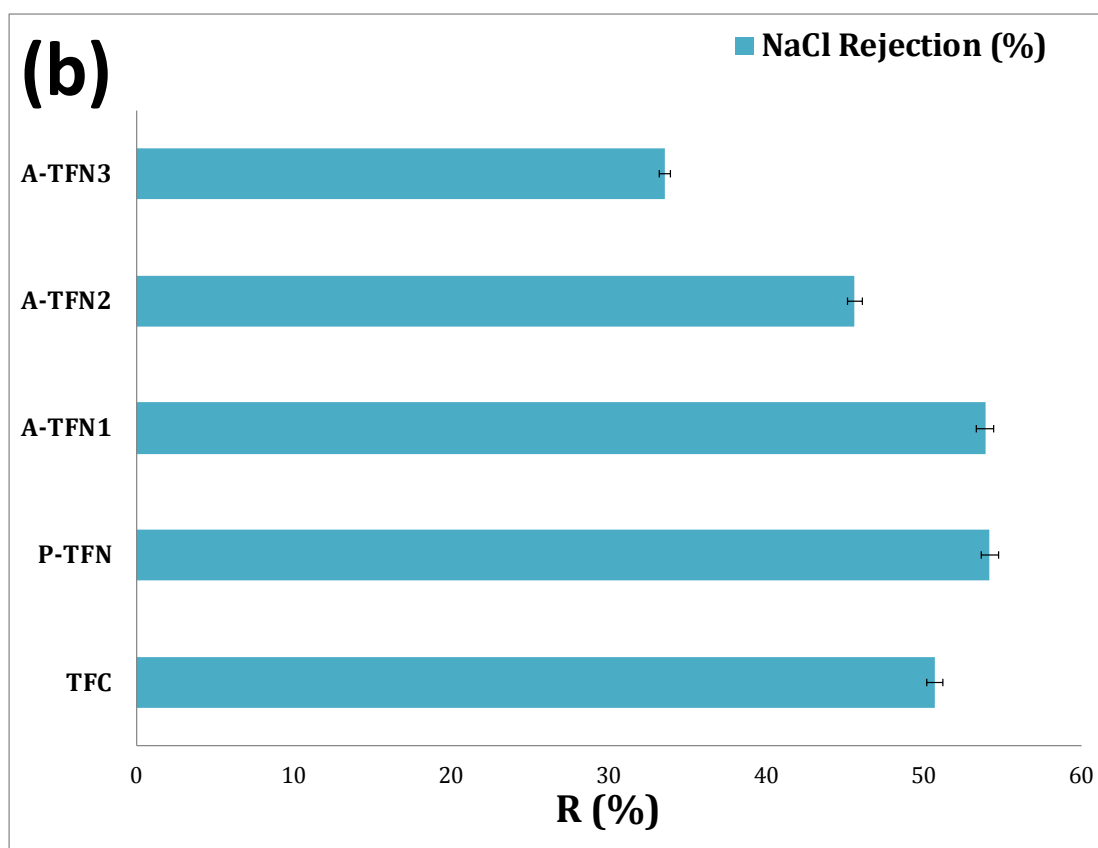
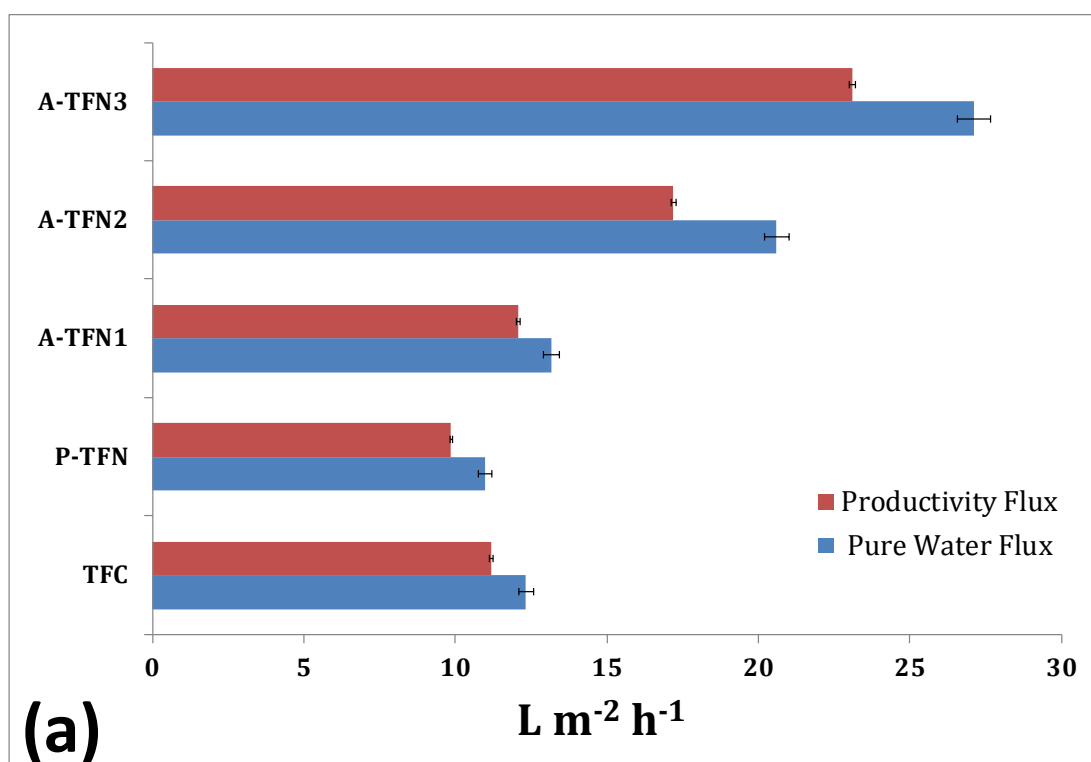


Figure 3.14 (a) Flux and (b) salty organic solution rejection behaviours of TFC and TFN nanofiltration membranes.

Transport properties and pore sizes of all NF membranes delineated from experimental data based on permeation of glucose inside the membranes are presented in Table 2. Unfortunately, the porosity of membrane (A_K) could not be determined from the model solution because this parameter was reported as a collective terms of $\Delta X/A_K$ [108]. However, by knowing the actual thickness (ΔX), A_K can be obtained from $\Delta X/A_K$ data. As it is clearly shown, the pore radius (r_p) is varied from 4.8 to 5.078 Å° with increasing concentration of modified TiO₂ nanoparticles from 0.005 to 0.1 wt%. This may be explained by the fact that higher concentrations of nanoparticles would disturb the reaction rate between amine and chloride monomers, therefore producing the larger pore size in the thin separating layer. As mentioned earlier, the idea is the incorporation of affordable concentration of TiO₂ nanoparticles to reach higher productivity flux as well as good solute rejection. Incorporation of 0.1 wt% pure TiO₂ nanoparticles results in not only a slight pore radius enhancement, but also a significant growth of the effective thickness/porosity ($\Delta X/A_K$) due to precipitation of pure TiO₂ nanoparticles on cross-linked polyamide layer. These characteristics caused lower permeability while the solute rejection did not change significantly.

Table 3.2 Structural and transport properties of TFC and TFN nanofiltration membranes

Membrane	Solute permeability, $J_v (\times 10^{-6} \text{ m s}^{-1})$	$\lambda (r_s/r_p)$	$r_p (\text{Å}^\circ)$	$\Delta x/A_K (\mu m)$
TFC	3.01779	0.7487	4.808	0.77
P-TFN	2.66158	0.7428	4.846	1.11
A-TFN ₁	3.25836	0.7494	4.804	0.89
A-TFN ₂	4.64103	0.7117	5.058	0.44
A-TFN ₃	6.2343	0.7089	5.078	0.27

3.4 Conclusions

A novel aromatic polyamide thin film nanocomposite nanofiltration membrane with appropriate structural and separation properties was developed by dispersing the aminosilanized TiO_2 nanoparticles inside the diamine monomer and polymerizing the monomer in the presence of the nanoparticles. The developed membrane has improved permeability as well as selectivity. Silane coupling agent (AAPTS) was grafted onto the external surface of TiO_2 to overcome the agglomeration normally encountered in the preparation of TFN membranes and to achieve the better interfacial adhesion between nanoparticles and polymer matrix. Upon incorporation of TiO_2 nanoparticles, thermal stability of TFN membrane was significantly improved in comparison with TFC membrane. TFN membrane with ultra-low concentration (0.005 wt%) of amine functionalized TiO_2 nanoparticles provides the best salt rejection as well water flux. Membrane flux can also be further improved by the incorporation of higher percentage of the modified TiO_2 nanoparticles.

Chapter 4 Synthesis, Characterization, and Antifouling Properties of TiO₂-PVA Thin Film Nanocomposite (TFN) Membranes

Abstract

In this chapter, a thin film nanocomposite membrane has been developed by dip-coating of a chemically surface-modified porous poly(vinylidene fluoride) support in different poly(vinyl alcohol) (PVA) aqueous solutions. TiO₂ nanoparticles were employed as inorganic fillers into PVA matrix. In order to improve the interfacial adhesion of nanoparticles in PVA blend, an endothermic carboxylation reaction under acidic condition was carried out onto the TiO₂ surface using chloroacetic acid (ClCH₂COOH). Glutaraldehyde (GA) was used as a cross-linker for the composite membranes in order to enhance stability of the coated layer. The presence of carboxyl (–COOH) content on the TiO₂ surface was confirmed by FTIR spectral analysis. Scanning electron microscopy (SEM) identified various topographies by the incorporation of TiO₂ nanoparticles. PEG 2000 and MgSO₄ solutions were used to evaluate the steric (hydrodynamic) and Donnan-type (electrostatic interactions) rejection properties of the prepared membranes in a batch stirred cell at 400 kPa and ambient temperature. Interestingly, a 40% improvement of bivalent salt was attained by the incorporation of 1.0 wt% surface-carboxylated TiO₂ nanoparticles into PVA solution. A simultaneous 57% PEG retention improvement also achieved. Antifouling properties of membranes were calculated using dilute bovine serum albumin (BSA) solution. After PVA coating with TiO₂ incorporation, the flux recovery ratio of PVDF membrane was significantly improved from 45 to 94%.

4.1 Introduction

Poly(vinylidene fluoride) (PVDF) membranes have long been used in several membrane processes including: reverse osmosis[109], nanofiltration[110], ultrafiltration[111, 112], microfiltration[113] and gas separation[114, 115]. In spite of superior intrinsic properties such as high mechanical strength, thermal and chemical stability, PVDF suffers from poor wettability and low water permeability for aqueous media application due to its strong hydrophobic nature. Thermodynamically, there is no electrostatic interaction between PVDF hydrophobic surface and water molecules due to the absence of hydrogen bonding interaction. Therefore, water molecules are free from hydrophobic PVDF surface, which is spontaneously ended up with an entropy increase in the boundary layer between the $(\text{CH}_2=\text{CF}_2)_n$ interface and water molecules [116]. As a result, water-soluble macromolecules such as proteins are significantly likely to be adsorbed onto the PVDF membrane surface which makes it susceptible to fouling. In fact, fouling is a consequence of pore blockage caused by the deposition of retained solute particles at the membrane surface or inside the pore which results in flux reduction[117]. Physical surface coating through a thin functional hydrophilic layer has been targeted by many researchers [118-121] as it is a simple and convenient way to improve the membrane surface hydrophilicity but to retain the physical and chemical stability of the bulk polymer. However, in case of the PVDF membrane with good chemical resistance, chemical surface modification can also be considered to achieve more strongly anchored coating layer. Poly(vinyl alcohol) (PVA) is a water-soluble biodegradable polymer with inherently good hydrophilicity, good film-forming characteristics and high antifouling potential accompanied by high water permeability[122, 123]. These good properties make PVA an attractive polymer in applications for membrane-based water treatment. However due to inherit water-solubility PVA, it must be crosslinked when fabricated for aqueous applications[123]. Many studies were focused on surface modification of the polymeric ultrafiltration membranes using a thin PVA-based film to improve the membrane performance in terms of selectivity, permeability and antifouling capability [124-126]. For this purpose, some research efforts have been placed on the nanofiller-reinforced thin film nanocomposite membranes recently [127, 128]. The interest of using nanoparticles is growing exponentially due to their new

properties arising from nanoscale effects. The use of nanoparticles in manufacturing these membranes allows for both a high degree of control over membrane fouling and the ability to produce desired structure with new functionalities[129]. The performance of nanocomposite membrane highly depends on matrix/filler adhesion and the quality of dispersion of filler particles into the polymer matrix[130]. Nano titanium dioxide (TiO_2 nanoparticle) as nanofiller has been the focus of numerous studies in recent years for improvement the permeability and antifouling properties of nanocomposite membranes [131-135]. Modification with certain functional groups is one of the mostly accepted methods to improve nanoparticles compatibilization and dispersion stability into the polymeric matrix [136, 137]. To our knowledge, using nanoparticles within PVA film to evaluate interfacial properties of the nanocomposite films in the preparation of nanofiltration membranes has rarely reported. Pourjafar et al. prepared a polyethersulfone/poly (vinyl alcohol)/titanium dioxide nanocomposite nanofiltration membrane by depositing the TiO_2 nanoparticles on the surface of PVA coated on PES ultrafiltration support [138]. They have found that Binding TiO_2 nanoparticles with PVA hydroxyl groups might plug any pinholes and local defects, and thus enhances the salt rejection. However, no characterizations on antifouling capability of fabricated nanocomposite membranes were reported. Baroña et al. [139] successfully improved the permeate water flux by incorporation of aluminosilicated single-walled nanotubes within PVA matrix without sacrificing the rejection data. However, they did not report the information about the antifouling property change before and after the embedding inorganic nanophase. In this study, the novel PVDF/PVA nanocomposite membrane synthesized by mixing of the PVA with functionalized TiO_2 nanoparticles was investigated. Besides, the PVDF ultrafiltration support was hydrophilized to overcome the instability of the PVA-deposited layer originating from weak adhesion between PVDF hydrophobic surface and the hydrophilic PVA film. The focus of this paper is on synergistic effects of TiO_2 nanoparticles and their surface chemistry on the structure, morphology, permeability and antifouling properties of resultant TiO_2 -PVA thin film nanocomposite membranes. For this purpose, an asymmetric PVDF ultrafiltration membrane was firstly hydrophilized to overcome the instability of the PVA-deposited layer originating from weak adhesion between PVDF hydrophobic surface and the hydrophilic PVA film. Then, TiO_2 nanoparticles were modified with chloroacetic acid (ClCH_2COOH) to introduce carboxylic groups ($-\text{COOH}$) on

particles' surfaces. Finally TiO₂ nanoparticles with or without chemical surface modification was incorporated inside the PVA matrix. The antifouling property was investigated using Bovine Serum Albumin as the foulant.

4.2 Experimental Section

4.2.1 Materials and Chemicals

Poly(vinylidene fluoride) [Radel A-300, Solvay Advanced Polymers, USA], and Polyvinylpyrrolidone (PVP, K40) [GAF® ISP Technologies Inc., Mw = 40,000] were used as a polymer matrix pore former respectively. 1-methyl-2-pyrrolidinone (NMP) (HPLC grade), Poly(vinylalcohol) (Mw 89,000-98,000, 99+% hydrolysed), titanium(IV) oxide nanopowder (SSABET = 35-65 m²/g; ca. 80% anatase, 20% rutile ~21 nm particle size, ≥99.5%), chloroacetic acid (ACS reagent, ≥99.0%), potassium hydroxide (KOH reagent grade, 90%, flakes) and bovine serum albumin (BSA) (agarose gel electrophoresis ≥98%, lyophilized powder) were purchased from Sigma-Aldrich. Glutaraldehyde (GA 25% solution) as cross linker was supplied by Ajax Finechem Pty Ltd. Potassium permanganate (KMNO₄) and ethanol (100% Denatured, 99.5% minimum purity) purchased from Chem-Supply, SA, Australia. Poly(ethylene glycol) (PEG 2000, 99% Mw = 1800) purchased from Merck. In addition, sulphuric acid (H₂SO₄ 98% AnalaR NORMAPUR®) and magnesium sulfate (MgSO₄ ≥98%) was purchased from RHEOCHEM LTD and BDH chemicals, Australia. Whatman glass microfiber filters (GF/B) was employed for the separation of TiO₂ nanoparticles from the solution. Deionized water has been used throughout this study unless otherwise indicated.

4.2.2 Carboxylation of TiO₂ nanoparticles

Carboxylation of TiO₂ nanoparticles was carried out by the simple reflux method which extensively was explained in previous chapter. Briefly, a TiO₂ suspension (10 g of TiO₂ in 1500 ml) was homogeneously stirred at ambient temperature for 1 h followed by 30 min ultrasonication. 12.5 g chloroacetic acid was added slowly to the resulted mixture under stirring by a magnetic stirrer. After stirring for 7 h at 100 °C,

the mixture was cooled down and repeatedly washed and filtered until the pH value of the mixture became neutral. The final separation of TiO₂ particles from the solution was carried out in a centrifuge at 4000 rpm for 30 min. The resulting particles were then dried in an oven at 80 °C for 24 h to further remove the impurities. The presence of organic groups on the surface of modified nanoparticles was confirmed by FTIR analysis.

4.2.3 Preparation of PVDF support membrane

The flat sheet membranes were prepared by phase inversion via immersion precipitation technique. The blend homogeneous solutions based on PVDF polymer were prepared by dissolving 15wt.% PVDF in NMP in the presence of 2 wt% PVP as pore former at around 40 °C with mechanical stirrer at 100 rpm for 20 h. The homogeneous polymer solution was evacuated overnight prior to the casting to remove the gas-bubbles. The compositions of casting solution were shown in Table 4.1. The solution was cast using a homemade casting knife with 120 µm thickness on polyester non-woven fabric. The polymer layer was immediately transferred to the non-solvent bath (water) at room temperature and had been kept there for 24 hours to complete the solidification process and leach out the solvent residual. At the final stage, the membranes were dried by placing between soft tissue papers at room temperature.

Table 4.1 Summary of the membranes' recipes

Membrane	PVDF (wt%)	PVP (wt%)	PVA (wt%)	TiO ₂ -COOH (wt%)	TiO ₂ -Pure (wt%)	NMP (wt%)
M-1	15	2	—	—	—	83
M-2	15	2	1	—	—	83
M-3	15	2	1	0.5	—	83
M-4	15	2	1	1	—	83
M-5	15	2	1	—	1	83

4.2.4 Preparation of composite and nanocomposite membranes

The first step of our coating process was hydrogen fluoride (HF) elimination of PVDF chain by using KMnO_4 and KOH with protocol described previously [140]. For the next step, PVA aqueous solution was employed as a hydrophilic coating media, which was prepared by dissolving of PVA in water at 90 °C. The above chemically-treated PVDF support was immersed inside 1 wt.% aqueous solution of PVA for 5 min. The excess solution was drained off by holding the substrate in a vertical position. Thereafter, the drenched membranes were immersed in 5 wt.% aqueous solution of glutaraldehyde as cross linker and 0.5 wt.% H_2SO_4 as catalyst for 1 min. The composite PVDF and PVA membrane was finally dried at 110°C for 2 min. TiO_2 -PVA nanocomposites were synthesised using the same procedure as mentioned above, except that various amount of pure and carboxylated TiO_2 nanoparticles were dispersed in PVA solution. In order to reach good dispersion of nanoparticles, ultrasonication was employed for 30 min immediately prior to the crosslinking reaction.

4.2.5 Membrane characterization

In order to examine the surface wetting characteristics of membranes, water contact angle was measured using the contact angle detecting instrument [KSV Cam Optical Contact Angle and Pendant Drop Surface Tension Software Version 3.81, Finland]. De-ionized water was used as the probe liquid in all measurements. Functional identification of the prepared membranes and the modified TiO_2 nanoparticles were demonstrated using FTIR spectral analysis. All FTIR spectra were recorded by the attenuated total reflection (ATR) technique using Spectrum 100-FT-IR Spectrometer (Perkin-Elmer). Morphologies of composite and nanocomposite membranes were observed using scanning electron microscopy (Zeiss EVO 40XVP). Gold sputtered coating was performed on the samples under vacuum before the morphological observation. TEM images were obtained using a JEOL 4000EX instrument operating at 400 kV. In order to investigate the dispersion quality of TiO_2 nanoparticles throughout the nanocomposite membranes, the EDX-mapping analysis was also carried out via the EDS X-ray detector equipped by the scanning electron microscopy.

4.2.6 Filtration performance and fouling analysis

All filtration experiments were carried out in a batch stirred cell as described elsewhere[134]. High purity nitrogen gas was used to pressurize the cell to the operating pressure. The flux and rejection rate of all membranes were determined under the 4 bars transmembrane pressure (P) at room temperature at fixed speed of 500 rpm. The flux (J) through the membrane may be described by the following equation:

$$J = \frac{m}{(A\Delta t)} \quad (1)$$

where m is the mass of permeated water, A the membrane area and Δt the permeation time. Fouling can be quantified by the resistance appearing during the filtration and cleaning can be specified by the removal of this resistance. The resistance is due to the formation of a cake or gel layer on the membrane surface. Therefore, after pure water flux measurement (J_{wi}), the solution reservoir was refilled with a 200 ppm BSA solution and the flux (J_p) was obtained. After 90 min filtration, the membrane was washed with deionized water for 10 min and the pure water flux of cleaned membranes was measured (J_{wc}). In order to evaluate the fouling-resistant capability of the membrane, the flux recovery ratio FRR (%) was calculated using the following expression:

$$FRR(\%) = \left(\frac{J_{wc}}{J_{wi}} \right) \times 100 \quad (4.2)$$

Here, R_t is the degree of the total flux loss caused by total fouling R_r and R_{ir} . Eqs. (4.3) and (4.4) show reversible deposition and irreversible fouling:

$$R_r(\%) = \frac{J_{wc} - J_p}{J_{wi}} \times 100 \quad (4.3)$$

$$R_{ir}(\%) = \frac{J_{wi} - J_{wc}}{J_{wi}} \times 100 \quad (4.4)$$

Obviously, R_t can be defined as the sum of R_r and R_{ir} :

$$R_t = R_r + R_{ir} \quad (4.5)$$

BSA rejection data was measured by UV-vis spectrometer over wavelength 280 nm (SP8001, Metertech Inc, Taiwan). Small organic solute and divalent salt retention data were determined for all prepared samples using 1000 ppm PEG 2000 Da and MgSO₄ solutions. The rejection can be described by following equation:

$$R(\%) = \left(1 - \frac{C_p}{C_f}\right) \times 100 \quad (4.6)$$

where C_p and C_f are the concentration in the permeate and the feed, respectively. Membrane rejection for NaCl was characterized by TPS WP-81 (Thermo Fisher Scientific Inc., Australia). The concentrations of glucose in permeate was analysed by Shimadzu TOC-5000 CE analyser. Determination of BSA concentration in permeates and feed solutions were also carried out by UV-vis spectrometer.

4.3 Results and discussion

4.3.1 Characterization of Carboxylated of TiO₂ nanoparticles

Due to their high surface area, inorganic nanoparticles are easily agglomerated driven by the decrease of surface energy. It is known that TiO₂ nanoparticles have a very high surface area to volume ratio. This will cause interaction of the particles' surfaces, resulting in tendency of nanoparticles to agglomerate. The particle agglomeration will impede its dispersion inside the polymer. Interfacial modification of nanoparticles with covalently bonded functional groups or molecules is an efficient approach to increase their dispersity throughout the polymer solution and achieve defect-free organic-inorganic mixed matrix structure because of its higher compatibility with polymer chains[135-137]. In case of TiO₂ nanoparticles, the problem is the existence of highly physisorbed water (including physically bonded or hydrogen-bonded water) on their surface which may affect the subsequent surface modifications. We anticipate that the addition of carboxyl groups on the TiO₂ enables a strong covalent binding between nanoparticles and PVA chain during crosslinking process[141].

Figure 4.1 shows further illustration of introducing carboxyl groups on the TiO_2 surface and its consequent influence on the resultant PVA- TiO_2 matrix structure. As can be seen, without carboxyl groups, no chemical linkage is established between the TiO_2 nanoparticles. This can be due to the poor interfacial interactions between the hydrophilic nanoparticles which originates from their high surface energy [142]. Nevertheless, it is hypothesized that there can be hydrogen bonding between the large TiO_2 agglomerates and the PVA chains which are condensed to covalent bonding during final heating and drying stages. Conversely, a good dispersion of carboxylated- TiO_2 nanoparticles in aqueous PVA solution is expected after applying carboxyl groups on their surfaces. Because of interaction between $-\text{COOH}$ and $-\text{OH}$ groups on the nanoparticle surface and $-\text{OH}$ in the PVA chains, PVA may act as a template during mixing and sonication step [143]. Furthermore, during the heat curing step, crosslinking reaction between $-\text{COOH}$ and $-\text{OH}$ in the PVA can be intensified by acting each nanoparticle as a crosslinking centre in the nanocomposite film. Therefore, dispersity and settlement of nanoparticles could be greatly improved.

Figure 4.2 shows FTIR adsorption of pure and carboxylated TiO_2 nanoparticles. The stretching and bending bands at 3300 and 1640 cm^{-1} can be assigned to vibrations of water molecules adsorbed on the surface of nanoparticles [144]. However, two new peaks emerged in carboxylated TiO_2 nanoparticles at 1710 cm^{-1} attributed to stretching of $\text{C}=\text{O}$ and 2923 cm^{-1} belongs to stretching vibration in the $-(\text{CH}_2)_n-$ groups of introduced chloroacetic acid molecules during carboxylation reaction[145].

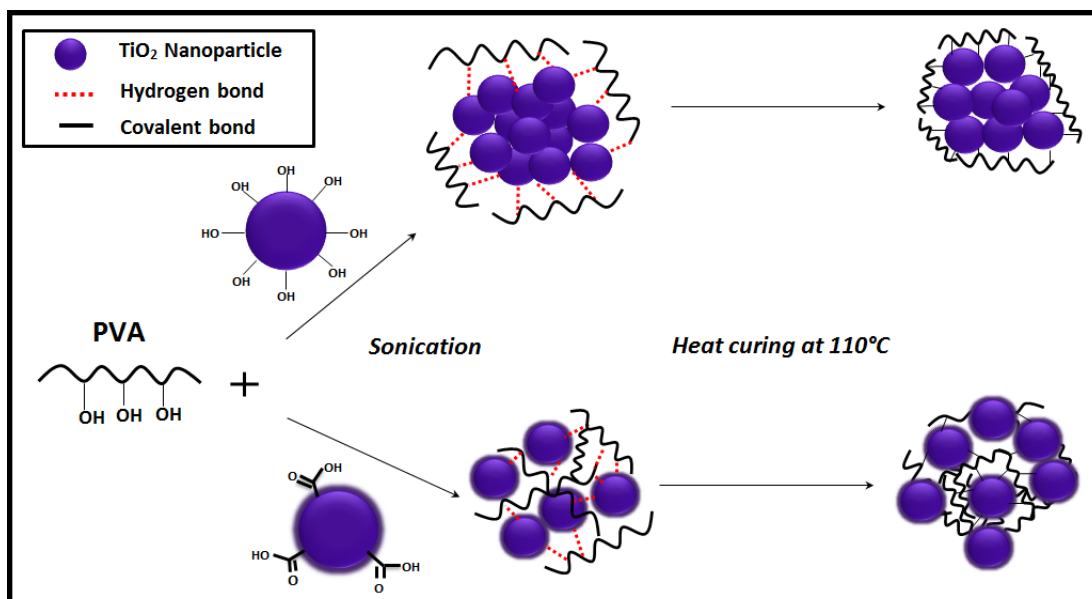


Figure 4.1 A depiction of the interactions between hydroxyl groups of PVA chains TiO_2 nanoparticles in raw and carboxylated forms

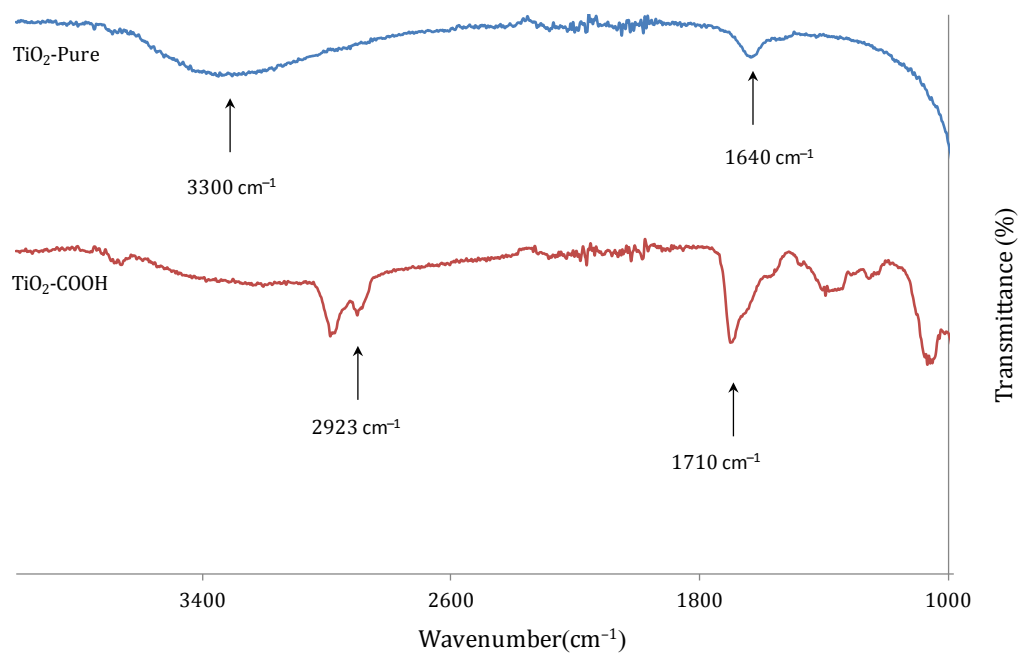


Figure 4.2 ATR-FTIR spectra of pure and carboxylated TiO_2 nanoparticles

The effect of the presence of carboxylate group on particle dispersity was examined by TEM analysis with result showing in Figure 4.3. Two particle mixture in water

with similar content of pure or carboxylated TiO_2 particles were prepared by ultrasonication. Figure 4.3(a) clearly shows an extensive aggregation of raw TiO_2 while striking better dispersion of carboxylated TiO_2 nanoparticles is displayed in Figure 4.3(b), which can be ascribed to the reduced hydrophilic property and the surface energy of the particles by the surface carboxylation reaction.

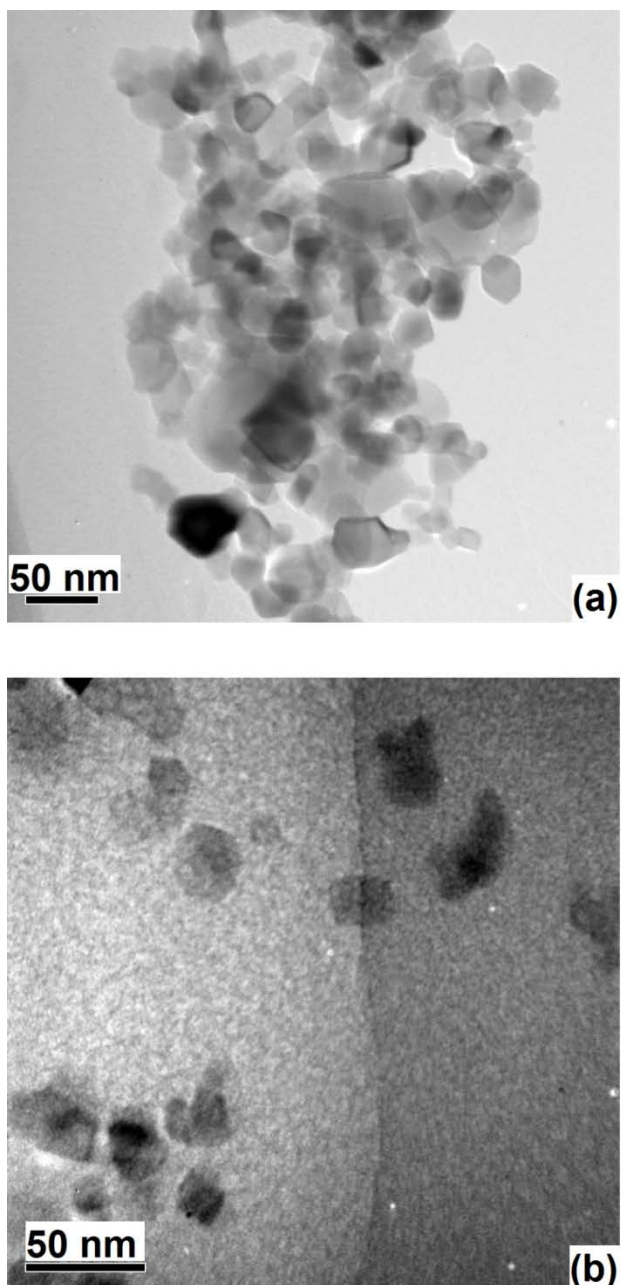


Figure 4.3 TEM observations of (a) raw and (b) carboxylated TiO_2 nanoparticles dispersed in deionized water followed by 10 min ultrasonication

4.3.2 Composite and Nanocomposite membranes characterized by FTIR and SEM

ATR-FTIR spectra of all prepared membranes over wave numbers of 700–4000 cm^{-1} are given in Figure 4.4. These characteristic peaks are closely related with certain chemical groups. The vibrational bands over 2850 to 2950 cm^{-1} is due to the C–H asymmetric stretching vibration of the methyl group of the PVP[146]. The peaks over 1650 to 1750 cm^{-1} region can be ascribable to stretching vibration of aldehyde (C=O) groups in glutaraldehyde crosslinker solution and also to the presence of PVP in the initial casting solution[147]. Appearance of the peak at around 3300 to 3500 cm^{-1} from the composite and nanocomposite membranes is assigned to asymmetric vibration of hydroxyl (–OH) groups introduced by PVA coating[148].

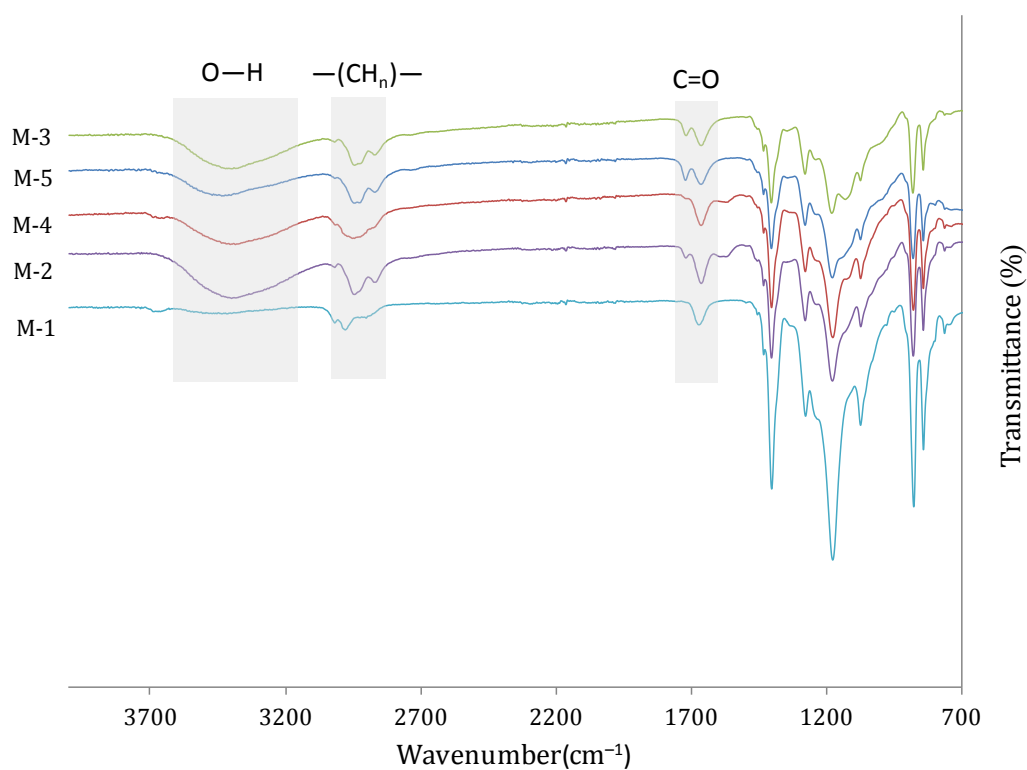


Figure 4.4 ATR-FTIR spectra of all prepared membranes

Figure 4.5 depicts the cross-sectional SEM micrographs of PVDF substrate (Figure 4.5(a) and b) and PVA-coated composite membrane (Figure 4.5(c)). Upon immersion of the casted polymer solution (PVDF/PVP/NMP) into the water coagulant bath, the fast solvent/non-solvent exchange took place across the interface of casting film and non-solvent. This is combined with the repulsive forces between polymers (PVDF) and water, leading to immediate precipitation of polymers at the interface. As a result, As a result, atypical asymmetric structure and developed macrovoids in sub-layer were formed[134]. Fig. 4.5(c) exhibits establishment of a thin film on the top of the PVDF membrane after coating procedure. This observation indicates that the PVA film is formed on the surface of PVDF ultrafiltration membrane

SEM images of the surface views are shown in Figure 4.6. A microcracked PVA film is clearly illustrated from unmodified PVDF membrane after PVA coating (Figure 4.6 (C)). In fact, the repulsive force between hydrophilic PVA macromolecules and the PVDF hydrophobic surface does not allow the coating layer sufficiently well-bonded to the substrate surface. Such consideration is very crucial in case of micro-cracks formed at the resultant surface. On the other hand, it is clearly exemplified that hydrophilic modification of PVDF surface before PVA coating can prevent the crack formation of the resulted PVDF-PVA composite membrane. Obviously, introducing the polymerizable carboxyl groups on the TiO_2 surface has intensified the compatibilization of nanoparticles inside the PVA layer through the crosslinking reaction (M-3 and M-4). In order to investigate the dispersion quality of modified TiO_2 nanoparticles, the EDX-mapping analysis was also carried out throughout the hybrid polyamide thin films. Fig. 4.7 shows the elemental mapping images of the corresponding areas for Ti. The low density dispersion of TiO_2 was shown in Fig. 4.7(a), where 0.5 of modified nanoparticles were dispersed. While, Fig. 4.7(c) depicts the incorporation of raw TiO_2 nanoparticles into the PVA solution, results in highly dense and concentrated dispersion throughout the inner structure of PVA/ TiO_2 mixed matrix. We believe that these aggregations can be attributed to the physical adsorption of hydroxyl groups at TiO_2 surfaces.

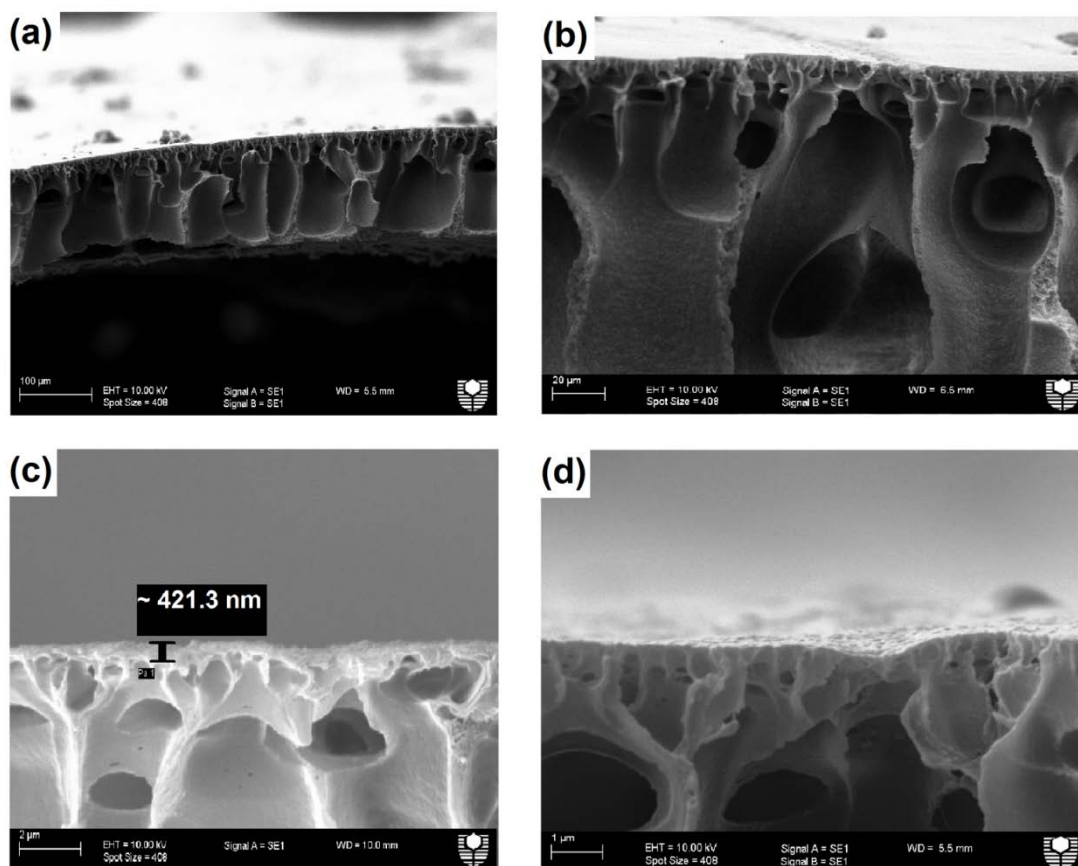


Figure 4.5 Cross-sectional SEM images of the cross-section of the M-1 (a, b and d) and M-2 (c) membranes, in different magnifications were 500 \times (a); 1000 \times (b); 3000 \times (c) and 5000 \times (d)

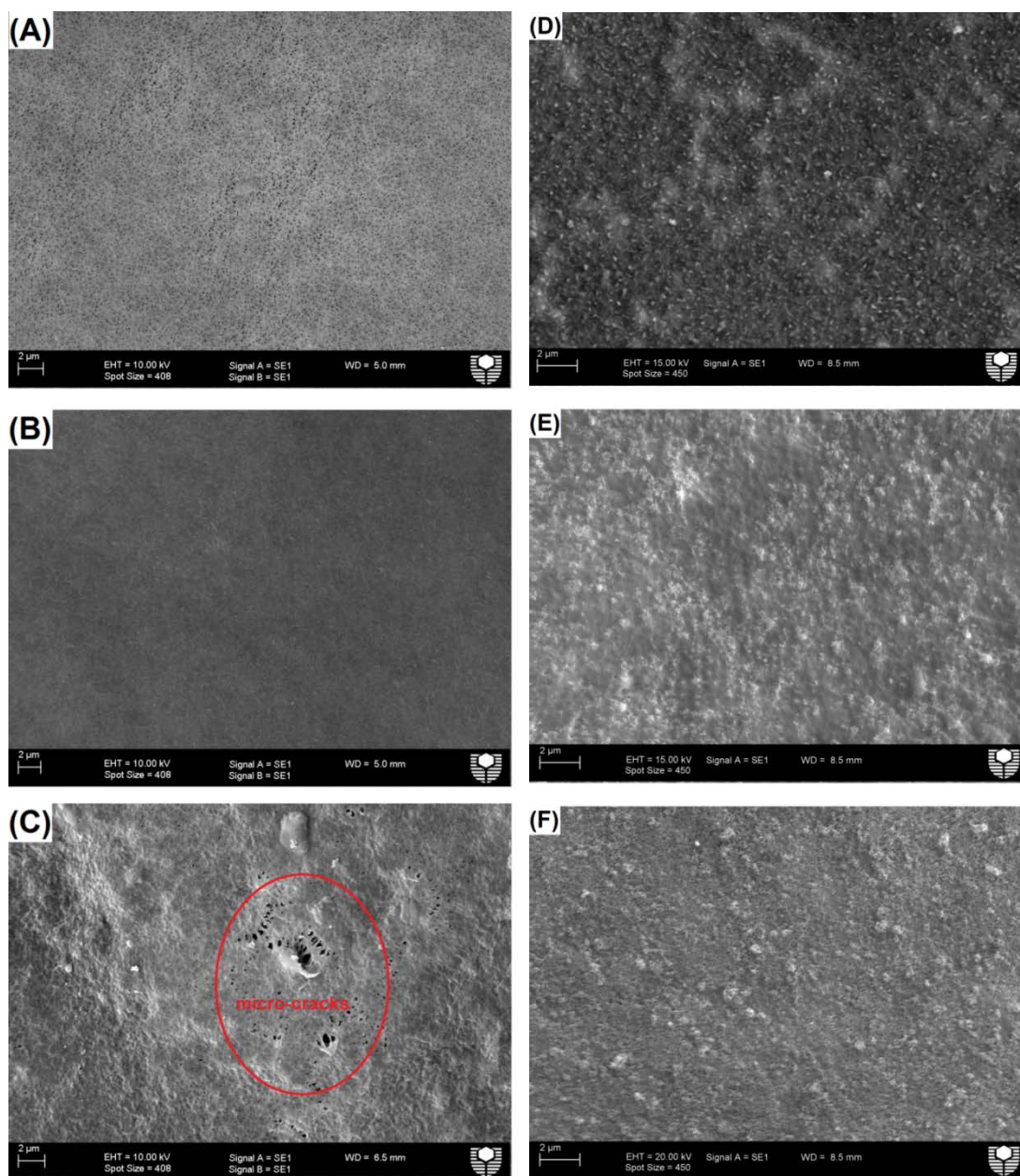


Figure 4.6 SEM surface images of composites and nanocomposites membranes: (A) M-1, (B) M-2, (C) M-2 (Supported by unmodified PVDF), (D) M-3, (E) M-4 and (F) M-5

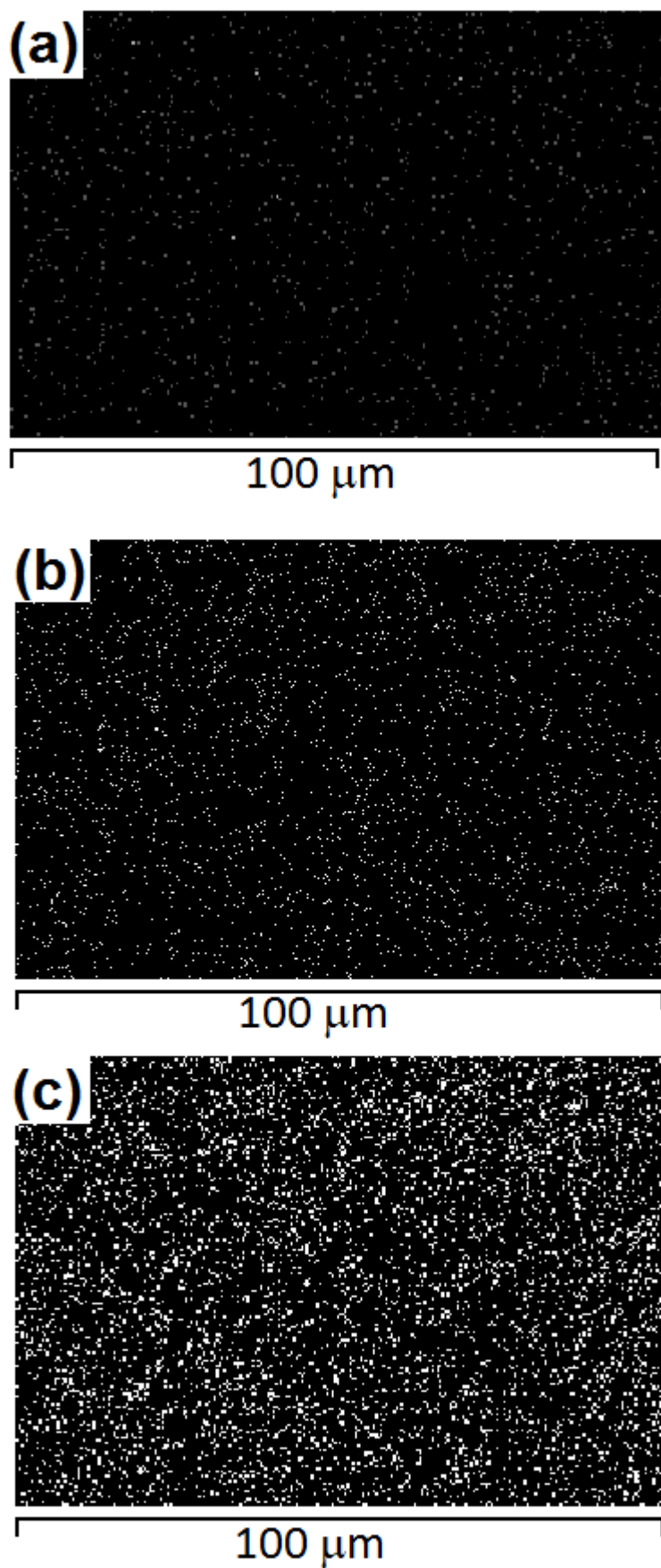


Fig. 4.7 EDX-mapping analyses of composites and nanocomposites membranes:
(a) M-3, (b) M-4 and (c) M-5

4.3.3 Membrane hydrophilicity, fouling resistance and performance evaluation

Table 4.2 shows the contact angle and the free energy of all membranes to evaluate the changes in the hydrophilicity of the membrane surface after and before modification with PVA as well as PVA-TiO₂ coating solutions. The free energy of interaction at the interface between the liquid and the surface (ΔG_{SL}) was attained by the equation given by Young–Dupré [149]:

$$(1 + \cos \theta) \gamma_L^{TOT} = -\Delta G_{SL} \quad (4.7)$$

where θ is the water contact angle at the triple air–liquid–surface contact point between a liquid drop (subscript L) and a surface (subscript S), and γ_L^{TOT} is the surface tension of water (72.8 mJ m⁻²). A quick look at contact angle data obviously reveals higher hydrophilicity of modified membranes in comparison with the hydrophobic PVDF substrate due to hydrophilic properties of the TiO₂ PVA macromolecules. For instance, the initial contact angle decreased from 76.08 (±5.0), to 57.07 (±1.04), 49.41(± 6.24), and 46.05 (±7.12), respectively as the modified TiO₂ addition into the solution was increased from 0% to 0.5 and 1.0 wt%, respectively. Consequently, the ΔG_{SL} values showed that after the TiO₂ modification by –COOH group, the membrane hydrophilicity was further improved as the contact angle was decreased to 46.05 (±7.12) with 1 wt% carboxylated-TiO₂ addition. Our results indicate that 1% of hydroxylated TiO₂ nanoparticles is an optimum amount to be added inside the PVA solution to improve its hydrophilicity but does not adversely affect the pore size distribution of the resultant composite membranes.

Table 4.2 The free energy of interaction between the surface and water droplet ($-\Delta G_{SL}$) calculated from water contact angle (θ)

Membrane	θ (°)	$-\Delta G_{SL}$ (mJ m ⁻²)
M-1	76.08 ± 5	90.3
M-2	57.07 ± 1.04	112.37
M-3	49.41 ± 6.24	120.16
M-4	46.05 ± 7.12	123.32
M-5	48.77 ± 5	120.77

Figure 4.8 describes the relationship between the pure water fluxes and the trans-membrane pressures for different kinds of composite membranes. The correlation can be described by Spiegler–Kedem Model[150]:

$$J_v = L_p (\Delta P - \sigma \Delta \Pi) \quad (4.8)$$

where J_v , L_p , ΔP , σ and $\Delta \pi$ are the water flux, the pure water permeability, the trans-membrane pressure, the reflection factor of the membrane, and the osmosis pressure, respectively. The osmotic pressure of inorganic and organic solutes is closely related to concentration polarization phenomena. However, for pure water this term is negligible. As can be seen, with the increase of the applied pressure, the permeability of all membrane samples is linearly increased, which is in a good agreement with Eq. (4.8) with average regression coefficients around 98%. Previous work implies that increasing the number of crosslinks throughout the PVA macromolecular chains will decrease its mesh size[151] and therefore result in flux declining. Indeed, incorporation of carboxylated TiO_2 nanoparticles can form a denser PVA- TiO_2 layer due to high adhesion of carboxylated nanoparticles to PVA chains, which leads to the decreased water permeability.

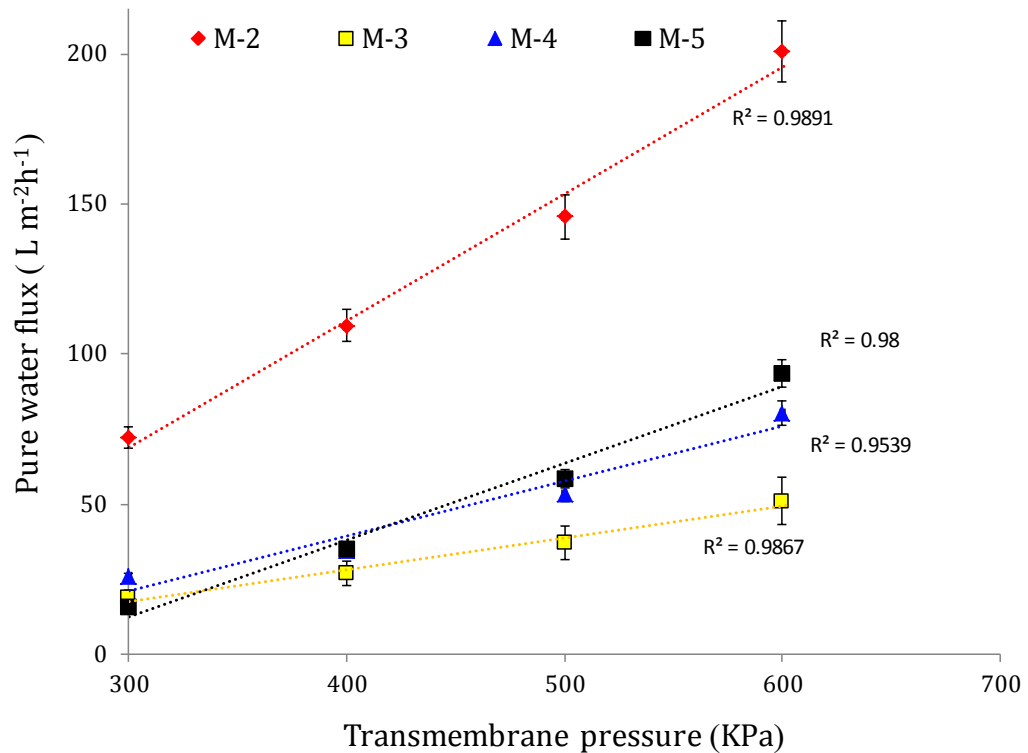


Figure 4.8 Effect of applied pressure on pure water flux values of developed membranes

Separation performance studies have been conducted to find out the membrane surface charging and sieving characteristics. The separation is influenced by both electrical (Donnan) and steric (sieving) size effects [150] as described by the extended Nernst-Planck equation[152]. Herein, PEG 2000, BSA and MgSO_4 were employed to investigate solute-to-pore size ratios and charge repulsion of the composite membranes, respectively, with results displaying in Figure 4.9. The improvement of ion repulsion as well as steric interactions in M-3 and M-4 nanocomposite membranes over M-2 membrane was clearly observed. Interestingly, an almost twofold increase in PEG rejection was achieved by incorporating 1 wt% carboxylated TiO_2 nanoparticles due to the changes of membrane pore size. However, inefficiency of raw TiO_2 into PVA matrix is perceived M-5 PEG and MgSO_4 rejection results. This can be due to the aggregation of the TiO_2 nanoparticles as a result of the van der Waals interactions between individual particles. Agglomeration and poor dispersion leads to more entanglements between TiO_2 nanoparticles and numerous nanogaps inhibiting rejection improvement.

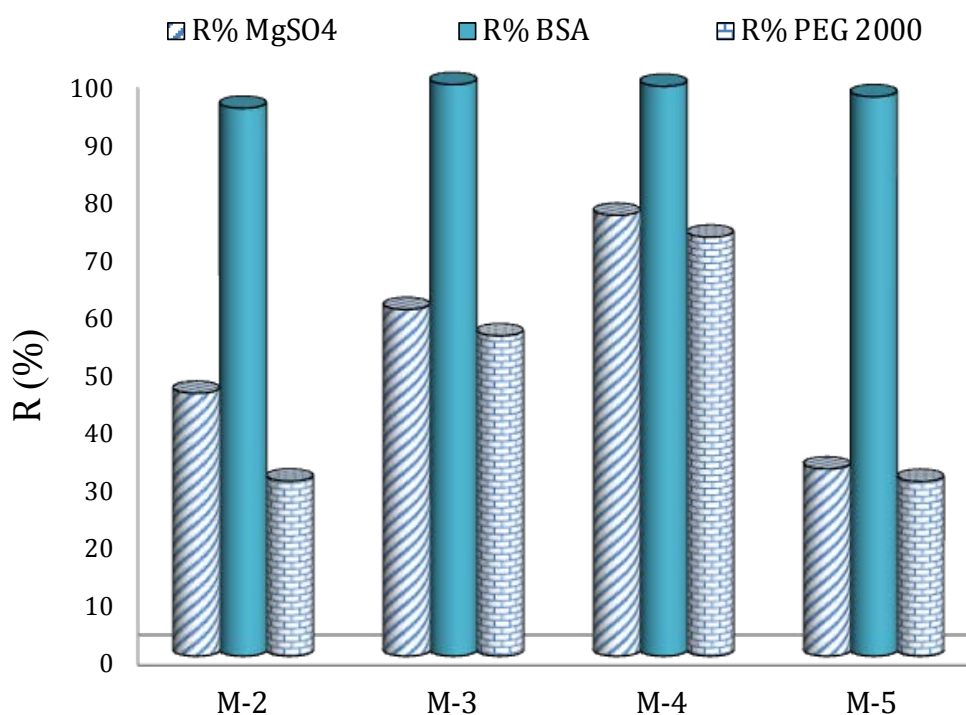


Figure 4.9 Rejection data for the composite and nanocomposite membranes

To evaluate the antifouling properties of membranes, the recovery ratios, flux losses and irreversible resistance of all membranes were calculated using BSA 200 ppm as a foulant. BSA retention data for all composite and nanocomposite membranes showed more than 95% rejection of BSA molecules in contrast to the 63% by PVDF membrane alone.

Figure 4.10 shows the BSA solution flux and pure water flux change before and after BSA filtration at different time periods. A quick look at pure water flux data reveals higher permeability of PVA composite membrane than the nanocomposite ones. This can corresponds to blockage the membrane surface pores by TiO_2 nanoparticles. However, the flux of M-1 membrane drastically decreased when pure water was switched to BSA solution. Nevertheless, for all nanocomposite membranes, the flux declining trend is not so large. The flux declining during BSA filtration can be attributed by membranes' fouling, while the effect of concentration polarization was considered negligible since a magnetic was continuously stirring over the membranes surface during the entire filtration process. The membranes' fouling caused by adsorption or deposition of the BSA macromolecules onto the membrane surface or within the pores plays the most important role for flux declining[153]. After 15 min washing, results at Figure 4.11 show that the pure water flux of the M-3 and M-4 nanocomposite membranes was mostly recovered with about 91 and 94 % respectively. By contrast, the recovery ratio for M-2 composite and PVDF membranes were only at 68% and 45%, respectively.

Based on Figure 4.11, PVDF membrane showed the highest amount of total fouling due to the hydrophobic interactions between the BSA and its hydrophobic sites. In fact, the surface of inorganic nanoparticles is less reactive to protein than organic polymer chains because of the hindrance of the protein molecules to penetrate into polymer chains.

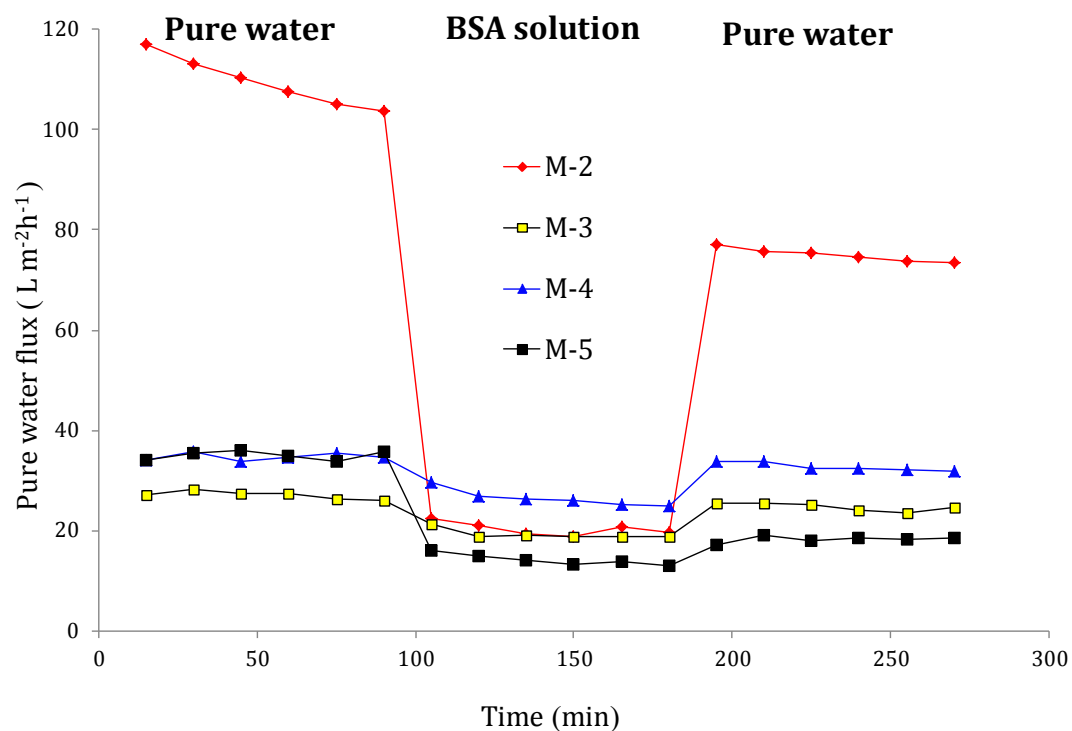


Figure 4.10 Three steps Flux versus Time for the developed membranes at 400 KPa: pure water flux for 90 min, BSA solution flux for 90 min, and pure water flux of cleaned membranes for 90 min

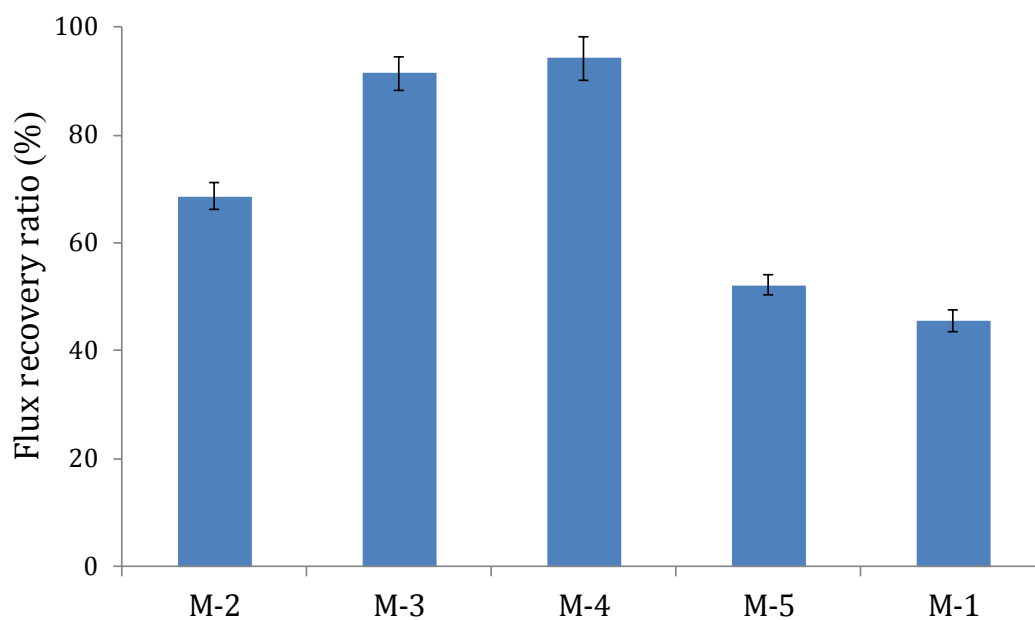


Figure 4.11 Pure water flux recovery after filtration of BSA solutions

A comparison between previews similar works and this study have also been made to highlight better understanding of the novelty of this study. Table 4.3 depicts a summary of previews literatures in compare with current study on recovery ratio for nanocomposite membranes incorporated by commercial and synthesized nanoparticles in pure and modified forms.

Figure 4.12 exhibits the total fouling ratio (R_t), reversible fouling ratio (R_r), and irreversible fouling ratio (R_{ir}) values for the all fabricated membranes. It is well known that the membranes with high hydrophilicity have lower tendency to the fouling. Therefore, hydrophobic adsorption between BSA protein and surface of TiO_2 modified membranes were diminished and deposited foulant were readily removed during filtration and washing process[154]. The obtained results clearly reveal that the total antifouling property was significantly improved by addition of TiO_2 nanoparticles. However, further improvements of total fouling resistance were also achieved by incorporating carboxylated TiO_2 nanoparticles into PVA solution. In fact, the surface of inorganic nanoparticles is less reactive to protein than organic polymer chains because of the hindrance of the protein molecules to penetrate into polymer chains.

Based on literatures the main mechanisms for fouling are adsorption of feed components accounting for reversible fouling and clogging of pores defined as irreversible fouling. According to reversible fouling data in Figure 4.11, M-5 exposes the best protein resistant surface while its total fouling value is higher than M-3 and M-4 nanocomposite membranes. This implies the irreversible fouling dominates the total fouling. It is hypothesized that, the incorporation of carboxylated nanoparticles reduces the number of active sites on which BSA molecules could be adsorbed due to covalently binding to hydroxylated nanoparticles. As a result, the possibility of interaction between BSA molecules and membrane surface will be decreased. Conversely, incorporation of raw TiO_2 nanoparticles into PVA matrix may broaden nanogaps dimension due to poor matrix-particle compatibilization which provide the membrane pores with entrapping sites for BSA molecules resulting in increasing irreversible fouling value of the M-5 membrane.

Table 4.3 Review of water flux recovery ratio (FRR) in nanocomposite membranes

FRR (%)	Inorganic nanophase	Nano-phase (wt%)	Polymer phase	Foulant	Ref.
86.2	Titania (Degussa P25)	4	poly (vinylidene fluoride) (PVDF)/sulfonated polyethersulfone (SPES)	BSA	[134]
66	Titania (Degussa P25)	2	Polyethersulfone (PES)	Non-skim milk	[155]
91.5	Silica (Sigma Aldrich, 5-15 nm)	3	Polysulfone (PSf)	Mixture of Palm oil/Tween 80/water	[156]
84	Titania (Degussa P25-aminosilane coupling agent modification)	2	Polyethersulfone (PES)	BSA	[137]
96.1	Boehmite (synthesized, 15-30 nm)	1	Polyethersulfone (PES)	whey	[157]
90.1	Boehmite (synthesized, 15-30 nm)	0.5	Polyethersulfone (PES)	whey	[157]
91.5	Alumina (10 nm)	2	poly (vinylidene fluoride) (PVDF)	Oily wastewater	[158]
87.7	Oxidized-multiwalled carbon nanotubes (MWCNTs)	0.04	Polyethersulfone (PES)	BSA	[159]
81.7	Titania (Degussa P25)	2	Polyethersulfone (PES)	whey	[160]
90.8	Titania (Degussa P25)	4	Polyethersulfone (PES)	whey	[160]
48	Amine functionalized-Multiwalled carbon nanotubes (MWCNTs)	0.5	Polyethersulfone (PES)	BSA	[161]
16.1	Polycaprolactone modified multiwall carbon nanotubes (PCL-MWCNTs)	0.5	Polyethersulfone (PES)	BSA	[162]
83	Oxidized-Multiwalled carbon nanotubes (MWCNTs) coated by synthesized Titania	1	Polyethersulfone (PES)	whey	[153]
91.5	Titania (Sigma Aldrich- carboxylated)	0.5	poly (vinylidene fluoride) (PVDF)/poly(vinyl alcohol) (PVA)	BSA	This work
94.1	Titania (Sigma Aldrich- carboxylated)	1	poly (vinylidene fluoride) (PVDF)/poly(vinyl alcohol) (PVA)	BSA	This work

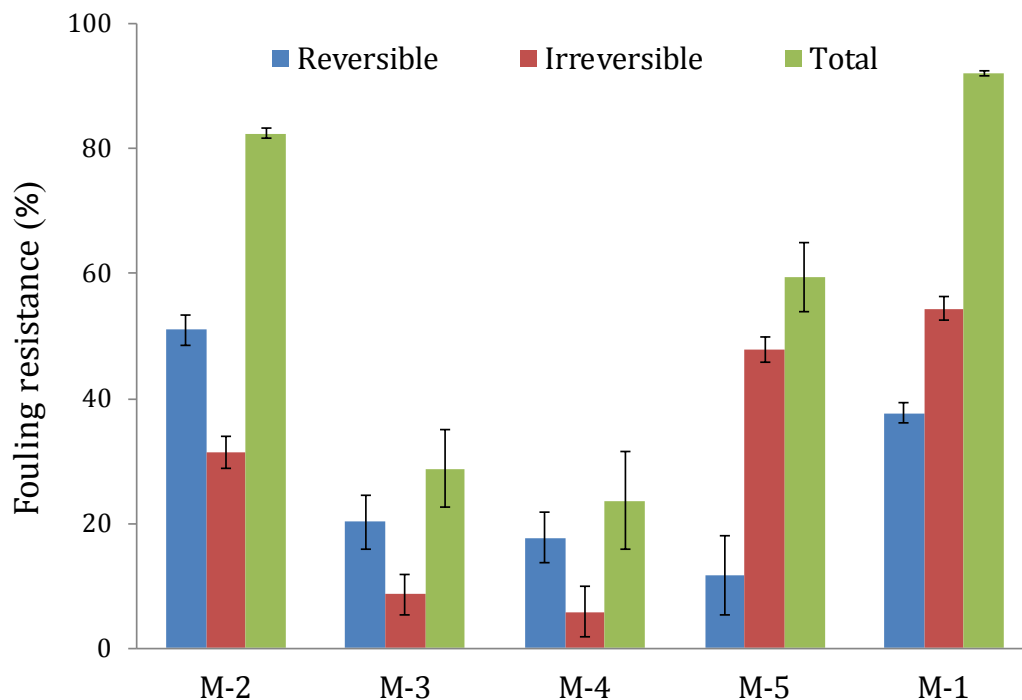


Figure 4.12 Fouling resistance ratios of all prepared membranes

4.4 Conclusion

A novel PVDF-based PVA and nanocomposite membrane with superior antifouling properties were developed using surface-modified TiO_2 nanoparticles. Surface hydrophilicity of TiO_2 nanocomposite membranes has been significantly improved. After carboxylation, the TiO_2 nanoparticles display better dispersion and adhesion with the polymer matrix membrane. The initial pure water fluxes of PVA/ TiO_2 nanocomposite membranes were lower compared to the PVA composite membrane but with significantly improved solute rejection and the antifouling properties. The best nanocomposite membrane performance was achieved by incorporating 1 wt% of carboxylated TiO_2 nanoparticles in PVA coated PVDF membranes.

Chapter 5 The effects of functionalized TiO₂ nanoparticles on properties and performance of polyimide-based thin film composite membranes in non-aqueous media

Abstract

In this chapter, a series of thin film nanocomposite solvent resistant nanofiltration membrane was developed by the conventional interfacial polymerization method on a porous polyimide support. TiO₂ nanoparticles were used as inorganic fillers into polyamide chain network. TiO₂ nanoparticles' surfaces were functionalized in order to improve their compatibilization inside the polyamide matrix. For this purpose, monoethanolamine (MEOA) and triethylenetetramine (TETA) agents were applied to aminate TiO₂ nanoparticles, while thionyl chloride (TCl) was used to chlorinateation. The morphologies and surface properties of IP-based membranes were characterised with Scanning Electron Microscopy (SEM) equipped with Energy Dispersive X-Ray Spectrometer (EDX). SEM images identified various topographies by incorporation of different TiO₂ nanoparticles. EDX-mapping analysis was also carried out to investigate the dispersion quality of the functionalized TiO₂ nanoparticles throughout the hybrid polyamide thin films. Mass transport properties of membranes were evaluated by two different dyes; positively-charged Crystal Violet (CV) (408 Da) and neutral Bromothymol Blue (BTB) (624 Da). Interestingly, the TFN membrane attained by the incorporation of TETA-functionalized TiO₂ nanoparticles (TETA-TFN) gave the best CV rejection (93.2%), while the lowest BTB rejection (80%). In case of TFN membrane fabricated by TCl-modified TiO₂ (TCl-TFN), roughly high levels of solute/dye rejections were achieved; where BTB and CV rejections were about 90 and 93% respectively. Further, this membrane represented the lowest permeability of either CV or BTB with about 97 Kg m⁻² h⁻¹ which can be attributed to formation of a dense structure after exposing the chlorinated TiO₂ nanoparticles into interfacial polymerization reaction on membrane surfaces.

5.1 Introduction

Nanofiltration membrane persistent to organic solvents has been recently considered as a high potential and low-cost platform for numerous applications including: pharmaceutical processing [163, 164], catalyst recovery [165], biofuels purification [166-168], organophilic dyes[169], and the separation of wide range of organic molecules which have molecular weight (MW) in the range of 200–1000 Da [170, 171].

These membrane materials are generally classified as ceramic [172, 173], polymer-silicone composite (PDMS)[174] and polymer [175, 176]. The interest of polymeric solvent resistant nanofiltration membranes is sharply increasing since the fabrication process is cost-effective and reproducible. Among these SRNF membranes mostly used in non-aqueous systems, two typical types are the membranes containing 10 to 30 wt% polymer in asymmetric skin layer fabricated by a phase inversion process induced by immersion precipitation technique [177] and polyamide composite membranes comprising a thin polymeric film formed by interfacial polymerization on a porous support [178].

Among all applicable polymeric supports in non-aqueous media, polyimide membrane possess ideal properties including excellent stability at relatively high temperatures excess of 300°C, high mechanical strength, and highly resistance to various solvents. However, the hydrophobic intrinsic of PI causes an insufficient wetting ability and adsorption of solutes onto the exposed surface in polar and semipolar systems. To overcome this issue, surface modification is frequently applied to induce hydrophilic covalently bound chemical groups on PI surface [179].

Recently, cross-linking of polyimides with polyethyleneimine (PEI) demonstrates a promising approach to prepare a positively charged membrane due to the existence of free amine group at the membrane surface. In particular, polyimide surface can be cross-linked by reacting with primary and secondary amines to improve the membrane separation efficiency and solvent resistance [180]. Vanherck et al. [181] investigated the effect of both post and simultaneous crosslinking treatment of polyimide support with diamine solution. They found an optimal crosslinking

condition by eliminating the additional post-synthesis step through dissolving diamine crosslinkers in the aqueous coagulation bath. In another different study, Kosaraju and Sirkar proposed propylene (PP)-based thin film composite SRNF membrane using interfacial polymerization reaction between poly(ethyleneimine) and isophthaloyl dichloride (IPD) [182]. These PP based TFC SRNF membranes have two obvious advantages. First, taking advantages of polypropylene endurance including high pH resistance, thermal, chemical and solvent stability which allow the use of the TFC membranes in solvent-stable nanofiltration; second, improving the hydrophilicity and selectivity of PP support for separation of organic dyes. The use of nanoparticles in the manufacturing process of polymeric membranes has received much attention as a new method to improve the flux and selectivity by assembling engineered nanoparticles throughout the surface or bulk structure[183]. Soroko and Livingston[183] reported the effect of the dispersed TiO_2 nanoparticles in polyimide matrix on the membrane preparation and performance. They found that the kinetics of the liquid–liquid demixing was delayed by introducing the TiO_2 nanoparticles as a nucleating agent. Roy et al.[184] fabricated high flux TFC solvent-resistant nanofiltration membranes using both hydrophilized and hydrophobized multi-walled carbon nanotubes (MWCNTs). The transport corridor between MWCNTs (nanogaps) and the surrounding polymer chains could also be optimised to reduce the resistance for solvent and water transport.

In this chapter, thin film composite and thin film nanocomposite solvent resistant nanofiltration membrane has been developed by conventional interfacial polymerization method on a porous polyimide support. Isophthaloyl chloride and ethylenediamine were employed as the organic and aqueous phase, respectively. TiO_2 nanoparticles were used as inorganic fillers into polyamide selective layer.

5.2 Experimental

5.2.1 Materials and Chemicals

Lenzing P84 polyimide (HP Polymers GmbH), n-dimethylformamide (DMF), monoethanolamine (MEOA) and, thionyl chloride (TCl), isophthaloyl chloride (IPC), ethylenediamine (EDA), tetrahydrofuran (THF), isopropyl alcohol (IPA), ethanol and methanol from Merck were used. Triethylenetetramine (TETA), crystal violet (CV) ($M_w = 408$ Da) and Bromothymol Blue (BTB) ($M_w = 624$ Da) purchased from Sigma Aldrich. Titanium dioxide nanoparticles (TiO_2 , particle size of 20 nm) was obtained from Degussa and Merck. Distilled water was used throughout this study.

5.2.2 TiO_2 functionalization procedure

Briefly, one gram of dry TiO_2 was placed in 200 ml of a 20:1 mixture of TCl and DMF. The solution was stirred overnight at ambient temperature. The resulting powder was washed with THF to remove excess TCl. After the acyl chlorination, TiO_2 nanoparticles from the solution were centrifuged at 10000 rpm for 15 min. The resulting particles were then dried in an oven at 100 °C for 24 h. As it is mentioned earlier, TCl was used as a coupling agent to chlorination of TiO_2 nanoparticles.

For amine functionalization of acyl chlorinated TiO_2 nanoparticles, two different amine agents were intentionally employed. Therefore, MEOA and TETA were used to prognosticate the relevancy of the number of amine functions on the surface of the resultant membranes. For each amine solution, 200 mg of dried acyl chlorinated TiO_2 nanoparticles were reacted with 100 ml amine and ethanol solution at 70°C for 5 h. After cooling to room temperature, the MWNTs were washed with pure ethanol for several times to remove excess amines. The product was then grounded with a mortar and pestle. The presence of organic groups on the surface of modified nanoparticles was confirmed by FTIR.

5.2.3 Ultrafiltration Polyimide (PI) membranes preparation

For the preparation of asymmetric PI ultrafiltration membrane as a solvent resistant support, a viscous solution consisting of 18 wt.% polyimide and dimethylformamide was stirred at speed of 200 rpm for 8 h at around 50 °C until the solution became completely homogenous. The polymer solution was allowed to stand for overnight at ambient temperature to remove air bubbles. The solution was sprinkled and cast using a homemade casting knife with 75 µm thickness on polyester non-woven fabric and then was moved to the non-solvent bath containing pure water for precipitation at room temperature. The prepared membranes were washed and stored in water bath for at least 1 day to completely leach out the residual solvents and additives. At the final stage, membrane was dried by placing between two sheets of filter paper for 24 h at room temperature.

5.2.4 Fabrication of TFC and TFN SRNF membranes

Preparation of TFC and TFN membranes has been accomplished by two stages. Firstly, the rudimentary poly (ethyleneimine) coating step was carried out on all polyimide UF supports as follows. Flat PI membranes were soaked with the 0.1 wt% PEI aqueous mixture of IPA and water (1:1 by volume ratio) for about 30 min and then thermally cured at 110 °C. To prepare pure co-polyamide composite membrane, the polyimide UF support was immersed in aqueous solution containing 2 wt% EDA for 5 min. In order to remove excess solution and eliminate any bubbles from the membrane surfaces, the submerged membranes were kept vertically for 1 min and then wiped off with a soft sponge in one direction. The saturated membrane was then drenched into 0.1 wt% IPC in *n*-hexane solution. After 60 soaking, the obtained membrane was cured at 80 °C for 5 min to ensure interfacial reaction fully completed. TiO₂ polyamide nanocomposite membranes were prepared by the same procedure as above, except that certain amount of aminated and chlorinated TiO₂ nanoparticles were dispersed in EDA and IPC solution, respectively. In order to reach good dispersion of nanoparticles, ultrasonication bath was employed for 1 hour at ambient temperature immediately prior to the interfacial polymerization. A Summary of the TFC and TFN membranes' recipes was shown in Table 5.1.

Table 5.1 Fabrication recipes of the TFC and TFN SRNF membranes

Membrane	PI (wt. %)	PEI (wt. %)	EDA (wt. %)	IPC (wt. %)
TFC	18	1	2	0.1
MEOA-TFN	18	1	2	0.1
TETA-TFN	18	1	2	0.1
TCI-TFN	18	1	2	0.1

5.2.5 Characterization of SRNF membranes

In order to identify the functional groups on the modified TiO₂ nanoparticles, FTIR spectra were obtained for spectroscopic investigation. All FT-IR spectra were recorded by the attenuated total reflection (ATR) technique using Bruker-IFS 48 FTIR spectrometer (Ettlingen, Germany) with horizontal ATR device (Ge, 45°). The spectrum was scanned from 1200 to 4000 cm⁻¹ at 4 cm⁻¹ resolution for the modified nanoparticles. The hydrophilicity of original TFC and TFN SRNF membranes were analyzed to examine the variations in wetting characteristics of membranes. The contact angles between water and surfaces of membranes were obtained using a contact angle measuring instrument (KSV Cam Optical Contact Angle and Pendant Drop Surface Tension Software Version 3.81, Finland) for evaluation of membrane hydrophilicity. De-ionized water was used as the probe liquid in all measurements. To minimize the experimental error, the contact angle was measured at three random locations for each sample and then the average value was reported. Top surface and cross-section of SRNF membranes was inspected by (Zeiss EVO 40XVP) scanning electron microscopes (SEM). Pt sputtered coating was performed on the samples under vacuum before the morphological observation. The elemental composition analysis was conducted using an EDS X-ray detector equipped by the scanning electron microscopy. The AFM images were obtained using a DualScopeTM scanning probe-optical microscope (DME model C-21, Denmark). Small squares of prepared membranes (approximately 1 cm²) were cut and glued on glass substrate. The membrane surfaces were imaged in a scan size of 10 μm × 10 μm. The surface

roughness parameters of the membranes which are expressed in terms of the mean roughness (S_a), the root mean square of the Z data (S_q) and the mean difference between the five highest peaks and lowest valleys (S_z) were calculated from AFM images by SPM DME software at scan area of $10\ \mu\text{m} \times 10\ \mu\text{m}$.

All filtration experiments were carried out in a batch stirred cell as described elsewhere [185]. The flux and rejection of all membranes were determined under the 5 bars transmembrane pressure (P) at room temperature at fixed speed of 200 rpm. The flux (J) through the membrane may be described by the following equation:

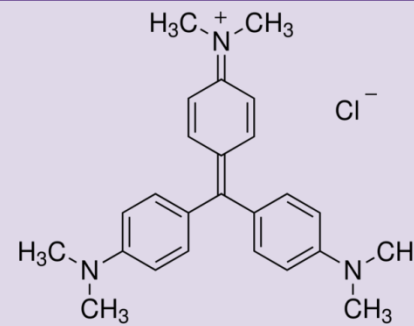
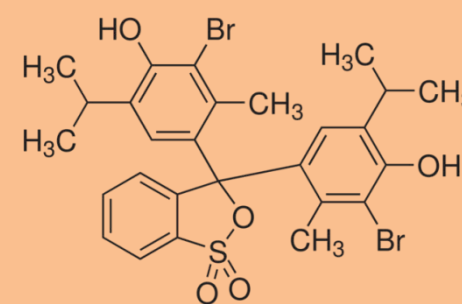
$$J = \frac{m}{(A\Delta t)} \quad (1)$$

where m (kg) is the total mass of permeate collected under transmembrane pressure P (bar) in a time scale Δt (h) and A is the effective area of membrane (m^2). The 50 ppm Bromothymol Blue (BTB) and 10 ppm of crystal violet (CV) were used as the feeds for SRNFs performance evaluation. All dyes properties were presented in Table 5.2. The dyes rejection ratio was calculated via the following the equation:

$$R(\%) = \left(1 - \frac{C_{dye}^{permeate}}{C_{dye}^{feed}}\right) \times 100 \quad (2)$$

where $C_{dye}^{permeate}$ and C_{dye}^{feed} represent dyes concentrations in permeate and feed solutions, respectively, measured by a UV–vis spectrophotometer (U-2800, Hitachi, Japan).

Table 5.2 Molecular structures and physical properties of Dye-Solutes in this study

Reagent dye M_w (g/mol)	UV absorption (λ_{\max})	Dyes structure
Crystal Violet [⊕] (407.98)	595 nm	
Bromothymol Blue [∘] (624.38)	420 nm	

5.3 Results and discussion

5.3.1 FTIR analysis

FTIR adsorption was carried out to investigate that the surface modification of TiO₂ nanoparticles with different function groups. According to Figure 5.1, the band at about 2870 cm⁻¹ observed in both samples can be assigned to the stretching from methylene groups (-CH₂-). It is also observed that only TETA-TiO₂ shows significant N-H bending at 1460 cm⁻¹ arising from secondary-amine (R-NH-R') in triethyrtetramine structure. Besides, band at around 1640 cm⁻¹ can be associated with primary-amine (R-NH₂) bending vibration in both MEOA and TETA modified TiO₂ samples. Meanwhile the peak at about 3450 cm⁻¹ is ascribable to the primary and secondary amine stretching.

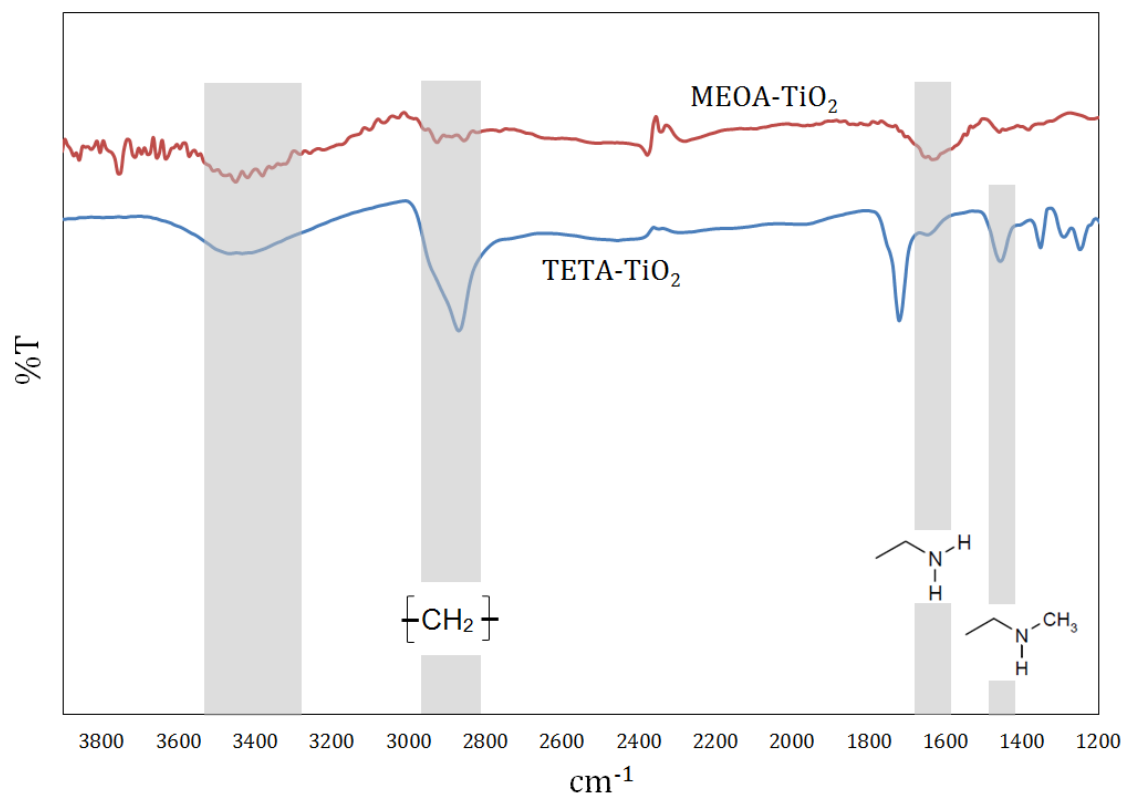


Figure 5.1 ATR-FTIR spectra of aminated TiO_2 nanoparticles

5.3.2 Membrane surface morphology

Figure 5.2 (a) represents a typical asymmetric structure of the TFN SRNF membrane originated from complete phase inversion of homogenous PI solution. As it is known, the presence of macro-voids in the sub layer would lead to higher porous structure as well as higher permeability for the membranes. Images at higher magnification reveal the establishment of distinctive layers on the surface of composite membrane. A dense film with a thickness less than $2\ \mu\text{m}$ is clearly shown in Figure 5.2(b) which was formed during the immersion of PI substrate into the 1 wt% PEI coating solution. Furthermore, Figure 5.2 (c) yields the formation of ultra-thin skin layer with about 100 nm thickness by the careful controlling of the interfacial polycondensation of ethylenediamine with isophthaloyl chloride. Fig. 3(a-d) shows top view SEM images of TFC and TFN surfaces on polyimide support. Based on Fig. 2 (a) it can be seen that a relatively smooth and homogeneous skin layer was uniformly coated on the porous substrate. This structure completely changed to the typical dense “nodular” structure after exposing the chlorinated

TiO₂ nanoparticles into interfacial polymerization reaction on membrane surfaces (Figure 5.3(b)). The formation of the more nodular as well as denser structure is more remarkable on TCI-TFN surface (Figure 5.3 (b)) compared to the original TFC membrane (Figure 5.3 (a)) which can be evidence for potentiality in achieving higher solute rejection[101]. Figure 5.3 (c and d) exhibits relatively ridge-and-valley structure obtained from amine-modified TiO₂ nanoparticles. In case of MEOA-TFN (Figure 5.3 (c)), uniform distribution of some spherical and cylindrical shapes on the surface is clearly seen.

Besides, the TETA-TFN membrane prepared with the involvement of triethylenetetramine attached on TiO₂ surface represents the roughest surface among all thin films with lots of “leaf-like” peaks on it. This morphology can be expected from substantial interaction between the external surfaces of amine-coated TiO₂ nanoparticles and the polyamide matrix during polymerization reaction.

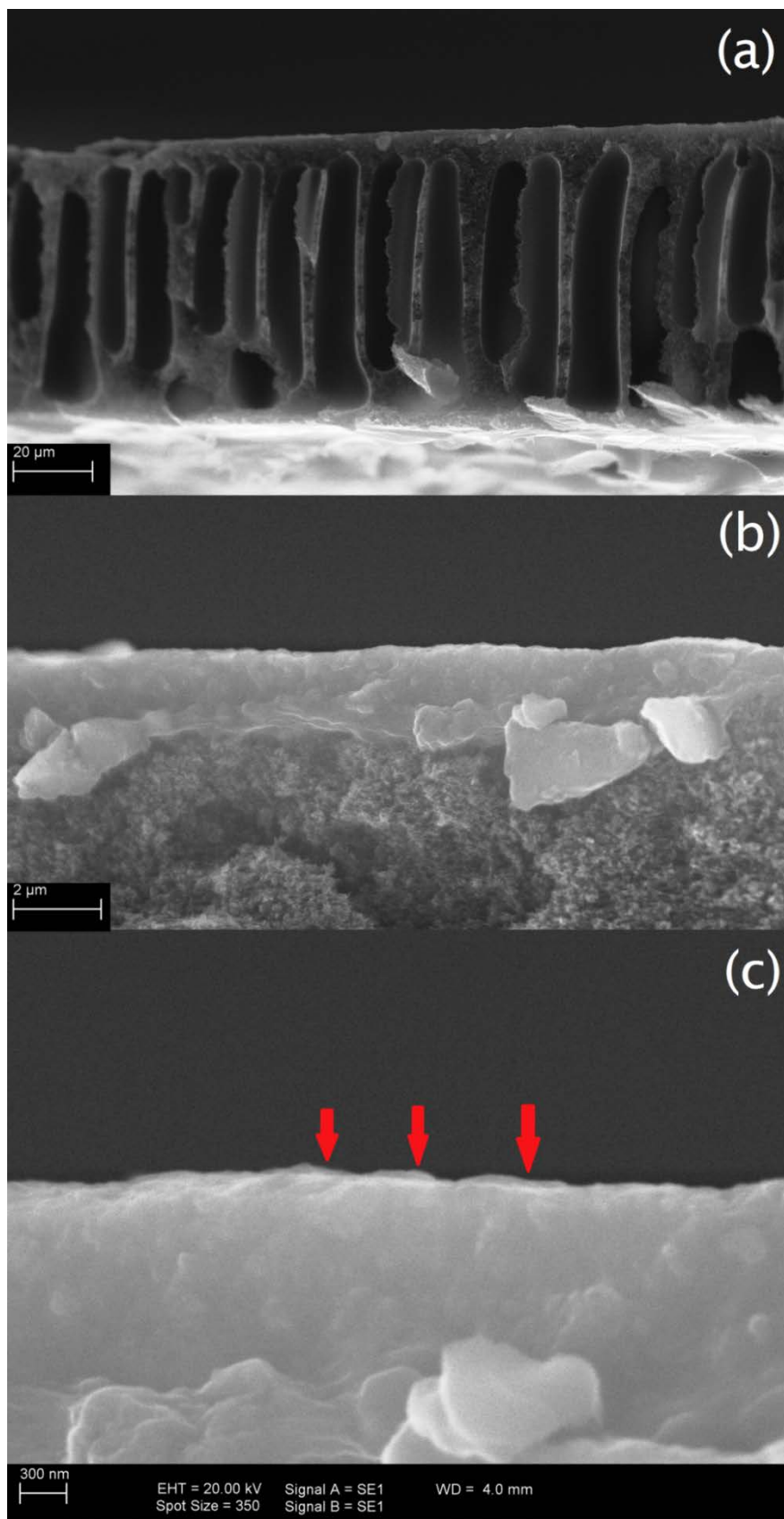


Figure 5.2 SEM images of the cross-section of the TFC SRNF membrane, in different magnifications were 1000 \times (top); 5000 \times (middle) and 20000 \times (bottom).

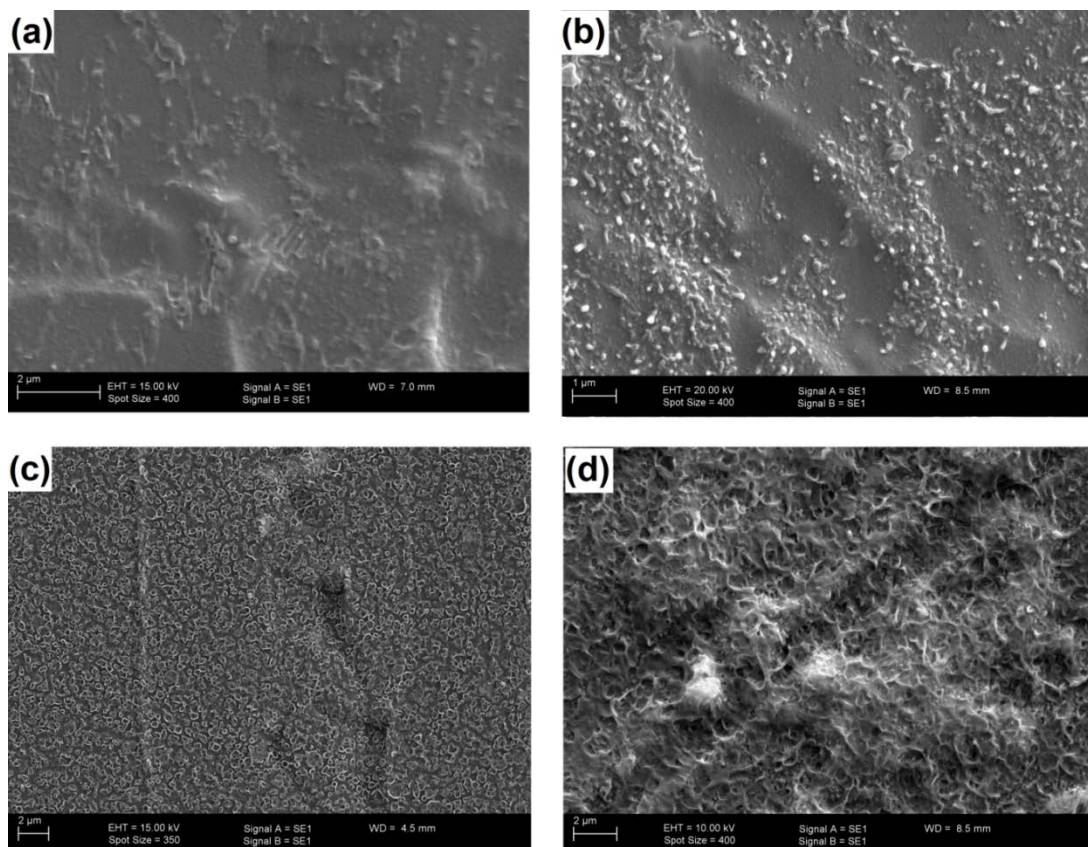


Figure 5.3 Surface SEM images of the TFC and TFN SRNF membranes

In order to investigate the dispersion quality of modified TiO_2 nanoparticles, the EDX-mapping analysis was also carried out on the hybrid polyamide thin films. Figure 5.4 shows the elemental mapping images of the corresponding areas for Ti. The low density dispersion of chlorinated TiO_2 nanoparticles has been obtained in case of TCI-TFN. The incorporation of modified TiO_2 nanoparticles into the aqueous solution (TEOA-TFN and TETA-TFN) results in the ununiformed and specifically highly dense and concentrated dispersion in case of TETA-TFN throughout the inner structure of polyamide matrix. We believe that these aggregations can be attributed to the physical adsorption of amine agent's molecules (i.e., monoethylamine and triethylenetetramine) at TiO_2 surfaces. A schematic of a single TETA molecule linking two TiO_2 nanoparticles is presented in this figure. In part (A) of the same figure, the amine is physically linked to the TiO_2 surface through the amine groups and no chemical linkage is established between the TiO_2 nanoparticles. While in part (B), the formation of long amine chain grafted on nanoparticle surfaces is illustrated. This allows for TiO_2 nanoparticles to be easily dispersed into polymer Matrix.

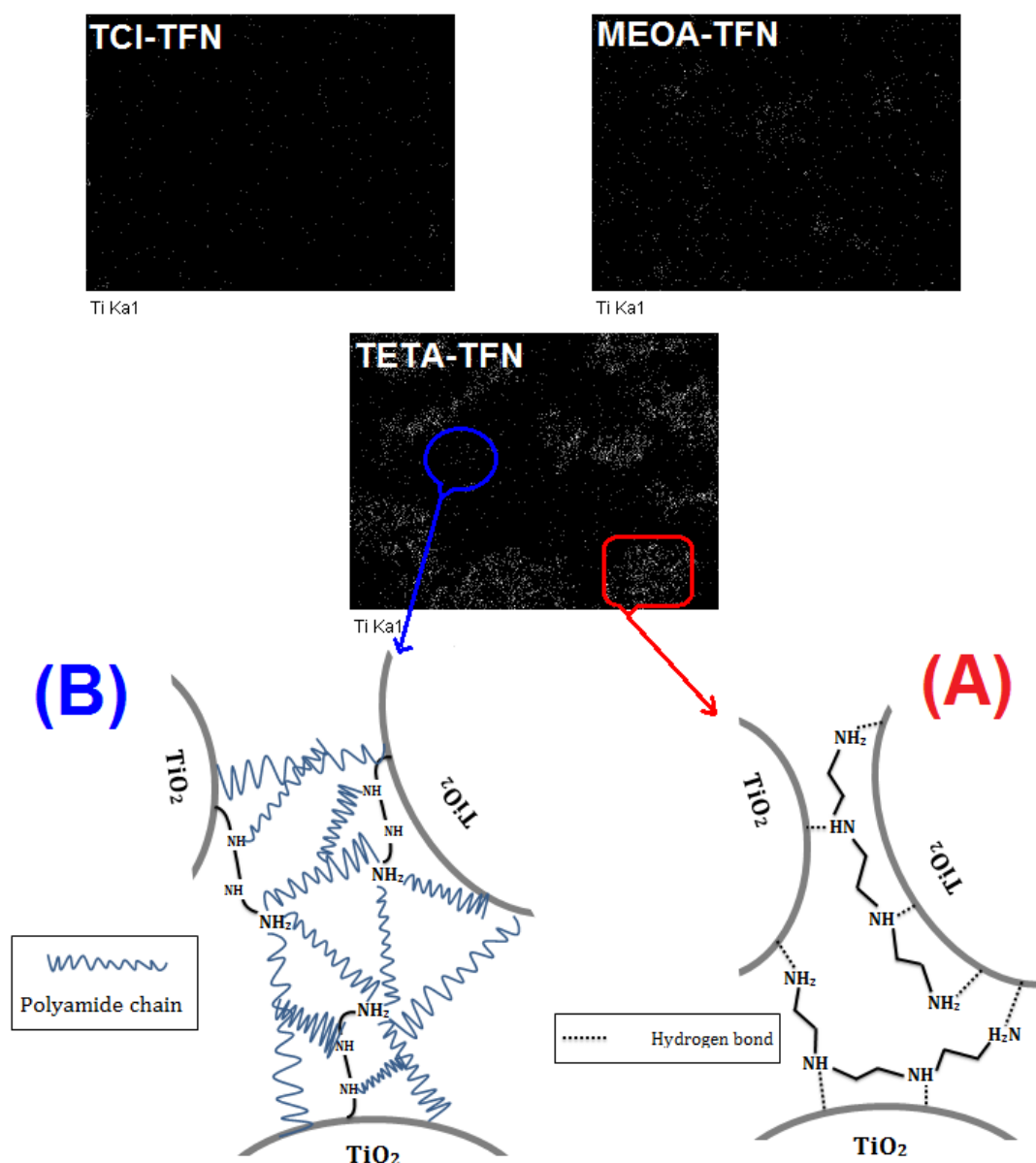


Figure 5.4 EDX-mapping analyses of nanocomposite SRNF membranes and schematic settlements of (A) physical, (B) chemical functionalization of TiO_2 nanoparticles by TETA

To investigate the topography of the fabricated membranes in a higher resolution, AFM imaging was also been performed at a small scan size of $10\mu\text{m} \times 10\mu\text{m}$. Table 5.3 reveals the surface roughness parameters of the membranes in terms of average roughness (S_a), root mean square roughness (S_q) and the mean difference between the five highest peaks and lowest valleys (S_z). A somewhat homogeneous bright and

dark areas corresponding to the peak and valleys, respectively, is clearly shown in all 3D AFM images (Figure 5.5). Interestingly, by the incorporation of TiO_2 nanoparticles with different chemistry, the variety of topography was obtained. The formation of various topographies demonstrates that the interfacial crosslinking reaction was successfully interfered by surface modification of TiO_2 nanoparticles. Based on Table 5.3, the roughest morphology is ascribable to TETA-TFN, while TFC membrane fabricated without TiO_2 nanoparticles incorporation represents the smoothest surface among all samples. Herein, we believe that the degree of crosslinking will be abounding with presence of the chemical functions on TiO_2 surface similar to chemical groups involving in amidation reaction. The comparison of the roughness profile between TEOA-TFN and TETA-TFN membranes reveals a significant increase in the value of S_z . This can be related to the presence of more amine groups in TETA, which leads to more progression in crosslinking reaction. Moreover, it should be noted that the nanoparticle surface modification with functional groups similar to crosslinking agents can also amplify the compatibilization of particles inside the polymer matrix.

Table 5.3 Surface roughness parameters of the TFC and TFN SRNF membranes

Membrane	Roughness		
	S_a (nm)	S_q (nm)	S_z (nm)
TFC	34	44.76	374.1
MEOA-TFN	48.41	64.9	541.2
TETA-TFN	82.36	104.46	695.75
TCI-TFN	62.52	78.2	556.17

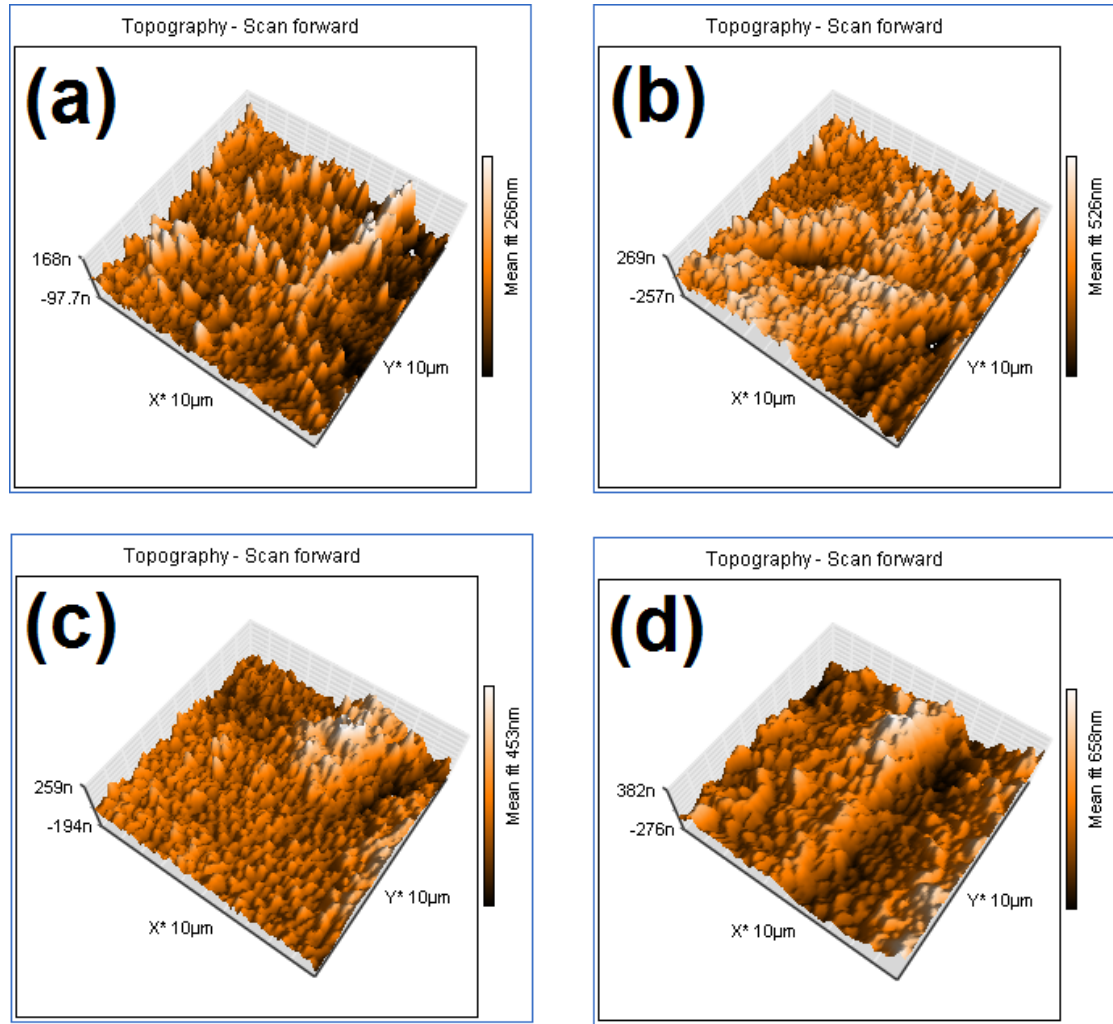


Figure 5.5 Three dimensional AFM images for the TFC and TFN SRNF membranes

5.3.3 Membrane hydrophilicity and performance evaluation

Flux and rejection behaviours for TFC and TFN membranes were evaluated by pure methanol and two different solute/dye solutions including Crystal Violet and neutral Bromothymol Blue. Figure 5.6 depicts the obvious high methanol flux in case of TETA-TFN and MEOA-TFN membranes equal to 110 and 107.6 Kg m⁻² h⁻¹ respectively. Meanwhile, the higher hydrophilicity of TETA-TFN than MEOA-TFN has also been approved by water contact angle data (Table 5.4). Besides that, TCl-TFN membrane yields 99.4 Kg m⁻² h⁻¹ methanol flux which is even lower than TFC membrane flux of 100.8 Kg m⁻² h⁻¹. On the other hand, the permeate flux is somewhat lower than the permeability for pure methanol because of the frictional

forces introduced by the solute to oppose the flux [186]. TETA-TFN and MEOA-TFN are yielding higher flux than TFC and TCI-TFN membranes.

We believe that these differences are caused by two key factors. Firstly, the rate of *IP* reaction interference by functionalized TiO_2 nanoparticles can result in the existence of so-called nanogaps between nanoparticles and polymeric phase. Secondly, deposition and affinity bindings between the external surfaces of functionalized TiO_2 nanoparticles and the surrounding polyamide chain could result denser polyamide structure. The flux increasing tendency can be interpreted by the interference of *IP* reaction with the amine-functionalized incorporation in aqueous phase. As a matter of fact, high density of amine groups on nanoparticle surfaces interact with polyamide matrix during *IP* reaction. Therefore, the adsorptive interactions of amine groups on the surface of TiO_2 nanoparticles around the aqueous-organic phase interface will accelerate the formation of dense polyamide thin film [184].

On the other hand, the incorporation of chlorinated TiO_2 nanoparticles into IPC organic solution would lead to the formation of a denser hybrid polyamide layer with reduced flux. Interestingly, the chlorination of TiO_2 nanoparticles would prevent the aggregation and consequently cause flux increasing. Moreover, due to the high amidation tendency of acyl chloride groups of IPC in amine solution, chlorine functions on TiO_2 nanoparticles are not able to strongly react with ethylenediamine. Instability of chlorinated- TiO_2 nanoparticles at aqueous-organic interface would also lead to the quicker hydroxylation of chlorine groups at nanoparticles' surfaces. Therefore, the anticipated hydrogen bindings between the hydroxylated nanoparticles and both carboxyl and amide groups of polyamide chain would lead to the formation of a dense TiO_2 -polyamide skin layer with flux declining.

Hydrophilicity measurements of SRNFs also confirm this interpretation. Accordingly, Table 5.4 shows lower water contact angle for TCI-TFN membrane than TETA-TFN and MEOA-TFN membranes which can be the result of the existence high dense hydroxyl groups on the resultant polyamide surface. However, the highest hydrophilicity is ascribable to TFC membrane where the higher density of hydrophilic amide groups in comparison with TFN membranes.

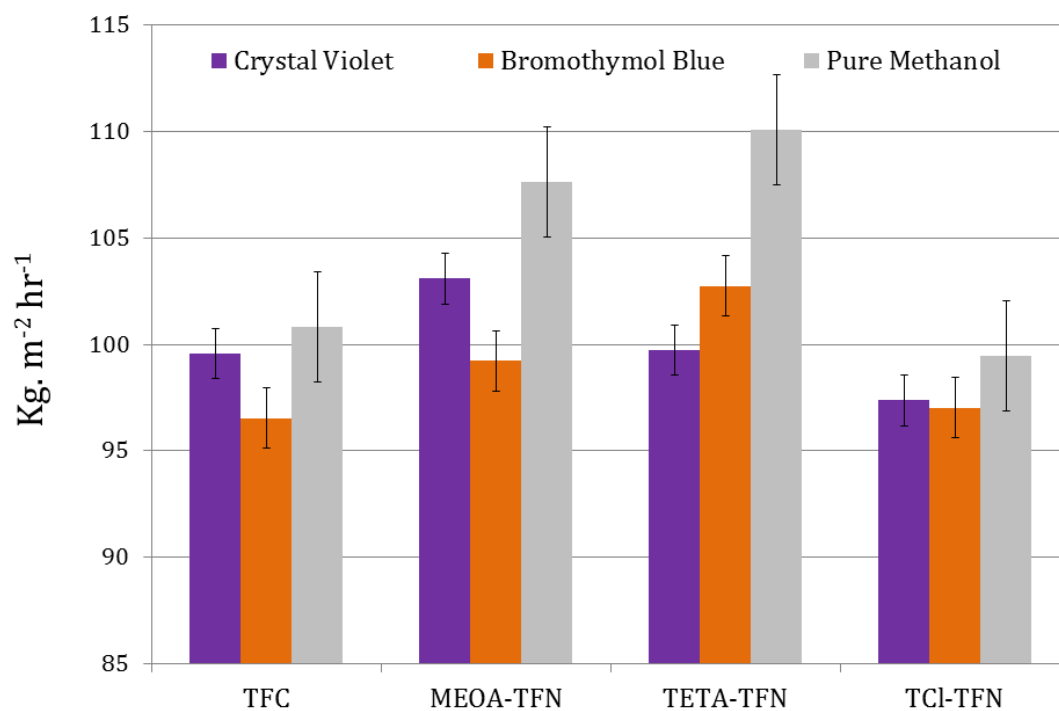


Figure 5.6 Fluxes of pure solvent (methanol) and two employed dye-solutes for composite and nanocomposite SRNF membranes

Table 5.4 Water contact angle measurements for the TFC and TFN SRNF membranes

Membrane	Contact angle (°)
TFC	49.32
MEOA-TFN	78.48
TETA-TFN	65.65
MEOA-TCI	63.37

The corresponding dye rejection results are shown in Figure 5.7. Rejection data for BTB can be interpreted by sieving mechanism across the membrane as it is uncharged solute/dye. For example, as there are no inorganic phase defects and consequent nanogaps in TFC membrane, the highest retention of BTB of 94.7% was illustrated. In case of TFN membranes, the more uniform dispersion of TiO_2 nanoparticles, the fewer nanogaps and consequently the more BTB rejection is achieved. Likewise, TETA-TFN showed lower BTB retention (79.9%) than MEOA-TFN (89.7%). These results are also in good agreement with dispersion quality observations obtained by EDX-mapping analysis (Figure 5.4).

On the other hand, the Crystal Violet which is positively charged dye in which both sieving and steric effects have to be considered for rejection analysis. As it is known, deposition of polyethyleneimine results in self-assembly formation of the positively charged layer on the Polyimide substrate[187]. The interfacial crosslinking of ethylenediamine and Isophthaloyl chloride produces a weak negatively charged placement of cross-linked subsurface throughout the PEI layer. Therefore, the resultant co-polyamide matrix exposed to feed solution acts as a denser layer with less positive charges than PEI. For that reason, the highest CV rejection is speculated upon TETA-TFN. We postulate that this can be due to the influence of positive charge accumulation of TETA-functionalized TiO_2 nanoparticles throughout the outermost cross-linked layer. TFC and MEOA-TFN exhibit somewhat the lowest percentage of CV rejection, equal to 76 and 74% respectively. The steric mechanism is also playing vital role where the molecular weight and consequently estimated molecular dimensions of crystal violet is lower than bromothymol blue. Therefore, the retention was declined for CV dye. In case of TCI-TFN, solute rejections remain roughly unaffected for both BTB (92.7%) and CV (90.1%). As it is mentioned earlier, this can be attributed to the formation of denser skin separation layer due to hydrogen bindings of hydroxylated nanoparticles to carboxyl, amine and amide groups of resultant polyamide network.

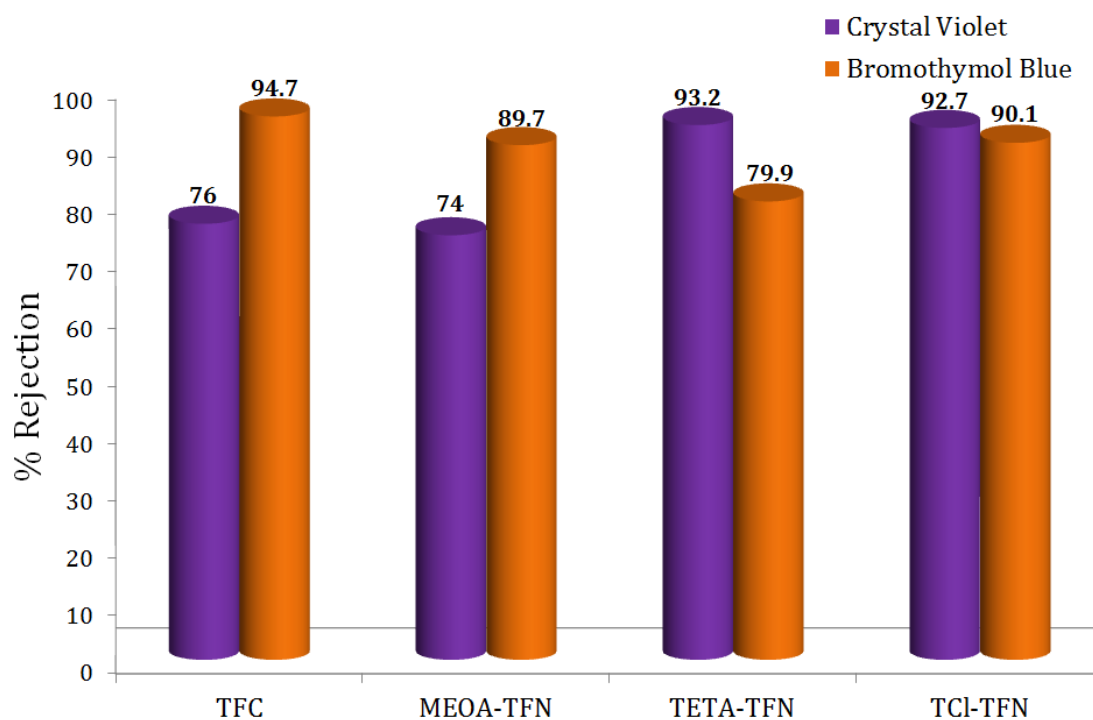


Figure 5.7 Dye-solute rejection behaviours of the TFC and TFN SRNF membranes

5.4 Conclusion

Novel thin film nanocomposite solvent resistant nanofiltration membranes were developed by interfacial polymerization method in the presence of TiO_2 nanoparticles on the porous polyimide support coated by polyethyleneimine. FTIR studies reveal that the dispersing or stabilizing agents was either covalently bonded to the TiO_2 nanoparticles or physically mixed which result in the only non-covalent interaction. Morphological studies have shown the remarkable changes before and after exposing the functionalized TiO_2 nanoparticles into interfacial polymerization reaction on membrane surfaces. Hydrophilicity and performance evaluation of membranes display a clear flux increasing tendency by the incorporation of amine-functionalized in aqueous phase. Conversely, incorporation of chlorinated TiO_2 nanoparticles into IPC organic solution resulted in the formation of a dense hybrid polyamide layer and thus the flux decrease.

Chapter 6 Conclusions and Recommendations

6.1 Conclusions

In this study, novel polymer-based thin film nanocomposite membranes have been synthesised for aqueous and non-aqueous applications. The thesis has focused on the effect of incorporation of TiO₂ nanoparticles into the thin skin layer during both polymerization and crosslinking reactions. The effects of incorporated TiO₂ nanoparticles on the surface chemistry, morphology and fouling performance of nanocomposite membranes fabricated through different techniques were explored. The following conclusions can be drawn from each developed technique.

Thin film nanocomposite polyamide membranes having an ultra-thin skin layer on the reinforced polyethersulfone barrier supported by porous α -Al₂O₃ ceramic hollow fibre membranes were prepared by interfacial polymerization. In order to achieve the highly permeable nanocomposite membranes, TiO₂ nanoparticles were dispersed inside the diamine monomer. Initially, a silane coupling agent called APTS was grafted on the external surface of TiO₂ to overcome the agglomeration normally encountered in the preparation of TFN membranes and to achieve the better interfacial adhesion between nanoparticles and polymer matrix. The structural and separation properties of the fabricated membranes were improved by incorporation of functionalized TiO₂ nanoparticles in the diamine monomer. Both of the permeability and selectivity of the developed membrane was improved. Upon incorporation of TiO₂ nanoparticles, thermal stability of TFN membrane was significantly enhanced in comparison with TFC membrane. Further, TFN membrane with ultra-low concentration (0.005 wt%) of amine functionalized TiO₂ nanoparticles provided the best salt rejection as well water flux. Membrane flux can also be further improved, approximately 2-fold, by the incorporation of higher percentage of the modified TiO₂ nanoparticles.

A novel PVDF/PVA composite and nanocomposite membranes were developed by blending the TiO_2 nanoparticles into the PVA coated layer. Herein, we focused on the synergistic effect of TiO_2 nanoparticles and their surface chemistry on the structure, morphology, permeability and antifouling properties of the resultant TiO_2 -PVA TFN membranes. Interfacial modification of TiO_2 nanoparticles with covalently bonded carboxyl groups revealed an efficient approach to increase their dispersity throughout the polymer solution. Besides, the antifouling properties and solute rejection of TFN membranes were significantly improved.

In chapter five, a novel thin film nanocomposite solvent resistant nanofiltration membrane has been synthesized by incorporating the TiO_2 nanoparticles during the interfacial polymerization reaction. A porous polyimide ultrafiltration membrane coated by polyethyleneimine has been used as a support. Amination and chlorination of TiO_2 nanoparticles were used to improve their compatibilization into the polyamide matrix. Hydrophilicity and performance evaluation of membranes confirm the flux increment after incorporation of amine-functionalized TiO_2 nanoparticles into the amine solution. Conversely, their incorporation into organic solution caused formation of a denser polyamide layer and increases the membrane flux.

6.2 Recommendations

Based on the results of this study, the following recommendations are made for future investigations of thin film nanocomposite membranes applicable to both aqueous and non-aqueous media.

1. Nanoparticles strongly tend to agglomerate due to their high specific surface area and surface energy. Functionalization of different nanoparticles is recommended as a straightforward method prior to incorporate them into skin layer of thin film nanocomposite membranes not only for liquid separation but also for gas separation.
2. For functionalization purposes, the use of other silicone-based coupling agents is also recommended to improve the quality of particles' dispersion and enhance the antifouling properties of the produced TFN membranes.

3. In comparison with the other potential materials, utilization of different ceramic membranes is recommended as a TFN membrane support. Ceramic membrane with high porosity offers not only chemical, mechanical and thermal resistance, but also absorption capacity to remove hazardous species during filtration process.

References

1. Agenson, K.O. and T. Urase, *Change in membrane performance due to organic fouling in nanofiltration (NF)/reverse osmosis (RO) applications*. Separation and Purification Technology, 2007. **55**(2): p. 147-156.
2. Studart, A.R., U.T. Gonzenbach, E. Tervoort, and L.J. Gauckler, *Processing Routes to Macroporous Ceramics: A Review*. Journal of the American Ceramic Society, 2006. **89**(6): p. 1771-1789.
3. Xiao, X., F. Chen, Q. Wei, and N. Wu, *Surface modification of polyester nonwoven fabrics by Al₂O₃ sol-gel coating*. Journal of Coatings Technology and Research, 2009. **6**(4): p. 537-541.
4. Baker, R., *Membrane technology and applications* 2012: Wiley.
5. Baker, R.W., *Membrane Technology*, in *Encyclopedia of Polymer Science and Technology* 2002, John Wiley & Sons, Inc.
6. Ji, J., J.M. Dickson, R.F. Childs, and B.E. McCarry, *Mathematical Model for the Formation of Thin-Film Composite Membranes by Interfacial Polymerization: Porous and Dense Films*. Macromolecules, 1999. **33**(2): p. 624-633.
7. Kim, K.J., S.B. Lee, and N.W. Han, *Kinetics of crosslinking reaction of PVA membrane with glutaraldehyde*. Korean Journal of Chemical Engineering, 1994. **11**(1): p. 41-47.
8. Stengaard, F.F., *Characteristics and performance of new types of ultrafiltration membranes with chemically modified surfaces*. Desalination, 1988. **70**(1): p. 207-224.
9. Jeong, B.H., E. Hoek, Y. Yan, A. Subramani, X. Huang, G. Hurwitz, A.K. Ghosh, and A. Jawor, *Interfacial polymerization of thin film nanocomposites: A new concept for reverse osmosis membranes*. Journal of Membrane Science, 2007. **294**(1-2): p. 1-7.
10. Roy, S., S.A. Ntim, S. Mitra, and K.K. Sirkar, *Facile fabrication of superior nanofiltration membranes from interfacially polymerized CNT-polymer composites*. Journal of Membrane Science, 2011. **375**(1): p. 81-87.
11. Baroña, G.N.B., M. Choi, and B. Jung, *High permeate flux of PVA/PSf thin film composite nanofiltration membrane with aluminosilicate single-walled nanotubes*. Journal of Colloid and Interface Science, 2012. **386**(1): p. 189-197.
12. Mulder, M., *Basic principles of membrane technology*. 1996. The Netherlands: Kluwer Academic Publishers.
13. ÇAPAR, G., *Development of a membrane based treatment scheme for water recovery from textile effluents*, 2005, Middle East Technical University.
14. Tang, C. and V. Chen, *Nanofiltration of textile wastewater for water reuse*. Desalination, 2002. **143**(1): p. 11-20.
15. Rahimpour, A., M. Jahanshahi, M. Peyravi, and S. Khalili, *Interlaboratory studies of highly permeable thin-film composite polyamide nanofiltration membrane*. Polymers for Advanced Technologies, 2011. **23**(5): p. 884-893.
16. Müller-Holst, H., M. Engelhardt, and W. Schölkopf, *Small-scale thermal seawater desalination simulation and optimization of system design*. Desalination, 1999. **122**(2): p. 255-262.
17. Le Dirach, J., S. Nisan, and C. Poletiko, *Extraction of strategic materials from the concentrated brine rejected by integrated nuclear desalination systems*. Desalination, 2005. **182**(1): p. 449-460.
18. Yilmaz, I., N. Kabay, M. Yuksel, R. Holdich, and M. Bryjak, *Effect of ionic strength of solution on boron mass transfer by ion exchange separation*. Separation Science and Technology, 2007. **42**(5): p. 1013-1029.

19. Veerapaneni, S., B. Long, S. Freeman, and R. Bond, *Reducing energy consumption for seawater desalination*. Journal American Water Works Association, 2007. **99**(6): p. 95-106.
20. Busch, M. and W. Mickols, *Reducing energy consumption in seawater desalination*. Desalination, 2004. **165**: p. 299-312.
21. Sanz, M.A., R.L. Stover, S. Degrémont, and E. Recovery. *Low energy consumption in the Perth seawater desalination plant*. in *Proceedings of the International Desalination Association Congress, Maspalomas, Gran Canaria, Spain*. 2007.
22. Semiat, R., *Energy issues in desalination processes*. Environmental science & technology, 2008. **42**(22): p. 8193-8201.
23. Elimelech, M. and W.A. Phillip, *The future of seawater desalination: Energy, technology, and the environment*. Science, 2011. **333**(6043): p. 712-717.
24. PIZZICHINI, M., *MEMBRANE APPLICATION IN FOOD INDUSTRY*. Membrane Technology: Applications to Industrial Wastewater Treatment, 1995. **1**: p. 151.
25. PEREIRA, N.S. and K.V. PEINEMANN, *Membrane technology in the chemical industry*, 2006, Wiley-VCH, Weinheim.
26. Li, N., E. Funk, Y. Chang, S. Kulkarni, A. Swamikannu, and L. White, *Membrane separation processes in the petrochemical industry*, 1987, Allied-Signal, Inc., Des Plaines, IL (USA). Engineered Materials Research Center.
27. Takht Ravanchi, M., T. Kaghazchi, and A. Kargari, *Application of membrane separation processes in petrochemical industry: a review*. Desalination, 2009. **235**(1): p. 199-244.
28. Ana Maria, S., P. Anil Kumar, and R. Syed, *Membrane Applications in Chemical and Pharmaceutical Industries and in Conservation of Natural Resources*, in *Handbook of Membrane Separations* 2008, CRC Press. p. 3-5.
29. Mehdizadeh, H., *Membrane desalination plants from an energy-exergy viewpoint*. Desalination, 2006. **191**(1): p. 200-209.
30. Koros, W. and G. Fleming, *Membrane-based gas separation*. Journal of Membrane Science, 1993. **83**(1): p. 1-80.
31. Scott, K., Hughes, R. , *Industrial membrane separation technology* 1996: Blackie Academic, London, UK.
32. Merten, U., *Desalination by reverse osmosis* 1966: The MIT Press.
33. Roh, I.J. and V.P. Khare, *Investigation of the specific role of chemical structure on the material and permeation properties of ultrathin aromatic polyamides*. J. Mater. Chem., 2002. **12**(8): p. 2334-2338.
34. Nunes, S.P. and K.V. Peinemann, *Membrane technology* 2001: Wiley Online Library.
35. Matsumoto, Y., M. Sudoh, and Y. Suzuki, *Preparation of composite UF membranes of sulfonated polysulfone coated on ceramics*. Journal of Membrane Science, 1999. **158**(1): p. 55-62.
36. Yunlan, G., S. Mingren, and H. Jiajun, *Optimization in the preparation of polysulfone ultrafiltration membranes*. Desalination, 1987. **62**(0): p. 173-182.
37. Chai, G.Y. and W.B. Krantz, *Formation and characterization of polyamide membranes via interfacial polymerization*. Journal of Membrane Science, 1994. **93**(2): p. 175-192.
38. Cadotte, J.E. and L. Rozelle, *In-situ formed condensation polymers for reverse osmosis membranes*. 1972.
39. Lang, K., S. Sourirajan, T. Matsuura, and G. Chowdhury, *A study on the preparation of polyvinyl alcohol thin-film composite membranes and reverse osmosis testing*. Desalination, 1996. **104**(3): p. 185-196.
40. Kim, H.I. and S.S. Kim, *Fabrication of reverse osmosis membrane via low temperature plasma polymerization*. Journal of Membrane Science, 2001. **190**(1): p. 21-33.
41. Enkelmann, V. and G. Wegner. *Mechanism of interfacial polycondensation and the direct synthesis of polyamide membranes*. 1975.

42. Chaufer, B., M. Rabiller-Baudry, L. Guihard, and G. Daufin, *Retention of ions in nanofiltration at various ionic strength*. Desalination, 1996. **104**(1-2): p. 37-46.
43. Ikeda, K., T. Nakano, H. Ito, T. Kubota, and S. Yamamoto, *New composite charged reverse osmosis membrane*. Desalination, 1988. **68**(2-3): p. 109-119.
44. Tsuru, T., M. Urairi, S.-I. Nakao, and S. Kimura, *Negative rejection of anions in the loose reverse osmosis separation of mono- and divalent ion mixtures*. Desalination, 1991. **81**(1-3): p. 219-227.
45. Bowen, W.R., A.W. Mohammad, and N. Hilal, *Characterisation of nanofiltration membranes for predictive purposes — use of salts, uncharged solutes and atomic force microscopy*. Journal of Membrane Science, 1997. **126**(1): p. 91-105.
46. Shin-ichi, N., *Determination of pore size and pore size distribution: 3. Filtration membranes*. Journal of Membrane Science, 1994. **96**(1-2): p. 131-165.
47. Bowen, W.R. and H. Mukhtar, *Characterisation and prediction of separation performance of nanofiltration membranes*. Journal of Membrane Science, 1996. **112**(2): p. 263-274.
48. van der Horst, H.C., J.M.K. Timmer, T. Robbertsen, and J. Leenders, *Use of nanofiltration for concentration and demineralization in the dairy industry: Model for mass transport*. Journal of Membrane Science, 1995. **104**(3): p. 205-218.
49. Deen, W.M., *HINDERED TRANSPORT OF LARGE MOLECULES IN LIQUID-FILLED PORES*. AIChE Journal, 1987. **33**(9): p. 1409-1425.
50. Schaep, J., B. Van der Bruggen, C. Vandecasteele, and D. Wilms, *Influence of ion size and charge in nanofiltration*. Separation and Purification Technology, 1998. **14**(1-3): p. 155-162.
51. Meihong, L., Y. Sanchuan, Z. Yong, and G. Congjie, *Study on the thin-film composite nanofiltration membrane for the removal of sulfate from concentrated salt aqueous: Preparation and performance*. Journal of Membrane Science, 2008. **310**(1-2): p. 289-295.
52. Rahimpour, A., M. Jahanshahi, M. Peyravi, and S. Khalili, *Interlaboratory studies of highly permeable thin-film composite polyamide nanofiltration membrane*. Polymers for Advanced Technologies, 2011: p. DOI: 10.1002/pat.1984.
53. Verhoef, A., A. Figoli, B. Leen, B. Bettens, E. Drioli, and B. Van der Bruggen, *Performance of a nanofiltration membrane for removal of ethanol from aqueous solutions by pervaporation*. Separation and Purification Technology, 2008. **60**(1): p. 54-63.
54. Yoshizuka, K., H. Ohta, K. Inoue, H. Kitazaki, and M. Ishimaru, *Selective separation of flavonoids with a polyvinyl alcohol membrane*. Journal of Membrane Science, 1996. **118**(1): p. 41-48.
55. Reinhart, C.T. and N.A. Peppas, *Solute diffusion in swollen membranes. Part II. Influence of crosslinking on diffusive properties*. Journal of Membrane Science, 1984. **18**: p. 227-239.
56. Jegal, J., N.-W. Oh, D.-S. Park, and K.-H. Lee, *Characteristics of the nanofiltration composite membranes based on PVA and sodium alginate*. Journal of applied polymer science, 2001. **79**(13): p. 2471-2479.
57. Jegal, J., N.-W. Oh, and K.-H. Lee, *Preparation and characterization of PVA/SA composite nanofiltration membranes*. Journal of applied polymer science, 2000. **77**(2): p. 347-354.
58. Jegal, J. and K.H. Lee, *Nanofiltration membranes based on poly(vinyl alcohol) and ionic polymers*. Journal of applied polymer science, 1999. **72**(13): p. 1755-1762.
59. Pendergast, M.T.M. and E.M.V. Hoek, *A review of water treatment membrane nanotechnologies*. Energy & Environmental Science, 2011. **4**(6): p. 1946-1971.
60. Lind, M.L., B.H. Jeong, A. Subramani, X. Huang, and E. Hoek, *Effect of mobile cation on zeolite-polyamide thin film nanocomposite membranes*. Journal of Materials Research, 2009. **24**(05): p. 1624-1631.

61. Lind, M.L., D. Eumine Suk, T.V. Nguyen, and E.M.V. Hoek, *Tailoring the structure of thin film nanocomposite membranes to achieve seawater RO membrane performance*. Environmental science & technology, 2010.
62. Fathizadeh, M., A. Aroujalian, and A. Raisi, *Effect of added NaX nano-zeolite into polyamide as a top thin layer of membrane on water flux and salt rejection in a reverse osmosis process*. Journal of Membrane Science, 2011. **375**(1-2): p. 88-95.
63. Lee, H.S., S.J. Im, J.H. Kim, H.J. Kim, J.P. Kim, and B.R. Min, *Polyamide thin-film nanofiltration membranes containing TiO₂ nanoparticles*. Desalination, 2008. **219**(1-3): p. 48-56.
64. Lee, S.Y., H.J. Kim, R. Patel, S.J. Im, J.H. Kim, and B.R. Min, *Silver nanoparticles immobilized on thin film composite polyamide membrane: characterization, nanofiltration, antifouling properties*. Polymers for Advanced Technologies, 2007. **18**(7): p. 562-568.
65. Kim, E.-S., G. Hwang, M.G. El-Din, and Y. Liu, *Development of nanosilver and multi-walled carbon nanotubes thin-film nanocomposite membrane for enhanced water treatment*. Journal of Membrane Science, (10.1016/j.memsci.2011.11.041).
66. Uyak, V., I. Koyuncu, I. Oktem, M. Cakmakci, and I. Toroz, *Removal of trihalomethanes from drinking water by nanofiltration membranes*. Journal of hazardous materials, 2008. **152**(2): p. 789-794.
67. Eriksson, P., *Water and salt transport through two types of polyamide composite membranes*. Journal of Membrane Science, 1988. **36**: p. 297-313.
68. Cadotte, J., R. Forester, M. Kim, R. Petersen, and T. Stocker, *Nanofiltration membranes broaden the use of membrane separation technology*. Desalination, 1988. **70**(1-3): p. 77-88.
69. Raman, L.P., M. Cheryna, and N. Rajagopalan, *Consider nanofiltration for membrane separations*. Chemical Engineering Progress;(United States), 1994. **90**(3).
70. Petersen, R.J., *Composite reverse osmosis and nanofiltration membranes*. Journal of Membrane Science, 1993. **83**(1): p. 81-150.
71. Eriksson, P., *Nanofiltration extends the range of membrane filtration*. Environmental progress, 1988. **7**(1): p. 58-62.
72. Williams, M.E., *A brief review of reverse osmosis membrane technology*, 2003, Williams Engineering Services Company, Inc.
73. Li, D. and H. Wang, *Recent developments in reverse osmosis desalination membranes*. J. Mater. Chem., 2010. **20**(22): p. 4551-4566.
74. Baker, R.W., *Membrane separation systems: recent developments and future directions*1991: William Andrew.
75. Strathmann, H., *Synthetic membranes and their preparation*. Handbook of industrial membrane technology. New Jersey: Noyes Publications, 1990.
76. Kesting, R.E., *Synthetic Polymeric Membranes, A Structural Perspective*, A Wiley-Interscience Publication, 1985, Wiley.
77. Cabasso, I., *Membranes*. Encyclopedia of Polymer Science and Engineering. *JI Kroschwitz*, 1987, New York, John Wiley & Sons.
78. Lonsdale, H.K., *The evolution of ultrathin synthetic membranes*. Journal of Membrane Science, 1987. **33**(2): p. 121-136.
79. Roh, I.J., J.J. Kim, and S.Y. Park, *Mechanical properties and reverse osmosis performance of interfacially polymerized polyamide thin films*. Journal of Membrane Science, 2002. **197**(1-2): p. 199-210.
80. Freger, V., *Nanoscale heterogeneity of polyamide membranes formed by interfacial polymerization*. Langmuir, 2003. **19**(11): p. 4791-4797.
81. Song, Y., P. Sun, L.L. Henry, and B. Sun, *Mechanisms of structure and performance controlled thin film composite membrane formation via interfacial polymerization process*. Journal of Membrane Science, 2005. **251**(1-2): p. 67-79.
82. Li, L., S. Zhang, X. Zhang, and G. Zheng, *Polyamide thin film composite membranes prepared from 3, 4', 5-biphenyl triacyl chloride, 3, 3', 5, 5'-biphenyl*

- tetraacyl chloride and m-phenylenediamine*. Journal of Membrane Science, 2007. **289**(1-2): p. 258-267.
83. Hoek, V. and A.K. Ghosh, *NANOCOMPOSITE MEMBRANES AND METHODS OF MAKING AND USING SAME*, 2010, US Patent App. 20,100/224,555.
84. Lind, M.L., A.K. Ghosh, A. Jawor, X. Huang, W. Hou, Y. Yang, and E.M.V. Hoek, *Influence of zeolite crystal size on zeolite-polyamide thin film nanocomposite membranes*. Langmuir, 2009. **25**(17): p. 10139-10145.
85. Jadav, G.L. and P.S. Singh, *Synthesis of novel silica-polyamide nanocomposite membrane with enhanced properties*. Journal of Membrane Science, 2009. **328**(1-2): p. 257-267.
86. Martin, M.N., J.I. Basham, P. Chando, and S.-K. Eah, *Charged Gold Nanoparticles in Non-Polar Solvents: 10-min Synthesis and 2D Self-Assembly*. Langmuir, 2010. **26**(10): p. 7410-7417.
87. Tan, X., S. Liu, and K. Li, *Preparation and characterization of inorganic hollow fiber membranes*. Journal of Membrane Science, 2001. **188**(1): p. 87-95.
88. Liu, S., K. Li, and R. Hughes, *Preparation of porous aluminium oxide (Al₂O₃) hollow fibre membranes by a combined phase-inversion and sintering method*. Ceramics international, 2003. **29**(8): p. 875-881.
89. Liu, S. and K. Li, *Preparation TiO₂/Al₂O₃ composite hollow fibre membranes*. Journal of Membrane Science, 2003. **218**(1-2): p. 269-277.
90. Nandi, B., R. Uppaluri, and M. Purkait, *Effects of dip coating parameters on the morphology and transport properties of cellulose acetate-ceramic composite membranes*. Journal of Membrane Science, 2009. **330**(1-2): p. 246-258.
91. Gekas, V. and B. Hallström, *Mass transfer in the membrane concentration polarization layer under turbulent cross flow : I. Critical literature review and adaptation of existing sherwood correlations to membrane operations*. Journal of Membrane Science, 1987. **30**(2): p. 153-170.
92. Bowen, W.R., A.W. Mohammad, and N. Hilal, *Characterisation of nanofiltration membranes for predictive purposes--use of salts, uncharged solutes and atomic force microscopy*. Journal of Membrane Science, 1997. **126**(1): p. 91-105.
93. Aimar, P., M. Meireles, and V. Sanchez, *A contribution to the translation of retention curves into pore size distributions for sieving membranes*. Journal of Membrane Science, 1990. **54**(3): p. 321-338.
94. Bowen, W.R. and J.S. Welfoot, *Modelling the performance of membrane nanofiltration—critical assessment and model development*. Chemical Engineering Science, 2002. **57**(7): p. 1121-1137.
95. Merkel, T., B. Freeman, R. Spontak, Z. He, I. Pinnau, P. Meakin, and A. Hill, *Ultraparpermeable, reverse-selective nanocomposite membranes*. Science, 2002. **296**(5567): p. 519-522.
96. Ge, L., M. Xu, and H. Fang, *Synthesis of titanium oxide layers on glass substrates with aqueous refluxed sols (RS) and photocatalytic activities*. Journal of Materials Science, 2007. **42**(13): p. 4926-4934.
97. Wang, X., Zhang, Niehaus, and T. Frauenheim, *Excited State Properties of Allylamine-Capped Silicon Quantum Dots*. The Journal of Physical Chemistry C, 2007. **111**(6): p. 2394-2400.
98. Ryu, Y.B., W.Y. Jung, M.S. Lee, E.D. Jeong, H.G. Kim, J.S. Yang, G.-D. Lee, S.S. Park, and S.-S. Hong, *Hydrothermal synthesis of titanium dioxides from peroxotitanate solution using basic additive and their photocatalytic activity on the decomposition of orange II*. Journal of Physics and Chemistry of Solids. **69**(5-6): p. 1457-1460.
99. Ye, L., R. Pelton, and M.A. Brook, *Biotinylation of TiO₂ Nanoparticles and Their Conjugation with Streptavidin*. Langmuir, 2007. **23**(10): p. 5630-5637.
100. Kim, H.S., H.S. Yang, H.J. Kim, and H.J. Park, *Thermogravimetric analysis of rice husk flour filled thermoplastic polymer composites*. Journal of thermal analysis and calorimetry, 2004. **76**(2): p. 395-404.

101. Kwak, S.-Y. and D. Woo Ihm, *Use of atomic force microscopy and solid-state NMR spectroscopy to characterize structure-property-performance correlation in high-flux reverse osmosis (RO) membranes*. Journal of Membrane Science, 1999. **158**(1-2): p. 143-153.
102. Zajac, R. and A. Chakrabarti, *Irreversible polymer adsorption from semidilute and moderately dense solutions*. Physical Review E, 1995. **52**(6): p. 6536.
103. Gentle, T., R. Schmidt, B. Naasz, A. Gellman, and T. Gentle, *Organofunctional silanes as adhesion promoters: direct characterization of the polymer/silane interphase*. Journal of Adhesion Science and Technology, 1992. **6**(2): p. 307-316.
104. Ghosh, A.K., B.-H. Jeong, X. Huang, and E.M.V. Hoek, *Impacts of reaction and curing conditions on polyamide composite reverse osmosis membrane properties*. Journal of Membrane Science, 2008. **311**(1-2): p. 34-45.
105. Wenzel, R.N., *Resistance of solid surfaces to wetting by water*. Ind. Eng. Chem, 1936. **28**(8): p. 988-994.
106. Vellenga, E. and G. Trägårdh, *Nanofiltration of combined salt and sugar solutions: coupling between retentions*. Desalination, 1998. **120**(3): p. 211-220.
107. Mohammad, A., R.K. Basha, and C. Leo, *Nanofiltration of glucose solution containing salts: Effects of membrane characteristics, organic component and salts on retention*. Journal of Food Engineering, 2010. **97**(4): p. 510-518.
108. Ahmad, A. and B. Ooi, *Optimization of composite nanofiltration membrane through pH control: Application in CuSO₄ removal*. Separation and Purification Technology, 2006. **47**(3): p. 162-172.
109. Vigo, F., G. Capannelli, C. Uliana, and S. Munari, *Asymmetric polyvinylidene fluoride (pvdf) radiation grafted membranes: preparation and performance in reverse osmosis application*. Desalination, 1981. **36**(1): p. 63-73.
110. Liu, J., Z. Xu, and Y. Zhang, *Preparation of Polyvinylidene Fluoride (PVDF) Hollow Fiber Composite Nanofiltration Membrane I. Fabrication of the Composite Nanofiltration Membrane*. JOURNAL-EAST CHINA UNIVERSITY OF SCIENCE AND TECHNOLOGY, 2006. **32**(3): p. 241.
111. Capannelli, G., F. Vigo, and S. Munari, *Ultrafiltration membranes--characterization methods*. Journal of Membrane Science, 1983. **15**(3): p. 289-313.
112. Bottino, A., G. Camera-Roda, G. Capannelli, and S. Munari, *The formation of microporous polyvinylidene difluoride membranes by phase separation*. Journal of Membrane Science, 1991. **57**(1): p. 1-20.
113. Madaeni, S.S. and A.H. Taheri, *Effect of Casting Solution on Morphology and Performance of PVDF Microfiltration Membranes*. Chemical Engineering & Technology, 2011. **34**(8): p. 1328-1334.
114. Wang, D., K. Li, and W. Teo, *Preparation and characterization of polyvinylidene fluoride (PVDF) hollow fiber membranes*. Journal of Membrane Science, 1999. **163**(2): p. 211-220.
115. Shih, H., Y. Yeh, and H. Yasuda, *Morphology of microporous poly (vinylidene fluoride) membranes studied by gas permeation and scanning electron microscopy*. Journal of Membrane Science, 1990. **50**(3): p. 299-317.
116. Liu, F., N.A. Hashim, Y. Liu, M.R.M. Abed, and K. Li, *Progress in the production and modification of PVDF membranes*. Journal of Membrane Science, 2011. **375**(1-2): p. 1-27.
117. Rana, D. and T. Matsuura, *Surface modifications for antifouling membranes*. Chemical reviews, 2010. **110**(4): p. 2448.
118. Nunes, S.P., M.L. Sforça, and K.-V. Peinemann, *Dense hydrophilic composite membranes for ultrafiltration*. Journal of Membrane Science, 1995. **106**(1-2): p. 49-56.
119. Wei, J., G.S. Helm, N. Corner-Walker, and X. Hou, *Characterization of a non-fouling ultrafiltration membrane*. Desalination, 2006. **192**(1-3): p. 252-261.

120. Boributh, S., A. Chanachai, and R. Jiratananon, *Modification of PVDF membrane by chitosan solution for reducing protein fouling*. Journal of Membrane Science, 2009. **342**(1–2): p. 97-104.
121. Du, J.R., S. Peldszus, P.M. Huck, and X. Feng, *Modification of poly(vinylidene fluoride) ultrafiltration membranes with poly(vinyl alcohol) for fouling control in drinking water treatment*. Water Research, 2009. **43**(18): p. 4559-4568.
122. Hirai, T., Y. Asada, T. Suzuki, and S. Hayashi, *Studies on elastic hydrogel membrane. I. Effect of preparation conditions on the membrane performance*. Journal of applied polymer science, 1989. **38**(3): p. 491-502.
123. Bolto, B., T. Tran, M. Hoang, and Z. Xie, *Crosslinked poly (vinyl alcohol) membranes*. Progress in polymer science, 2009. **34**(9): p. 969-981.
124. Gohil, J.M. and P. Ray, *Polyvinyl alcohol as the barrier layer in thin film composite nanofiltration membranes: Preparation, characterization, and performance evaluation*. Journal of Colloid and Interface Science, 2009. **338**(1): p. 121-127.
125. Peng, F., X. Huang, A. Jawor, and E.M.V. Hoek, *Transport, structural, and interfacial properties of poly(vinyl alcohol)–polysulfone composite nanofiltration membranes*. Journal of Membrane Science, 2010. **353**(1–2): p. 169-176.
126. Peng, F., Z. Jiang, and E.M.V. Hoek, *Tuning the molecular structure, separation performance and interfacial properties of poly(vinyl alcohol)–polysulfone interfacial composite membranes*. Journal of Membrane Science, 2011. **368**(1–2): p. 26-33.
127. Ng, L.Y., A.W. Mohammad, C.P. Leo, and N. Hilal, *Polymeric membranes incorporated with metal/metal oxide nanoparticles: A comprehensive review*. Desalination, 2010.
128. Pendergast, M.M., A.K. Ghosh, and E.M.V. Hoek, *Separation performance and interfacial properties of nanocomposite reverse osmosis membranes*. Desalination, (0).
129. Kim, J. and B. Van der Bruggen, *The use of nanoparticles in polymeric and ceramic membrane structures: Review of manufacturing procedures and performance improvement for water treatment*. Environmental Pollution, 2010. **158**(7): p. 2335-2349.
130. Kim, S., R. Roque, B. Birgisson, and A. Guarin, *Porosity of the dominant aggregate size range to evaluate coarse aggregate structure of asphalt mixtures*. Journal of Materials in Civil Engineering, 2009. **21**(1): p. 32-39.
131. Bae, T.-H. and T.-M. Tak, *Effect of TiO₂ nanoparticles on fouling mitigation of ultrafiltration membranes for activated sludge filtration*. Journal of Membrane Science, 2005. **249**(1–2): p. 1-8.
132. Li, J.-F., Z.-L. Xu, H. Yang, L.-Y. Yu, and M. Liu, *Effect of TiO₂ nanoparticles on the surface morphology and performance of microporous PES membrane*. Applied Surface Science, 2009. **255**(9): p. 4725-4732.
133. Ebert, K., D. Fritsch, J. Koll, and C. Tjahjawiguna, *Influence of inorganic fillers on the compaction behaviour of porous polymer based membranes*. Journal of Membrane Science, 2004. **233**(1–2): p. 71-78.
134. Rahimpour, A., M. Jahanshahi, B. Rajaeian, and M. Rahimnejad, *TiO₂ entrapped nano-composite PVDF/SPES membranes: Preparation, characterization, antifouling and antibacterial properties*. Desalination, 2011. **278**(1–3): p. 343-353.
135. Yang, Y., H. Zhang, P. Wang, Q. Zheng, and J. Li, *The influence of nano-sized TiO₂ fillers on the morphologies and properties of PSF UF membrane*. Journal of Membrane Science, 2007. **288**(1–2): p. 231-238.
136. Rajaeian, B., A. Rahimpour, M.O. Tade, and S. Liu, *Fabrication and characterization of polyamide thin film nanocomposite (TFN) nanofiltration membrane impregnated with TiO₂ nanoparticles*. Desalination, 2013. **313**(0): p. 176-188.
137. Razmjou, A., J. Mansouri, and V. Chen, *The effects of mechanical and chemical modification of TiO₂ nanoparticles on the surface chemistry, structure and fouling*

- performance of PES ultrafiltration membranes*. Journal of Membrane Science, 2011. **378**(1–2): p. 73-84.
138. Pourjafar, S., A. Rahimpour, and M. Jahanshahi, *Synthesis and characterization of PVA/PES thin film composite nanofiltration membrane modified with TiO₂ nanoparticles for better performance and surface properties*. Journal of Industrial and Engineering Chemistry, 2012. **18**(4): p. 1398-1405.
139. Baroña, G.N.B., M. Choi, and B. Jung, *High Permeate Flux of PVA/PSf Thin Film Composite Nanofiltration Membrane with Aluminosilicate Single-Walled Nanotubes*. Journal of Colloid and Interface Science, 2012.
140. Xu, Z., L. Li, F. Wu, S. Tan, and Z. Zhang, *The application of the modified PVDF ultrafiltration membranes in further purification of Ginkgo biloba extraction*. Journal of Membrane Science, 2005. **255**(1): p. 125-131.
141. Huang, R. and J. Rhim, *Modification of poly (vinyl alcohol) using maleic acid and its application to the separation of acetic acid-water mixtures by the pervaporation technique*. Polymer international, 1993. **30**(1): p. 129-135.
142. Rong, M., M. Zhang, and W. Ruan, *Surface modification of nanoscale fillers for improving properties of polymer nanocomposites: a review*. Materials science and technology, 2006. **22**(7): p. 787-796.
143. Lou, Y., M. Liu, X. Miao, L. Zhang, and X. Wang, *Improvement of the mechanical properties of nano-TiO₂/poly (vinyl alcohol) composites by enhanced interaction between nanofiller and matrix*. Polymer Composites, 2009. **31**(7): p. 1184-1193.
144. Blin, J.L., C. Gérardin, L. Rodehüser, C. Selve, and M.J. Stébé, *Influence of Alkyl Peptidoamines on the Structure of Functionalized Mesoporous Silica*. Chemistry of Materials, 2004. **16**(24): p. 5071-5080.
145. Max, J.J. and C. Chapados, *Infrared spectroscopy of aqueous carboxylic acids: Comparison between different acids and their salts*. The Journal of Physical Chemistry A, 2004. **108**(16): p. 3324-3337.
146. Sivaiah, K., K.N. Kumar, V. Naresh, and S. Buddhudu, *Structural and Optical Properties of Li⁺: PVP & Ag⁺: PVP Polymer Films*. Materials Sciences and Applications, 2011. **2**(11): p. 1688-1696.
147. Kesting, R.E., *Synthetic polymeric membranes* 1971: McGraw-Hill New York.
148. Mansur, H.S., R.L. Orefice, and A.A.P. Mansur, *Characterization of poly (vinyl alcohol)/poly (ethylene glycol) hydrogels and PVA-derived hybrids by small-angle X-ray scattering and FTIR spectroscopy*. Polymer, 2004. **45**(21): p. 7193-7202.
149. Kinsella, J., D. Whitehead, J. Brady, N. Bringe, and P. Fox, *Milk proteins: possible relationships of structure and function*. Developments in dairy chemistry. 4. Functional milk proteins., 1989: p. 55-95.
150. Pusch, W., *Determination of Transport Parameters of Synthetic Membranes by Hyperfiltration Experiments Part I: Derivation of Transport Relationship from the Linear Relations of Thermodynamics of Irreversible Processes*. Berichte der Bunsengesellschaft für physikalische Chemie, 1977. **81**(3): p. 269-276.
151. Dai, W.S. and T.A. Barbari, *Hydrogel membranes with mesh size asymmetry based on the gradient crosslinking of poly(vinyl alcohol)*. Journal of Membrane Science, 1999. **156**(1): p. 67-79.
152. Ikeda, K., T. Nakano, H. Ito, T. Kubota, and S. Yamamoto, *New composite charged reverse osmosis membrane*. Desalination, 1988. **68**(2–3): p. 109-119.
153. Vatanpour, V., S.S. Madaeni, R. Moradian, S. Zinadini, and B. Astinchap, *Novel antibifouling nanofiltration polyethersulfone membrane fabricated from embedding TiO₂ coated multiwalled carbon nanotubes*. Separation and Purification Technology, 2012. **90**(0): p. 69-82.
154. Rahimpour, A., M. Jahanshahi, B. Rajaeian, and M. Rahimnejad, *TiO₂ entrapped nano-composite PVDF/SPES membranes: Preparation, characterization, antifouling and antibacterial properties*. Desalination, 2011. **278**(1): p. 343-353.

155. Rahimpour, A., S.S. Madaeni, A.H. Taheri, and Y. Mansourpanah, *Coupling TiO₂ nanoparticles with UV irradiation for modification of polyethersulfone ultrafiltration membranes*. Journal of Membrane Science, 2008. **313**(1-2): p. 158-169.
156. Ahmad, A.L., M.A. Majid, and B.S. Ooi, *Functionalized PSf/SiO₂ nanocomposite membrane for oil-in-water emulsion separation*. Desalination, 2011. **268**(1-3): p. 266-269.
157. Vatanpour, V., S.S. Madaeni, L. Rajabi, S. Zinadini, and A.A. Derakhshan, *Boehmite nanoparticles as a new nanofiller for preparation of antifouling mixed matrix membranes*. Journal of Membrane Science, 2012. **401-402**(0): p. 132-143.
158. Yan, L., S. Hong, M.L. Li, and Y.S. Li, *Application of the Al₂O₃-PVDF nanocomposite tubular ultrafiltration (UF) membrane for oily wastewater treatment and its antifouling research*. Separation and Purification Technology, 2009. **66**(2): p. 347-352.
159. Vatanpour, V., S.S. Madaeni, R. Moradian, S. Zinadini, and B. Astinchap, *Fabrication and characterization of novel antifouling nanofiltration membrane prepared from oxidized multiwalled carbon nanotube/polyethersulfone nanocomposite*. Journal of Membrane Science, 2011. **375**(1-2): p. 284-294.
160. Vatanpour, V., S.S. Madaeni, A.R. Khataee, E. Salehi, S. Zinadini, and H.A. Monfared, *TiO₂ embedded mixed matrix PES nanocomposite membranes: Influence of different sizes and types of nanoparticles on antifouling and performance*. Desalination, 2012. **292**(0): p. 19-29.
161. Rahimpour, A., M. Jahanshahi, S. Khalili, A. Mollahosseini, A. Zirepour, and B. Rajaeian, *Novel functionalized carbon nanotubes for improving the surface properties and performance of polyethersulfone (PES) membrane*. Desalination, 2012. **286**(0): p. 99-107.
162. Mansourpanah, Y., S.S. Madaeni, A. Rahimpour, M. Adeli, M.Y. Hashemi, and M.R. Moradian, *Fabrication new PES-based mixed matrix nanocomposite membranes using polycaprolactone modified carbon nanotubes as the additive: Property changes and morphological studies*. Desalination, 2011. **277**(1-3): p. 171-177.
163. Cao, X., X.Y. Wu, T. Wu, K. Jin, and B.K. Hur, *Concentration of 6-aminopenicillanic acid from penicillin bioconversion solution and its mother liquor by nanofiltration membrane*. Biotechnology and Bioprocess Engineering, 2001. **6**(3): p. 200-204.
164. Sheth, J.P., Y. Qin, K.K. Sirkar, and B.C. Baltzis, *Nanofiltration-based diafiltration process for solvent exchange in pharmaceutical manufacturing*. Journal of Membrane Science, 2003. **211**(2): p. 251-261.
165. van der Gryp, P., A. Barnard, J.P. Cronje, D. de Vlieger, S. Marx, and H. Vosloo, *Separation of different metathesis Grubbs-type catalysts using organic solvent nanofiltration*. Journal of Membrane Science, 2010. **353**(1-2): p. 70-77.
166. Othman, R., A.W. Mohammad, M. Ismail, and J. Salimon, *Application of polymeric solvent resistant nanofiltration membranes for biodiesel production*. Journal of Membrane Science, 2010. **348**(1-2): p. 287-297.
167. Othman, R., A.W. Mohammad, M. Ismail, and J. Salimon, *SELECTIVITY OF POLYMERIC SOLVENT RESISTANT NANOFILTRATION MEMBRANES FOR BIODIESEL SEPARATION*. Sustainable Membrane Technology for Energy, Water, and Environment, 2012: p. 277.
168. Tarleton, E., J. Robinson, and J. Low, *Nanofiltration: A technology for selective solute removal from fuels and solvents*. 2009.
169. Darvishmanesh, S., J. Degrève, and B.V. Bruggen, *Performance of solvent-pretreated polyimide nanofiltration membranes for separation of dissolved dyes from toluene*. Industrial & Engineering Chemistry Research, 2010.

170. Vandezande, P., L.E.M. Gevers, and I.F.J. Vankelecom, *Solvent resistant nanofiltration: separating on a molecular level*. Chem. Soc. Rev., 2007. **37**(2): p. 365-405.
171. Rohani, R., M. Hyland, and D. Patterson, *A refined one-filtration method for aqueous based nanofiltration and ultrafiltration membrane molecular weight cut-off determination using polyethylene glycols*. Journal of Membrane Science, 2011. **382**(1-2): p. 278-290.
172. Tsuru, T., M. Miyawaki, H. Kondo, T. Yoshioka, and M. Asaeda, *Inorganic porous membranes for nanofiltration of nonaqueous solutions*. Separation and Purification Technology, 2003. **32**(1-3): p. 105-109.
173. Tsuru, T., T. Sudoh, T. Yoshioka, and M. Asaeda, *Nanofiltration in non-aqueous solutions by porous silica-zirconia membranes*. Journal of Membrane Science, 2001. **185**(2): p. 253-261.
174. Linder, C., M. Nemas, M. Perry, and R. Katrar, *Silicon-derived solvent stable membranes*, in *US Patent* 1993, Membrane Products Kiryat Weitzman Ltd. (Rehovot, IL)
175. White, L.S., *Transport properties of a polyimide solvent resistant nanofiltration membrane*. Journal of Membrane Science, 2002. **205**(1-2): p. 191-202.
176. Vanherck, K., P. Vandezande, S.O. Aldea, and I.F.J. Vankelecom, *Cross-linked polyimide membranes for solvent resistant nanofiltration in aprotic solvents*. Journal of Membrane Science, 2008. **320**(1): p. 468-476.
177. Strathmann, H., *Asymmetric polyimide membranes for filtration of non-aqueous solutions*. Desalination, 1978. **26**(1): p. 85-92.
178. LIVINGSTON, A.G., Y.S. Bhole, and M.F. Jimenez Solomon, *SOLVENT RESISTANT POLYAMIDE NANOFILTRATION MEMBRANES*, 2012, WO Patent WO/2012/010,889.
179. Zhu, B., H. Iwata, I. Hirata, and Y. Ikada, *Hydrophilic modification of a polyimide film surface*. Journal of Adhesion Science and Technology, 2000. **14**(3): p. 351-361.
180. Ba, C., J. Langer, and J. Economy, *Chemical modification of P84 copolyimide membranes by polyethylenimine for nanofiltration*. Journal of Membrane Science, 2009. **327**(1-2): p. 49-58.
181. Vanherck, K., A. Cano-Odena, G. Koeckelberghs, T. Dedroog, and I. Vankelecom, *A simplified diamine crosslinking method for PI nanofiltration membranes*. Journal of Membrane Science, 2010. **353**(1-2): p. 135-143.
182. Kosaraju, P.B. and K.K. Sirkar, *Novel solvent-resistant hydrophilic hollow fiber membranes for efficient membrane solvent back extraction*. Journal of Membrane Science, 2007. **288**(1-2): p. 41-50.
183. Soroko, I. and A. Livingston, *Impact of TiO₂ nanoparticles on morphology and performance of crosslinked polyimide organic solvent nanofiltration (OSN) membranes*. Journal of Membrane Science, 2009. **343**(1): p. 189-198.
184. Roy, S., S.A. Ntim, S. Mitra, and K.K. Sirkar, *Facile fabrication of superior nanofiltration membranes from interfacially polymerized CNT-polymer composites*. Journal of Membrane Science, 2011. **375**(1-2): p. 81-87.
185. Peyravi, M., A. Rahimpour, M. Jahanshahi, A. Javadi, and A. Shockravi, *Tailoring the surface properties of PES ultrafiltration membranes to reduce the fouling resistance using synthesized hydrophilic copolymer*. Microporous and Mesoporous Materials, 2012. **160**(0): p. 114-125.
186. Whu, J.A., B.C. Baltzis, and K.K. Sirkar, *Nanofiltration studies of larger organic microsolute in methanol solutions*. Journal of Membrane Science, 2000. **170**(2): p. 159-172.
187. Cheng, S., D.L. Oatley, P.M. Williams, and C.J. Wright, *Positively charged nanofiltration membranes: Review of current fabrication methods and introduction of a novel approach*. Advances in Colloid and Interface Science, 2011. **164**(1-2): p. 12-20.